CONTENTS

Abstract

Over a century of research has revealed the richness of stereoscopic vision in generating percepts of the three dimensional (3D). Since Wheatstone invented the stereoscope, it has been known that the different views projected to our two eyes contain information that is used to recover depth. It also has been realized that the two eyes which have slightly different views of the world contribute to the perception of depth. Many of the organisms, including humans, perceive the outside world with both eyes, grasping a two-dimensional retinal image which is captured by each eye as a common single image. This phenomenon is known as binocular fusion which means that similar images presented to the two eyes appear as one and are processed simultaneously rather than successively.

Fusion limit (i.e. diplopia threshold) denotes the largest retinal disparity between two images for which the impression of a single fused image can be maintained. It has pronounced influence on the generation of the percepts of 3D because goods are sterically recognized by the deviation of the retinal image generated in the position of the two eyes (i.e. binocular parallax). In contrast, viewing dissimilar images yields perceptual alternations competing for dominance, and this is known as binocular rivalry. Although various techniques have recently received much attention in the broadcast research community as a promising technology for three-dimensional television systems, the dominant problem associated with binocular vision still is that of explaining how a single unified visual percept is formed from the inputs from two eyes since any optical instrument, especially 3D displays, should be designed to avoid the unpleasant and annoying binocular rivalry. When we view a stereogram whose left and right images are of different, but uniform, colors, we perceive a stereoscopic image whose color differs from the color of either image. This property is explained by the theory of binocular color mixing. Then, one of the fundamental problems in understanding the color rivalry process was to measure how much difference of color is permitted before the visual field turns inhomogeneous. Many experiments have already been performed. Therefore,

previous works concerning the fusion limit of binocular vision are all based on normal visions. Few works are reported upon the cataract vision.

Along with the arrival of the aging society, the optical instruments design for elders has become an earnest demand. It is necessary to measure the vision difference that can be permitted before the rivalry occurs for elderly people. In this study, a cataract experiencing goggle is used to provide the vision as close appearance of age-related (senile) cataract as possible. It is evident that the main cause of visually significant cataracts is ageing, and age-related cataracts are the focus of many seminars. In this thesis, we measure the limit of binocular color fusion in the normal vision and the cataract experiencing vision which is used to simulate the elderly vision using a 3D display connected to a computer to present experimental stimuli conveniently. The results show that the color fusion limit curves in cataract experiencing vision are very similar with those in normal vision. In the normal vision, the color fusion limit $\Delta\lambda_{dn}$ is within a range of about 11 ~ 65 nm on central vision, 15 ~ 67 nm on the retinal eccentricity of 3°, 21 ~ 69 nm on the retinal eccentricity of 6°, and 25 ~ 70 nm on the retinal eccentricity of 9°. In the cataract experiencing vision, the color fusion limit $\Delta\lambda_{dc}$ is within a range of about 28 ~ 75 nm on central vision, 30 ~ 76 nm on the retinal eccentricity of 3°, 32 ~ 77 nm on the retinal eccentricity of 6°, and 33 ~ 79 nm on the retinal eccentricity of 9°. On the other hand, compared with the binocular color fusion limit in the normal vision $\Delta\lambda_{dn}$, the binocular color fusion limit in cataract experiencing vision $\Delta\lambda_{dc}$ is approximately 3~39 nm increased on the central vision, 4~22 nm on the retinal eccentricity of 3°, 5~23nm on the retinal eccentricity of 6°, and 5~24 nm on the retinal eccentricity of 9°. The results also reveal that a similar limit is observed in the range of 520~560 nm in both normal and cataract experiencing visions, and the minimum value of the binocular color fusion limit exists at 590 nm either in the normal vision or in the cataract experiencing vision during all retinal eccentricities, which might give some potential evidences for designing 3D equipments.

Recently, advances in brain wave research is remarkable, the function of the nervous system is being elucidated. To give more certification on the fusion limit, we carried out EEG based experiments to find out the relationship between the binocular fusion and

the brainwave rhythm. In EEG based experiments, the fast and middle alpha-variant rhythms on the front of the brain (locations Fp1, Fpz and Fp2) were recorded and analyzed. The EEG-based experimental results show that the middle alpha-variant rhythm is bigger than the fast alpha-variant rhythm when binocular fusion appears, while it becomes smaller when binocular rivalry appears either in normal vision or in experiencing cataract vision. In addition, the values of energy variation diagram of EEG when the binocular color fusion occurs were depicted, which the peaks (i.e. the middle alpha-variant rhythm) were located at 9 Hz ~11 Hz, suggesting that the subject was under relaxation. Furthermore, the difference of the wavelength between two eyes becomes larger, the ratio decreases, suggesting that it is more difficult to view fusional images.

Chapter 1

Introduction

1.1 General research background

Over a century of research has revealed the richness of stereoscopic vision in generating percepts of the three dimensional (3D) form Anderson and Nakayama (1994). Since Wheatstone (1938) invented the stereoscope, it has been known that the different views projected to our two eyes contain information that is used to recover depth. It also has been realized that the two eyes which have slightly different views of the world contribute to the perception of depth. Many of the organisms, including humans, perceive the outside world with both eyes, grasping a two-dimensional retinal image which is captured by each eye as a common single image. This phenomenon is known as binocular fusion which means that similar images presented to the two eyes appear as one and are processed simultaneously rather than successively. Fusion limit (i.e. diplopia threshold) denotes the largest retinal disparity between two images for which the impression of a single fused image can be maintained. It has pronounced influence on the generation of the percepts of 3D because goods are sterically recognized by the deviation of the retinal image generated in the position of the two eyes (i.e. binocular parallax). Recently, the success of the stereoscopic 3D cinema industry has been greatly achieved. As a result, the stereoscopic 3D content services have also been the subject of great interests from a variety of industries, such as the 3D broadcasting producing equipments, and so on. Nevertheless, there still remain many kinds of bottlenecks which might prevent the proliferation of stereoscopic 3D services from going into the mass market. These bottlenecks are the concerns over the visual fatigue and visual discomfort which might be induced from a number of stages. Such inducing scenarios involve the rendering on stereoscopic displays, the stereo shooting and 3D production, the coding and transmission in visual systems, etc (Lambooij et al., 2009).

In contrast, viewing dissimilar images yields perceptual alternations competing for dominance, and this is known as binocular rivalry. Although various techniques have recently received much attention in the broadcast research community as a promising technology for three-dimensional television (3D) systems, the dominant problem associated with binocular vision still was that of explaining how a single unified visual percept is formed from the inputs from two eyes since any optical instrument, especially 3D displays, should be designed to avoid the unpleasant and annoying binocular rivalry.

The binocular asymmetry might be one of the most well-known cautions of visual fatigue and discomfort in stereopsis. It is also well accepted that the perception has become more and more difficult in the events of binocular fusion once the level of asymmetries is larger than a certain limit which is called fusion limit (Hovis, 1989; Howard, 2002). The binocular asymmetries include different kinds of aspects, such as the chromaticity asymmetry, the luminance asymmetry, the structure asymmetry, and so on (Ikeda and Sagawa, 1979). To be specific, the differences in the color of two view fields also can yield rivalry, which is known as “Color Rivalry”. In other words, the color rivalry (i.e., superimposition) is regarded as the non-fused impressions in dichoptic color viewing (Hovis, 1989), and it is a periodic alternation of the image in each eye occurring in either the spatial or temporal domain.

On the other hand, when we view a stereogram whose left and right images are different, but uniform, colors, we perceive a stereoscopic image whose color differs from the color of either image. This property is explained by the theory of binocular color mixing. Then, one of the fundamental problems in understanding the color rivalry process was to measure how much difference of color was permitted before the visual field turns inhomogeneous. Many experiments have already been performed. Since Hering (1864) observed that dichoptic color mixtures were more stable with small stimuli than that with large stimuli, and then after that this had been confirmed by Thomas et al. (1961). Dawson (1917) and Johannsen (1930) reported that the color mixture became more stable as the luminance of the colors decreased. The literature concerning the binocular color mixing had been reviewed by Hovis (1989). Although some qualitative statements had reported previously, quantitative investigations were

firstly carried out by Ikeda and Sagawa (1979) as the great needs to investigate and quantitatively determine the chromatic fusion limit in dichoptic viewing. The importance of the quantitative research results of the fusion limit is reflected in the various real applications, aiming to provide customers with comfortable and relaxing viewing. These applications include the automatic stereo analyzer to guide the content creator for the creation of visually stereoscopic contents, the image safety guidelines for users who view 3D equipments, the automatic content adaption to reduce the level of visual discomfort, and the manufacturing guidelines to produce more and much safer optical instruments (Ujike et al., 2005; Shigeru, 1996; Huynh-Thu et al., 2010; Jung et al., 2011).

There are many previous reports in the literature concerning the quantitative research of fusion limit. Some of the representative researches can be introduced in the following. Ikeda and Sagawa (1979) measured the wavelength difference of binocular color fusion (i.e. $\Delta\lambda$) qualitatively for a 2^{o} field less than 10~100nm depending on the spectral region with wavelength regions from 420 nm to 680nm. They reconfirmed the value of the fusion limit that was determined by the color difference between two eyes. It was verified that the binocular color rivalry would occur whenever mutually opposing color components, such as red and green, which were perceived in respective eyes. Thereafter, Ikeda and his colleagues (Ikeda and Sagawa, 1979; Ikeda and Nakashima, 1980) found out that how $\Delta\lambda$ for each λ changed by varying the luminance and size of the stimuli, and that the binocular color fusion ceased when the color difference introduced between the left and right eyes exceeded a certain threshold value. More recently the conditions for binocular color fusion with non-spectral colors were studied systematically by Qin et al. (2009). The range of binocular color fusion limit was qualitatively measured, suggesting that its value was less than 10~80 nm with the wavelength regions from 450 to 650nm. The limit of binocular color fusion became smaller with the increase of the brightness of the stimulus. They also elucidated that the color fusion occurred more difficultly within the central visual field than that within the peripheral visual field. Thereafter, Jung et al. (2011) reported the quantitative measurement of binocular color fusion limit for non-spectral colors. In their experiment, they performed an experiment

concerning the binocular color fusion limit within the color gamut for non-spectral colors. The results were measured using a conventional 3D Liquid Cristal Display (LCD) by utilizing eight chromaticity points which can generally represent the whole visual area according to the standard CIE chromaticity diagram. Their results were also compared with those reported in the research by Ikeda and Sagawa to find out the consistency of the two results. To reduce the experiments trials which might take very long time to observe all the stimuli, only one single trichromat which might cover all eight chromaticity points was used in the experiment because over 2,000 trials should be recorded and analyzed in a single observation if all the eight points are adopted, and it also might induce visual fatigue including eye strain by the long time observation for the asymmetrical visual stimuli. The color fusion limit was quantified by ellipses in the chromaticity diagram, suggesting that the semi-minor axis of the ellipses ranges from 0.0415 to 0.0923 and the semi-major axis ranges from 0.0640 to 0.1560 (Jung et al., 2011).

All previous studies were based upon the natural color system. Nevertheless, with the problem of the coming acceleration of global population ageing, population ageing in nowadays is unprecedented and pervasive. Therefore, the optical instruments design for binocular vision has become an earnest demand towards the arrival of an aging society. And furthermore, that is necessary to measure how color differences between left and right images of initiate color rivalry by elderly people.

Human visual functions decline with age. Yellowing of the human lens is well-known age-related change of the ocular media. It decreases the transmittance of visible light especially in the short wavelength range (Pokorny et al., 1987; Weale, 1988; van den Berg and Tan, 1994; Xu et al., 1997). It has been found that the elderly showed symptoms of tritan-like defects in the color discrimination (Knoblauch et al., 1987). However, the elderly also have a compensation mechanism for preserving constant color appearance (Werner and Schefrin, 1993; Werner, 1996). Moreover, it has been demonstrated from many researches that the reason of the age-related declines in the visual performance realized in the reduction in the retinal illuminance due to changes in

the ocular media and the loss of efficiency at the neural level (Werner and Steele, 1988; Werner et al., 1990; Hardy et al., 2005; Suzuki et al., 2006).

On the other hand, it is well known that human visual functions decline with age, which the crystalline lens transmission in the visible spectrum decreases with age, and such decrease is greater for short wavelengths. The transmission of visible light decreases, especially for the elderly after the age of 65 years, resulting in that the crystalline color becomes yellower and saturated (Asbell, PA., 2005). Most cataracts are due to age-related changes in the lens. A cataract is a clouding of the clear lens in the eye and is one of the leading causes of vision decline. While cataracts most commonly occur in those who are older, they can develop in younger people as well. Some people are born with a cataract. More than half of all adults over the age of 65 have cataracts in one or both eyes, eventually, everyone gets cataracts. The main cause of visually significant cataracts is ageing, and age-related cataracts are the focus of many seminars.

1.2 Research purpose and organization of the thesis

Previous works concerning the fusion limit of binocular vision are all based on normal visions. Few works are reported upon the cataract vision. Along with the arrival of the aging society, the optical instruments design for elders has become an earnest demand. It is necessary to measure the vision difference that can be permitted before the rivalry occurs for elderly people. In this study, a cataract experiencing goggle is used to provide the vision as close appearance of age-related (senile) cataract as possible. It is well known that human visual functions decline with aging. To be specific, the crystalline lens transmission in the visible spectrum decreases with aging, and such decrease is greater for short wavelengths. The transmission of visible light decreases, especially for the elderly after the age of 70 years old, resulting in that the crystalline color becomes yellower and saturated. More than half of all adults over the age of 65 have cataracts in one or both eyes, eventually, everyone gets cataracts. It is evident that the main cause of visually significant cataracts is ageing, and age-related cataracts are the focus of many seminars.

In this study, we measured the limit of binocular color fusion in the normal vision and the cataract experiencing vision which is used to simulate the elderly vision using a 3D display connected to a computer to present experimental stimuli conveniently. In addition, the brain wave research related to vision is remarkable recently, to give more certification on the fusion limit, we carried out EEG based experiments to find out the relationship between the fusion limit and the brainwave rhythm.

To realize these objectives, we carried out two kinds of experiments. In the first experiment, we analyze the difference between the normal vision and the experiencing cataract vision on binocular color fusion limit. To be specific, the optical instruments design for binocular vision has become an earnest demand towards the arrival of an ageing society. It is necessary to measure how color difference between left and right images by elderly people, which the color rivalry occurs. In this study, we measured the limit of binocular color fusion in the normal vision and the cataract experiencing vision which is aiming to simulate the elderly vision. The result shows that the color fusion limit curves in cataract experiencing vision are very similar with those in normal vision. In the normal vision, the color fusion limit $\Delta\lambda_{dn}$ is within a range of about 11 ~ 65 nm on central vision, 15 ~ 67 nm on the retinal eccentricity of 3°, 21 ~ 69 nm on the retinal eccentricity of 6°, and 25 ~ 70 nm on the retinal eccentricity of 9°. In the cataract experiencing vision, the color fusion limit $\Delta\lambda_{dc}$ is within a range of about 28 ~ 75 nm on central vision, 30 ~ 76 nm on the retinal eccentricity of 3°, 32 ~ 77 nm on the retinal eccentricity of 6°, and 33 ~ 79 nm on the retinal eccentricity of 9°. On the other hand, compared with the binocular color fusion limit in normal vision $\Delta\lambda_{dn}$, the binocular color fusion limit in cataract experiencing vision $\Delta\lambda_{dc}$ is approximately 3~39 nm increased on the central vision, 4~22 nm on the retinal eccentricity of 3°, 5~23 nm on the retinal eccentricity of 6°, and 5~24 nm on the retinal eccentricity of 9°. The results also reveal that a similar limit is observed in the range of 520~560 nm in both normal and cataract experiencing visions, which might give some potential evidences for designing 3D equipment. In addition, the minimum value of the binocular color fusion limit exists at 590 nm either in the normal vision or the cataract experiencing vision during all retinal eccentricities.

In the second experiment, we give empirical and EEG evidences on the fusion limit of binocular vision in the two visions. In details, the relating issues regarding the second experiment can be described in the following. The EEG-based experimental results show that the middle alpha-variant rhythm is bigger than the fast alpha-variant rhythm when binocular fusion appears, while becomes smaller when binocular rivalry appears either in normal vision or in cataract experiencing vision. In addition, the values of energy variation diagram of EEG when the binocular color fusion occurs were depicted, which the peaks (i.e. the middle alpha-variant rhythm) were located at 9 Hz ~11 Hz, suggesting that the subject was under relaxation. Furthermore, the difference of the wavelength between two eyes becomes larger, the ratio of α/ β decreases, suggesting that it is more difficult to view fusional images in the two visions.

This thesis is organized as follows. Chapter 2 describes the visual perception and color vision. Chapter 3 presents the binocular vision. Chapter 4 shows the experimental apparatus. Chapter 5 depicts binocular color fusion limit in experiencing cataract. Chapter 6 introduces the empirical and EGG evidences of binocular color fusion. Finally, Chapter 7 gives conclusion.

Chapter 2

Visual perception and color vision

2.1 Light

Light is a form of energy known as electromagnetic radiation. Electromagnetic radiation originates from the Sun, but can also be produced artificially. Although EM exhibits both wave and particle characteristics, it is most commonly described as waves and characterized by its wavelength (measured in nanometers, nm). At one end of the EM spectrum are the very long radio waves, some of them meters in length. Towards the other end are tiny x-rays and gamma rays, which have wavelengths smaller than a billionth of a metre.

As the diagram below suggests, the part of the electromagnetic spectrum that our eyes can actually detect ("*visible light*") is tiny, less than 1%. It stretches from about 380 nanometres in wavelength (i.e. 0.00000038 metres) up to 780nm in Fig. 2.1 (http://solar-center.stanford.edu/SID/activities/GreenSun.html).

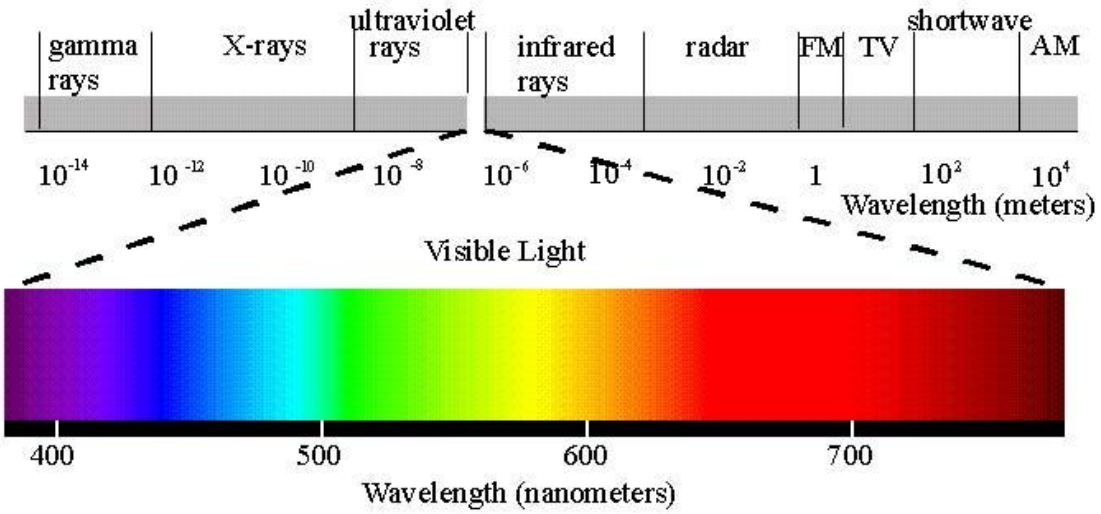

Fig. 2.1. Electromagnetic radiation from the Sun.

2.1.1 Light Sources

Since light is a form of electromagnetic energy, anything that emits, re-emits or conducts energy in sufficient quantities will produce light. Light sources (or 'illuminants') generally produce light in one of three ways:

- Incandescence – where a solid or liquid is hot enough to emit light
- Gas discharge – an electric current is passed through gas, producing light (e.g. a mercury lamp or neon light)
- Photoluminescence – phosphors absorb and then re-emit light, either concurrently or later on

A standard fluorescent tube uses a combination of gas discharge and photoluminescence. It is a phosphor-lined tube containing a mercury lamp. The lamp lights the phosphors, which then re-emit the light we see.

However, light sources can also be characterized by the quality of their light. Two light sources can have the same color temperature but be very different in the composition of waves. One might be made up of a fairly even distribution of wavelengths, while the other might have a very uneven distribution with some wavelengths missing and others spiked up. Although these two sources will give the same overall color cast to a scene the one with the very uneven spectral distribution is likely to strike particular 'colored' objects in odd and unpredictable ways. Some colors may appear washed out, with others overemphasized.

2.1.2 Substance

The second key element in our experience of color is the substance upon which, or through which, light falls. Objects in the world are not really 'colored'- they simply absorb, transmit or reflect particular wavelengths from visible light. If a collection of objects appear to us to be different colors, this is because each object differs in the way it responds under a light source. A 'white' object reflects all or most of the light that

falls upon it, while a ‘black’ object absorbs all or most of the light. Plants appears green because they have pigments which absorb wavelengths from the red and blue parts of the visible spectrum and only allow the ‘green’ wavelengths to be reflected on to a viewer.

This process of absorbing parts of the spectrum not only occurs when light is being reflected off solid surfaces, but also when it is transmitted through substances such as filters – or, indeed, the atmosphere. A bluish camera filter, for example, will absorb many of the longer green and red wavelengths approaching the camera and pass through more of the shorter ‘bluer’ wavelengths. Note that such a blue filter could be used to help correct the red-orange cast in the candlelit scene described above by suppressing the preponderance of red wavelengths within the scene.

In the same way that light sources can appear to produce light of the same color, but actually be emitting very different combinations of light waves, substances can appear to us to be the same color but actually be absorbing and reflecting light waves in quite different ways. This is an important point to grasp. As we’ll see below, most of the “natural” colors we see in the world around us are capable of being simulated by different intensities of just three fairly narrow bands of the spectrum (Red, Green and Blue, RGB, or Cyan, Magenta and Yellow, CMY).

2.1.3 Additive and subtractive color processes

Colors can be created in one of two ways. *Firstly*, certain wavelengths can be subtracted from the full spectrum (by being absorbed by a substance) leaving *the others* to pass into our eyes where they are experienced as particular colors. This is known as the subtractive color process.

An alternative approach to producing color is to project lights that are already limited to particular bands of the spectrum (e.g. red and blue lights) and allow their light-waves to combine to form other colors (in this example, magenta). Because this process adds light-waves, it is known as the additive color process. This is the way color is reproduced on television and computer screens. If you were to put a magnifying glass to

a white area of this monitor, you would see that it is actually composed of tiny dots of red green and blue light. These are small enough so that the light they omit seems to our eyes to be superimposed. When each of these three little colored lights is at full strength, we will think we see white. When they are at varying strengths or intensities, our eyes and brains will interpret the light-waves as other colors.

When reproducing color, it is obviously more efficient and economical to use as few colors as possible. For centuries, philosophers, scientists and particularly artists have sought to identify the 'primary colors' that can be used to mix every other color. Within the additive color process, red, green and blue are the best choice for primaries, this is why lights of these colors are used within monitor displays. Red, green and blue work best because they directly match the way our eyes detect color and light, with their red-, green- and blue-sensitive cones.

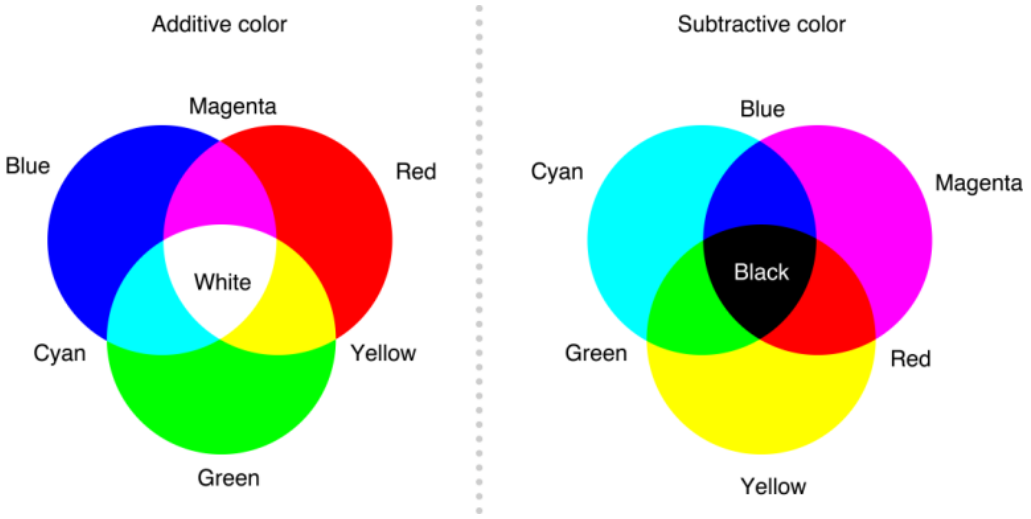

Fig. 2.2. Additive colors (left) and Subtractive colors (right).

However in a subtractive color process, like commercial printing, red green and blue are not the best choice of primary colors, because these colors subtract too much light. Imagine a blue dot on a page, with a red dot printed over the top of it. Light would hit the red dot and almost all of the green and blue light-waves would be absorbed, leaving red waves to pass on. The blue dot would then subtract the red light-waves and any of the remaining green, leaving little, if any, light at all to be reflected off the page. Within

a subtractive system (Fig. 2.2) of color reproduction Red, Green and Blue are incapable of producing the full range of colors we can see. The best choices are Cyan, Magenta and Yellow. This choice is not arbitrary: these colors have a special, 'complimentary,' relationship with red, green and blue.

Subtractive colors (left) as if reflected from a printed page; Additive colors (right) as if projected by colored lights. Illustrates the relationship between the additive primaries (Red, Green, Blue) and subtractive primaries (Cyan, Magenta, Yellow)

Here is how it works. Red, Green and Blue absorb most of the spectrum leaving only one band of wavelengths to transmit or reflect. Cyan, Magenta and Yellow, in contrast, subtract only one band of the spectrum (Red, Green or Blue, respectively) leaving the remaining wavelengths to reflect and mix together. The color we identify as 'Cyan' is actually a mixture of light-waves from the green and blue parts of the spectrum. A dot of cyan ink will subtract the red wavelengths from white light, leaving the green and blue wavelengths to reflect and combine to form the color we call cyan.

2.2 Visual system

2.2.1 Human eye

Vision is a complicated process that requires numerous components of the human eye and brain to work together. The initial step of this fascinating and powerful sense is carried out in the retina of the eye. Specifically, the photoreceptor neurons (called *photoreceptors*) in the retina collect the light and send signals to a network of neurons that then generate electrical impulses that go to the brain. The brain then processes those impulses and gives information about what we are seeing.

The human eyes are an organ of approximately spherical shape. The sphere has a radius of about 12 mm with a transparent protuberance towards the front. In the protective envelope, which preserves the eye's shape, are inserted three pairs of extrinsic muscles that move the eye in its bony orbit (the eye socket), a cone shaped

cavity pointing slightly outward relative to the central plane of the head. A change of the position of the eye caused by a well coordinated contraction and relaxation of the extrinsic muscles. Fixation of the external point is maintained also when the head is moved. The intricate mechanisms of eye movements have been studied extensively, and the interested reader is referred to Doolan et al. (1962); Robinson (1968); Monty and Senders (1976); and Cerrolaza et al. (2012).

Fig. 2.3 (Romany, F.M., 2012) shows the general plan of the human eye with the names of its principal parts. Brief descriptive notes on the optic media (cornea, lens, aqueous humor, and vitreous body) and on the retina are given below. Detailed accounts of the structure of the human eye, as well as of other eyes, are given, for example, by Walls (1942), Smelser (Ed., 1961), Davson (Ed., 1962), and Davson (1972).

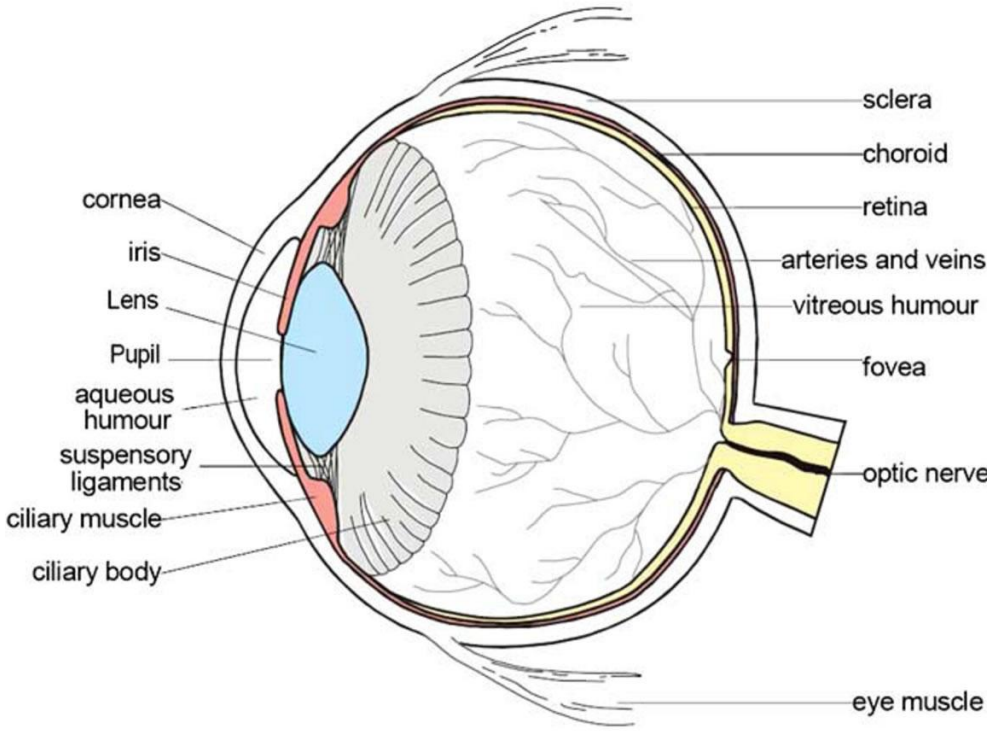

Fig. 2.3. The chematic near horizontal median section of right eye seen from above (Mansour, R.F., 2012).

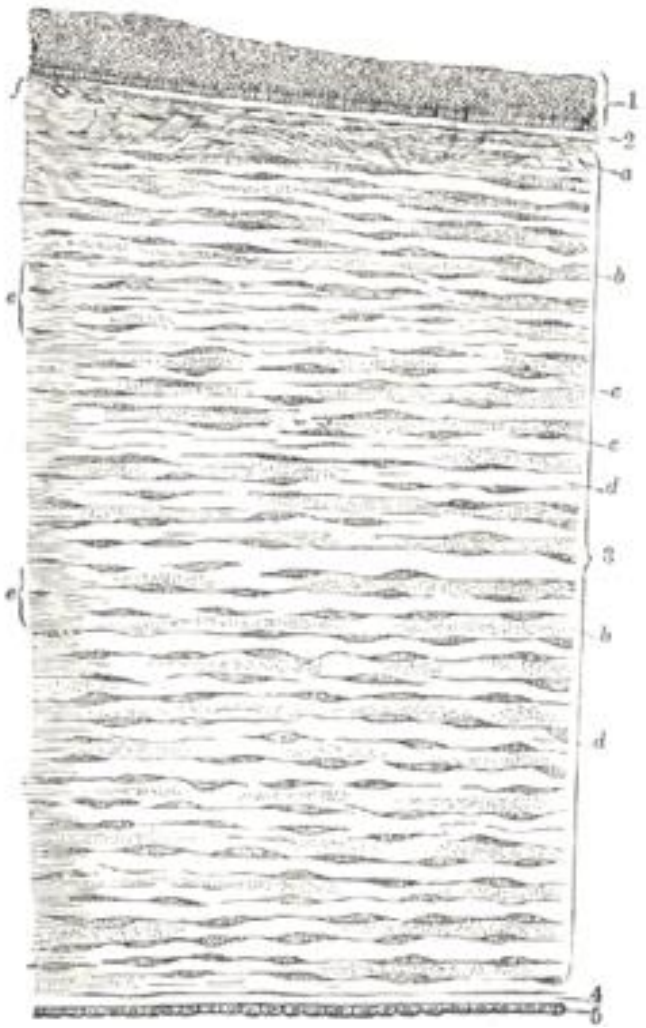

Fig. 2.4. Vertical section of human cornea from near the margin, where (1) Epithelium. (2) Anterior elastic lamina. (3) Substantia propria.(4) Posterior elastic lamina. (5) Endothelium of the anterior chamber (Gray, H., 1918).

Cornea

The cornea is the transparent front part of the eye that covers the iris, pupil, and anterior chamber, providing most of an eye's optical power. Together with the lens, the cornea refracts light and, as a result, helps the eye to focus. The cornea contributes more to the total refraction than the lens does, but, whereas the curvature of the lens can be adjusted to "*tune*" the focus, the curvature of the cornea is fixed. Fig. 2.4 (Gray, H., 1918) shows vertical section of human cornea from near the margin. The cornea has unmyelinated nerve endings sensitive to touch, temperature and chemicals; a touch of

the cornea causes an involuntary reflex to close the eyelid. In humans, the refractive power of the cornea is approximately 43 dioptres, roughly three-fourths of the eye's total refractive power.

Lens

The lens is a *biconvex multilayered structure*, enclosed in a sheath which is connected to the ciliary muscle by means of the zonule fibers. The shape of the lens changes during accommodation, the process that permits bringing the image of an object in the external field to a sharp focus in the fovea of the retina. The change of the shape in the lens during accommodation occurs mostly at its anterior surface which touches the iris. When the eye is focused for an object "*at infinity*", the zonule fibers, attached to the sheath of the lens, exert their maximum pull and hold the lens in a flattened position. In that position, the cornea provides most of the refractions needed to bring the beam of the parallel rays to a sharp focus in the fovea. When the object is nearer, the ciliary muscle contracts to release some of the tension exerted by the zonule fibers, thus allowing the anterior surface of the near object into the fovea from its position behind where it would be otherwise.

Aqueous humor and vitreous body

Between the cornea and the lens lies the anterior chamber of the eye which is filled with a clear liquid, *the aqueous humor*. This liquid, continuously generated and absorbed, controls the intraocular pressure, which is greater than the atmospheric pressure, to maintain the structural integrity of the eye. In health the aqueous humor does not mix with the firm, gel-like vitreous humor because of the lens and its suspensory ligaments between the two. The *aqueous humor* is secreted into the posterior chamber by the ciliary body, specifically the ciliary processes, and flows through the narrow cleft between the front of the lens and the back of the iris, to escape through the pupil into the anterior chamber, and then to drain out of the eye via the trabecular meshwork into the aqueous veins and eventually into the veins of the orbit.

In the space between the lens and the retina, about two thirds of the volume of the eye, is *the vitreous body* which consists of a transparent jelly interlaced with fibers. The solution is *99%* water, but has a gelatinous viscosity two to four times that of water. The remaining solutes include salts, sugars, phagocytes, and a network of collagen fibers. The phagocytic cells are present to remove unwanted debris in the visual field. The primary purpose of the vitreous humor is to provide a cushioned support for the rest of the eye, as well as a clear unobstructed path for light to travel to the retina. The metabolic exchange and equilibration between systemic circulation and vitreous humor is so slow that vitreous humor is sometimes the fluid of choice for postmortem analysis of glucose levels or substances which would be more rapidly diffused, degraded, excreted, or metabolized from the general circulation. A *vitrectomy* is a surgery to remove some or all of the vitreous humor from the eye.

The retina

The retina is a complex and multilayered structure lining most of the choroids, the vascular and pigmented layer attached to the sclera, the protecting envelope of the eye. A schematic cross section of the retina is given in Fig. 2.5 (Klob, H., 1995) which illustrates its structure as revealed through a light microscope. The illustration is taken from Pollack's well known treatise, i.e., The Retina (Polyak, 1941). Poleax's intensive study of the retina of primates covers and extends much of the earlier work. More recent preparations of primate retina, including those from human eyes, have confirmed the main features of the retinal fine structure illustrated in Fig. 2.5.

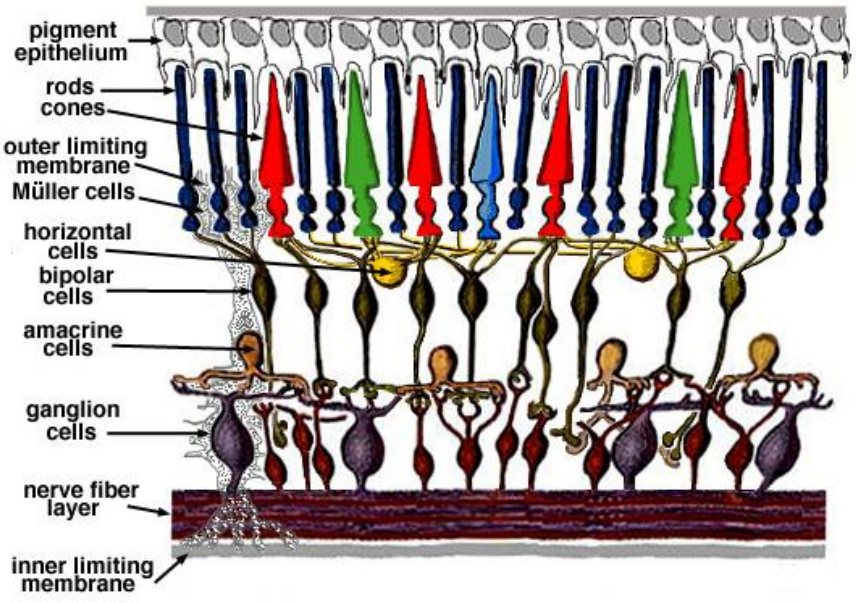

Fig. 2.5. Schematic diagram of the structures of the primate retina (Klob, H., 1995).

In accordance with Fig. 2.5, the following are the main retinal layers containing the different kinds of nerve cells (or neurons) and fibers that can be distinguished by means of light microscope:

1. *Pigment epithelium*. Cells with processes interdigitating to a small degree the outer segments and containing non-photosensitive melanin pigment in which most of the light transverse the retina is finally absorbed.

2. *Rod and cone layer (bacillary layer)*

   - Outer segments of the rods and cones
   - Inner segment

3. *Outer limiting membrane*. Thin sheet made up of fibers of the cells (Muller's fibers) sustaining the framework of the retina.

4. *Outer nuclear layer*. Mainly cell bodies (nuclei) of the rod and cone cells.

5. *Outer plexiform layer*. Inner fibers of the rod and cone cells and their synaptic contacts with outer fiber expansions of cells of layer.

6. *Inner nuclear layer*. Mainly nuclei of various types of bipolar cells and horizontal and amacrine cells.

7. *Inner plexiform layer*. Inner fiber expansions of bipolar cells and dendritic expansions of ganglion cells of all kinds.

8. *Layer of ganglion cells*. The cytoplasmic body of ganglion cell has an axon that becomes a fiber of the optic nerve.

9. *Layer of optic nerve fibers*. Fibers from the ganglion cells proceeding across the retina to leave the eyeball at the optic disk.

10. *Inner limiting membrance*. Thin sheet made up of the inner terminations of Muller's fibers.

The fovea

The fovea, also known as *the fovea centralis*, is a part of the eye, located in the center of the macula region of the retina. The fovea is responsible for sharp central vision, which is necessary in humans for reading, watching television or movies, driving, and any activity where visual detail is of primary importance. The fovea is surrounded by the parafovea belt, and the parafovea outer region: the parafovea is the intermediate belt where the ganglion cell layer is composed of more than five rows of cells; the parafovea is the outermost region where the ganglion cell layer contains two to four rows of cells, and is where visual acuity is below the optimum. This, in turn, is surrounded by a larger peripheral area that delivers information of low resolution.

The fovea in the retina is particular interest as this is the retinal area where vision is most acute. A pit or depression is seen in the retina vitreous surface, the inner limiting membrane. The retinal layer 5 to 9, redrawn as bands are considerably thinner near the center, while at the same time, the retinal layers 2 to 4 are somewhat thicker than in the outer region. The nearly flat central area of the fovea pit, where layers 5 to 9 are almost

absent, is called the fovea. There are no blood vessels in the fovea. It is the high density of cones in the fovea which gives this retinal region its exceptional capacity to resolve fine detail in an optical image focused there. Between 100,000 and 150,000 cones are estimated to be packed in the fovea. The fovea cones have a somewhat different structure than the cones in other retinal regions, and the relative number of pathways from the fovea to the brain is also greater than from other regions. These features are believed to be responsible for the higher sensitivity of the fovea to visual stimuli as compared to that of other retinal regions, when the eye is light adapted.

2.2.2 Mechanism of eye compared to camera

The eye as an optical instrument may be compared to a camera on a tripod (Fig. 2.6, http://www.r-s-c-c.org/node/45). The eyeball is the camera, and a bony socket in the skull, the orbit, is the tripod. The eyeball is moved from side to side and up and down and obliquely by six voluntary muscles. Each of these muscles is attached at one end to the eyeball and at the other to the edge of the orbit. The visual centers of the brain are so trained that these muscles move both eyes together so that synchronous vision is obtained.

The optic nerve passes from the back of the eyeball through a hole in the back of the orbit into the visual center of the brain. This center has many connections with other centers controlling bodily movements, and the close association of the visual and motor centers allows us to direct motions accurately. When vision is lost, when in a dark room, we can still move eyes muscles, but we make the hesitating uncontrolled motions of a blind person.

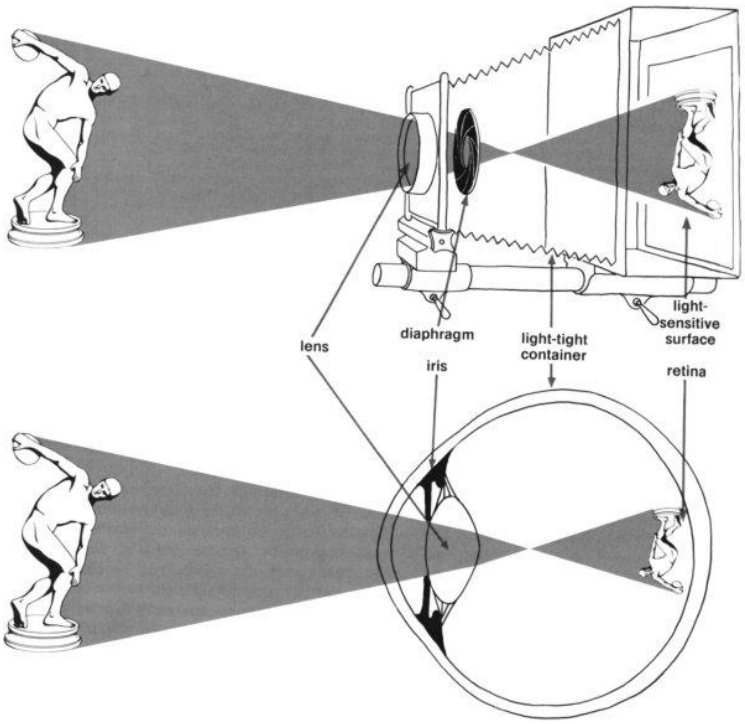

Fig. 2.6 Camera vs. Eye Ball.

2.2.3 The fine structure of the retina

A more recent subdivision of the retina into layers takes account of the functional properties of the neural network (Cao et al., 2015). Between the pigment epithelium and inner limiting membrane, the neurons are segregated into three layers:

- *Layer of photoreceptor cell* (rods and cones) (includes layers of outer and inner segments and layer of photoreceptor cell bodies; that is, the outer nuclear layer).
- *Layer of intermediate neurons* (or inner nuclear layer, containing bipolar cells, horizontal cells and amacrine cells).
- *Layer of ganglion cells*

First synaptic layer (or outer plexiform layer): interconnects the processed of photoreceptor and intermediate neurons.

Second synaptic layer (or inner plexiform layer): interconnects the processes of intermediate neurons and ganglions cells.

Fig. 2.7 (http://ibbiology.wikifoundry.com/page/Label+a+diagram+of+the+structure+of+the+human+eye+and+retina) is a reproduction of the summary diagram assembled by Dowling and Boycott (1966) which, in a highly schematic manner, illustrates the main nerve cells and their interconnections. The subdivision into layers, described above, is also indicated.

The human retina covers an area inside the eye of about 1100 m^2 and its average thickness is about 250 μm, giving it a volume of tissue of about 27.5 m^3. Within this rather small volume are estimated to be about 200 million nerve cells of different kinds that are directly involved with the early stages of the processing of the visual stimulus reaching the retina.

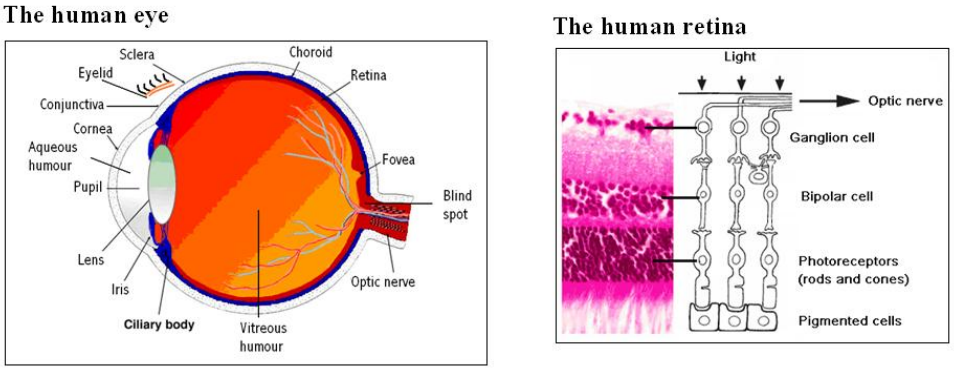

Fig. 2.7. Schematic diagram assembled of ultrafine structure of the primate retina.

A closer inspection suggests an organized hierarchy of signal generation in Fig. 2.7, transmission and coding in the retina and it is interesting to follow the steps that seem to constitute the retinal processes.

Color vision has been thought to be mediated entirely by the cones. However, the "wiring diagram", shown in Fig. 2.7 and discussed above, strongly supports certain other experimental evidence that rods can, under favorable circumstances such as at appropriate levels of stimulation and location in the retina, interact with cones. The

potential interactions are indicated by the existence of *direct contact between rod spherules and cone pedicles, indirect connections between rods and cones through horizontal cells* and *indirect connections between rod bipolars and cone bipolars through amacrine and ganglion cells*.

Main topographical features of the retina

Inspection of the whole surface area of the retina reveals a number of easily identifiable features and major regions. There are the following:

1. *Optic disk, papilla.* The gap in the retina proper, occupied by the optic disk which is not light sensitive and corresponds to the blind spot in the visual field.

2. *Approximate dimensions:* Vertical, 2 to 2.4 mm (7 to 8°); horizontal 1.5 to 1.8 mm (5 to 6°).

3. *Approximate position of center:* 4.8 mm to nasal side of visual pole and 0.47 mm above horizontal meridian (16° temporal and 1.6° below in external field).

4. *Ora serrata.* The abrupt boundary of the retina toward the front of the eye. Vision is impossible for stimuli beyond the ora serrata, but in fact many not reach as far as this.

5. *Fovea.* Small region about the visual pole.

6. *Rod free area.* Small area centered on the visual pole that is blind to weak stimuli in dark adaptation.

7. *Central avascular region.* This area is also centered on the visual pole.

8. *Yellow spot (macula lutea).* A central area extending beyond the fovea in which a yellow pigmentation can be seen in retinal preparations and associated with the Maxwell spot.

9. *Parafovea area.* Retinal region immediately surrounding the fovea.

10. *Peripheral area.* Region between the parafovea and the ora serrata.

Rod cells and cone cells of the retina

A microscopic view of the rod cells of a zebrafish shows us how these cells actually look in an animal. Additional research showed that the rod and cone cells were responsive to light.

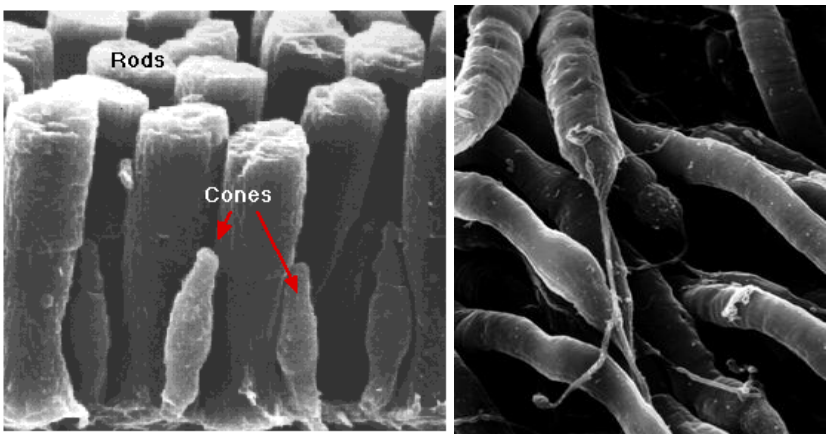

Fig. 2.8. A microscopic view of the rod cells and cone cells.

In the human eye, there are many more rod cells in the retina than there are cone cells (Fig. 2.8, http://users.rcn.com/jkimball.ma.ultranet/BiologyPages/V/Vision.html). The number of rod cells and cone cells in animals is often related to the animal's instincts and habits. For example, birds such as hawks have a significantly higher number of cones than do humans. This let them to see small animals from a long distance away, allowing them to hunt for food. Nocturnal animals, on the other hand, have relatively higher numbers of rod cells to allow them better night vision. A schematic drawing of rod and cone cells is shown in Fig. 2.9 (Wandell, B.A., 1995). The cells are divided into two sections. The bottom portion is called the inner segment. It contains the nucleus and the synaptic ending. The synaptic ending attaches to the neurons which produce signals that go to the brain. The top portion is called the outer segment. The outer segment is comprised of a membrane which is folded into several layers of disks. The disks are comprised of cells that contain the molecules that absorb the light.

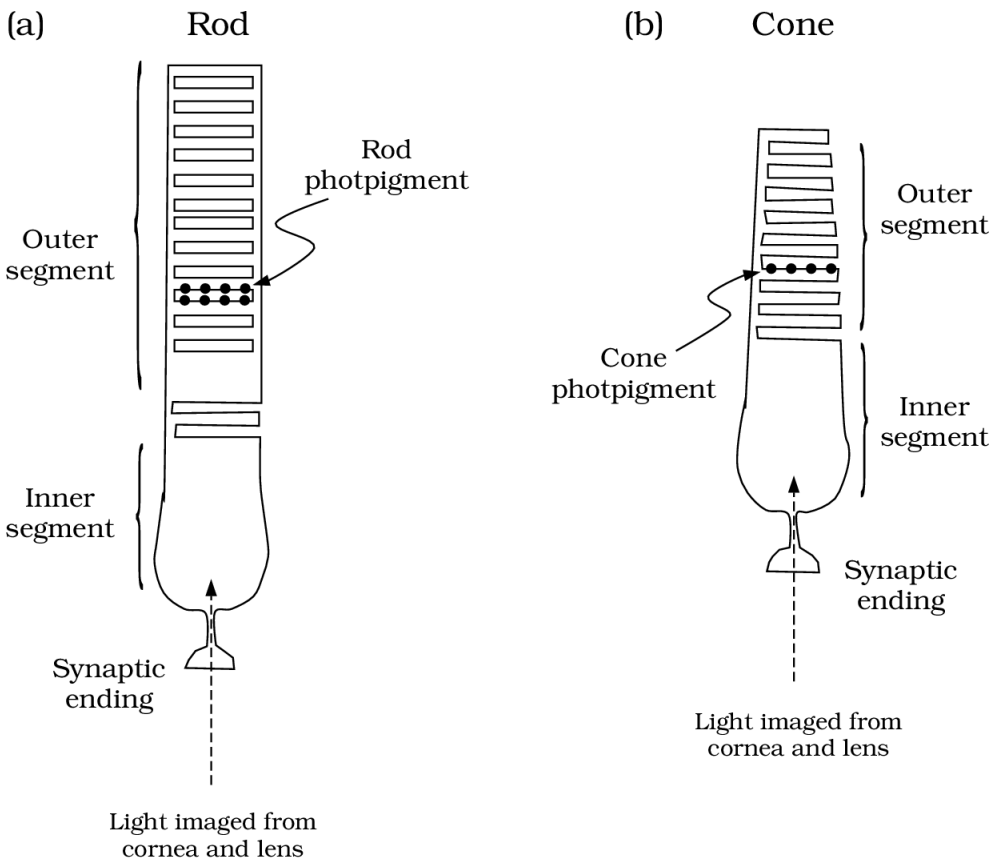

Fig. 2.9. A schematic drawing of rod and cone cells (Wandell, B.A., 1995).

Table. 2.1 Comparison of rod and cone cells.

Rods	**Cones**
used for night vision	used for day vision
very light sensitive; sensitive to scattered light	not very light sensitive; sensitive only to direct light
loss causes night blindness	loss causes legal blindness
low visual acuity	high visual acuity; better spatial resolution
not present in fovea	concentrated in fovea
slow response to light, stimuli added over time	fast response to light, can perceive more rapid changes in stimuli
have more pigment than cones, so can detect lower light levels	have less pigment than rods, require more light to detect images
stacks of membrane-enclosed disks are unattached to cell membrane	disks are attached to outer membrane
20 times more rods than cones in the retina	no reported
one type of photosensitive pigment	three types of photosensitive pigment in humans
confer achromatic vision	confer color vision

2.2.4 The photoreceptors

The photoreceptors are optically inhomogeneous and it is difficult, if not impossible, to assign representative single values for refractive index, absorptance, scattering, and so on to a cone or a rod photoreceptor.

The outer segment of the photoreceptor is of special interest because it is generally accepted that this is the part of the photoreceptor wherein the interaction of visual pigment occurs and light that initiates the visual process. In the outer segment of the rod, the laminations have the shape of double membrane disks that are not connected with the outer membrane and seem to float within it. An exception to this arrangement occurs at the lower end of the outer segment where the discs are actually infoldings or ingrowths or the outer membranes. In time, these infoldings are pinched off the outer membrane and new disks are thus generated. The replenishing process causes the stack of disks to move upwards gradually. It has been estimated that stack moves at a rate of about 10 μm per day. The disks pushed off the top are absorbed in the pigment epithelium, into which the upper portion of the outer segment protrudes (Young, 1976).

The visual pigments that have been extracted from primate retina as well as from retina of many other species are combinations of the chromophores, 11-cis retina l1, or 11-cis retina l2, and various proteins called opsins. It is interesting to note that the visual pigments extracted so far from primate retina all come from the outer segments of rod photoreceptors. No extractions of cone pigments have been reported. However, physical techniques of measurement, such as microspectrophotometry, show that three types of cone pigment must exist with absorptance maxima in the short, middle, and long wavelength region, respectively. The three types of cone pigment reside in different cones.

2.2.5 Retinal circuitry and lateral inhibition

Although there are some 120 million rods and 6 million cone cells in the retina, there are less than a million optic nerve fibers which connect them to the brain. This means

that there cannot be a single one-to-one connection between the photoreceptors and the nerve fibers. The number of receptors connecting to each fiber is location dependent. In the outer part of the retina, as many as 600 rods are connected to each nerve fiber, while in the fovea there is an almost one-to-one connection between cones and fibers. In addition to the rods and cones there are a number of other cell types whose function is to gather and process the information produced by the photoreceptors. The ganglion cells serve as terminators for the nerve fibers connecting to the brain. Between them and the photoreceptors are three other types of cells: bipolar, amacrine and horizontal cells.

Fig. 2.10 (http://www.catalase.com/retina.htm) shows the arrangement of these cells in the retina. Notice that the arrangement is counter intuitive, with light passing through the connecting "circuitry" before falling on the light sensitive receptors. The complexity of the connections in Fig. 2.10 indicates the retina is capable of some quite complex signal processing operations.

Fig. 2.11 (Jacobson, M., 1993) shows the effects of very simple model for lateral inhibition. Parts (a) and (b) of the figure show the sensory system operating without the effects of inhibition. In part (a) a uniform stimulation is applied to an array of sensors. The result is a constant level of output from the sensors. In part (b), the level of stimulation is decreased over the rightmost sensors. This has a direct on the output from the sensors. Part (c) of the figure shows the effect when inhibition is introduced to the system. As well as outputting its signal, each sensor has an inhibitory effect on its two neighbors. The resulting sensor output is quite similar to (b), but at the boundary between the two levels of excitation, the difference in the output is accentuated. In image processing, treating signals in this way is known as edge enhancement.

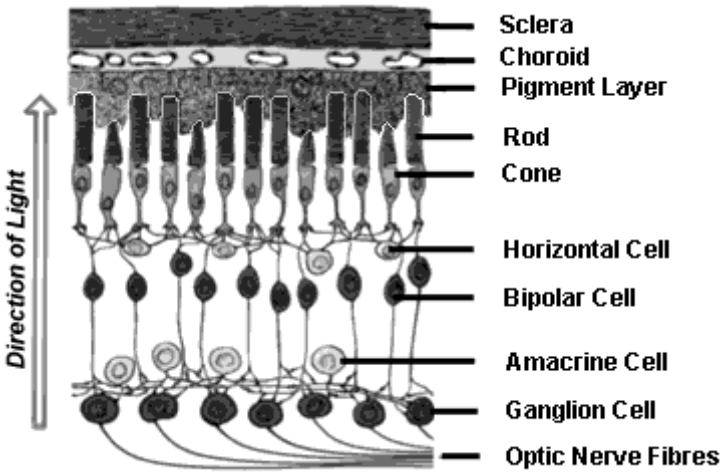

Fig. 2.10. The arrangement of cells in the retina.

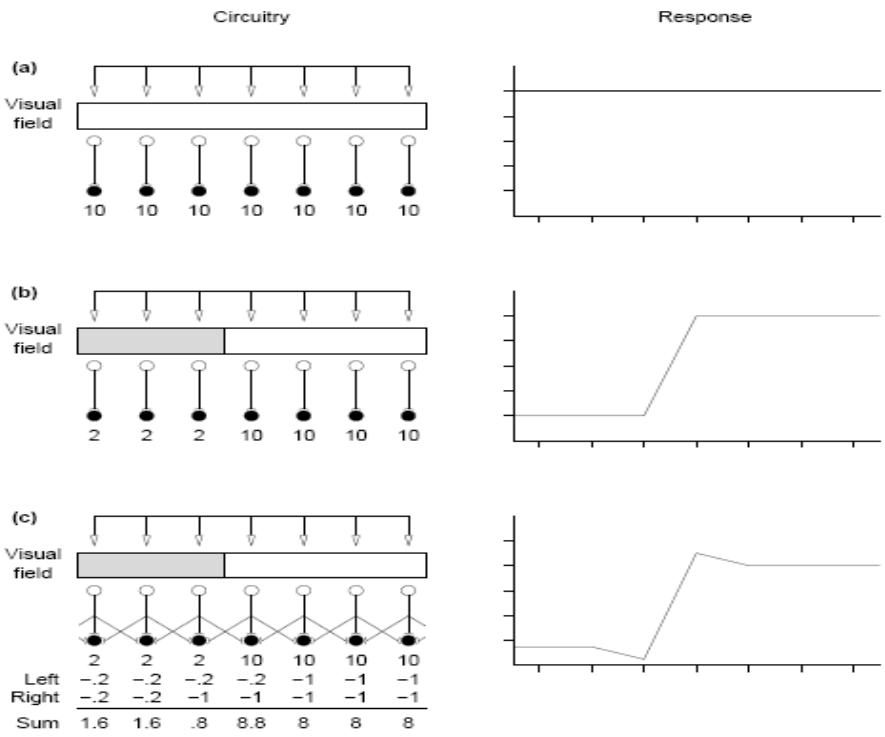

Fig. 2.11. The effects of lateral inhibition (Jacobson, M., 1993).

2.2.6 Visual processing in the brain

Fig. 2.12 (Emery, S.E., 2015) shows the general structure of the visual system. The signals produced in the retina are propagated backward through the head along the optic fiber tract, which is linked via the lateral geniculate nucleus to the visual cortex. The signals from the right side of each eye are propagated to the right side of the brain and those from the left side of each eye to the left side of the brain. The images on the retina are reversed so that the right part of the brain processes the left part of the visual field and vice versa.

From the optic chiasm the optical fibers terminate in the lateral geniculate bodies. From these, optic radiations extend into the primary areas of the visual cortex. These in turn are connected to secondary visual association areas, and from there to the general interpretive area of the brain.

The six layers of the lateral geniculate nucleus are divided equally between information supplied from each retina and therefore provide the first stages of stereoscopic vision. The cell arrangements each lateral geniculate nucleus are similar to those of the ganglion cells of the retina, but far more are devoted to contrast and movement, and fewer to luminosity. Similarly he paired responses for red-green and yellow-blue are also found in the lateral geniculate nucleus, suggesting that its main function is to carry out further processing of incoming signals.

The cells of the visual cortex also have a spatial relationship with the ganglion receptive fields of the eyes. About 50% they are devoted to the macula, with the fields from the other retinal areas being represented in their correct spatial relationship. The visual association areas of the brain appear to deal with more complex processing of the visual signal. In particular they appear to handle the processing of complex shapes and arrangements. Some evidence for this has been derived from people with brain damage in these areas, whose ability to identify or recognize shapes has been destroyed or severely impaired.

Although the lateral geniculate nucleus appears to concentrate on the contrast at edges and the discrimination of form, the primary visual cortex carries the process of form analysis even further. It appears that the cortex has columns of cells, extending through six layers, and particular directions. Some of these arrangements appear to be devoted to recognizing lines or bars or particular lengths and at particular orientations. The overall impression gained of how the brain processes visual information is as a series of steps, each taking the output of the previous steps and building up progressively more complex and abstract "impressions" of the input.

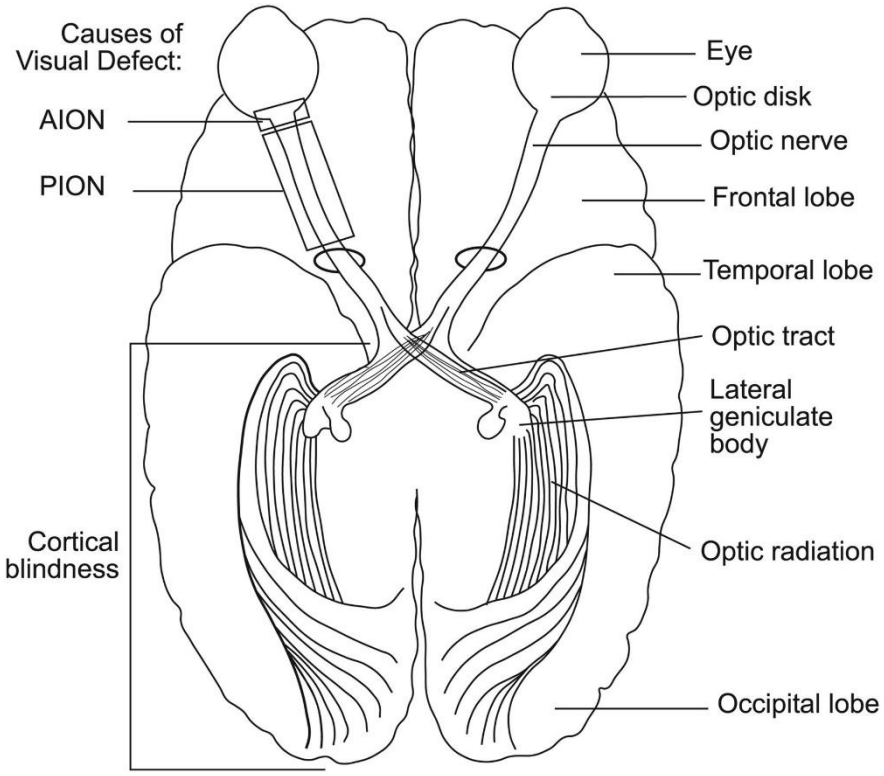

Fig. 2.12. The human visual system (Emery, S.E., 2015).

2.2.7 Human perception

The third key element in our experience of color is the human visual system (Fig. 2.13, Fuensanta, A.V.D., and Doble, N, 2012). Vision is a very personal, subjective experience, but the basic mechanics are the same for most of us. Light enters our eyes through the lens at the front of the eye and is focused onto the retina inside the back of

the eye. The retina is covered with millions of light sensitive cells which pass on signals to the brain via the optic nerve.

There are two types of light sensitive cells in the retina, called *rods* and *cones* because of their shape. Each eye has about 120 million rods, which tend to be concentrated more around the outer edges of the retina. Rods are not sensitive to color differences, but record information about lightness and darkness. They are good for detecting motion and for seeing in low light-levels.

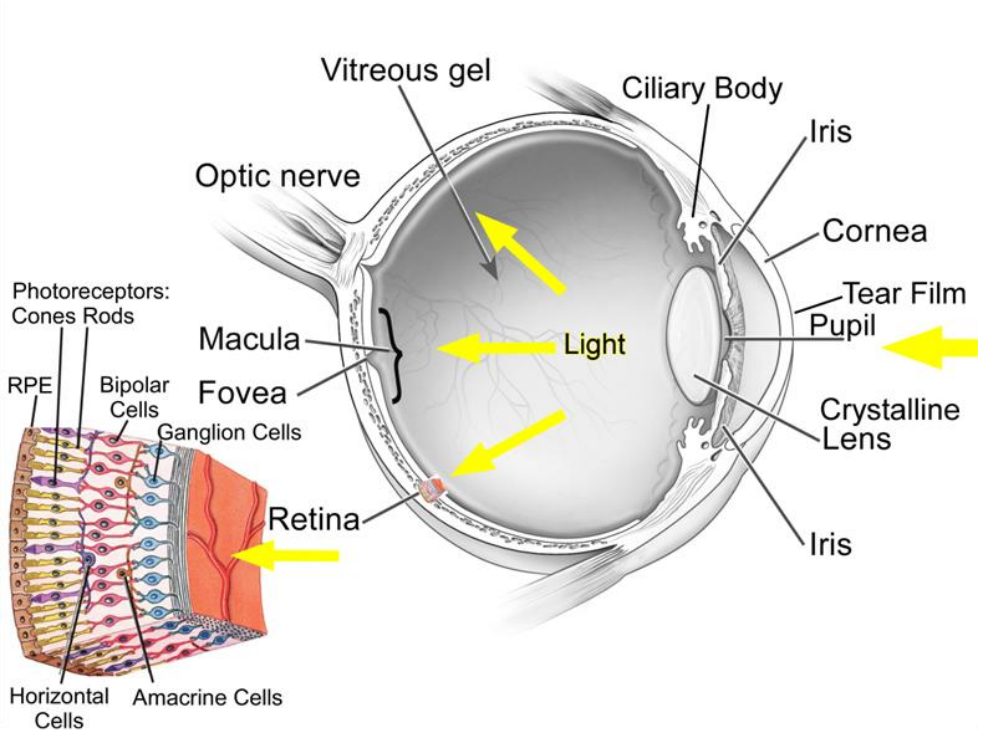

Fig. 2.13. The process of human perception (Fuensanta, A.V.D., and Doble, N., 2012).

The 6 million cones in each eyeball are sensitive to color rather than lightness and are concentrated towards the centre of the retina where there is more light. In humans there are three main sorts of cone, which respond to either long, medium or short wavelengths. They're usually called *red, green or blue cones* because these are the predominant colors within each band. However, the spectral bands they detect are actually quite wide and overlap each other. The way the information from the cones combines to provide our experience of color is still not entirely understood, but it seems most likely that the

outputs from all three cones are used to determine the color and quality of the light by comparing the responses from the different cones.

As we'll see below, a '*trichromatic*' model of color perception was developed in the nineteenth century. This argued that the eye must have three different types of receptors for color: each sensitive to red, green or blue; each combining to represent different colors. An alternative nineteenth-century theory, the 'opponent' model, argued that there were three very different sorts of receptors. These determined whether the color was: black or white; red or green; or yellow or blue. Twentieth-century science has offered some support to both theories. Studies of the eye have found that there are indeed three different cones that react to '*red*', '*green*', and '*blue*' wavelengths, while studies of human perception – such as our experience of contrasting colors and afterimages - and from color deficiencies, like color blindness, have suggested that there are red-green and blue-yellow oppositions involved in our perception of color.

The most popular theory today, the 'opponent-process' theory, brings together both of the earlier theories. It suggests that the *red-green-blue* information recorded by the three cones is further processed within the retina to produce three different "channels" of information which are communicated, electrochemically, to the brain: *red-green*; *yellow-blue*; and *white-black.* According to this theory, information received from the red cones and green cones is compared to determine the blackness or whiteness of the light; information from the red and blue cones is compared with information from the green channel to determine its 'redness' or 'greenness'; and information from the blue cones is put against information from the green and red cones to determine its 'blueness' or 'yellowness'.

2.3 Cataract vision

Human visual functions decline with age. Yellowing of the human lens is well-known age-related change of the ocular media. It decreases the transmittance of visible light especially in the short wavelength range (Pokorny et al., 1987; Weale, 1988; van den Berg and Tan, 1994; Xu et al., 1997). It has been found that the elderly showed symptoms of tritan-like defects in the color discrimination (Knoblauch et al., 1987). However, the elderly also have a compensation mechanism for preserving constant color appearance (Werner and Schefrin, 1993; Werner, 1996). Moreover, it has been demonstrated from many researches that the reason of the age-related declines in the visual performance realized in the reduction in the retinal illuminance due to changes in the ocular media and the loss of efficiency at the neural level (Werner and Steele, 1988; Werner et al., 1990; Hardy et al., 2005; Suzuki et al., 2006).

Cataracts occur when there is a buildup of protein in the lens that makes it cloudy. This prevents light from passing clearly through the lens, causing some loss of vision. Since new lens cells form on the outside of the lens, all the older cells are compacted into the center of the lens resulting in the cataract. On the other hand, it is well known that all most human visual functions decline with age, which the crystalline lens transmission in the visible spectrum decreases with age, and such decrease is greater for short wavelengths. The transmission of visible light decreases, especially for the elderly after the age of 65 years, resulting in that the crystalline color becomes yellower and saturated. Most cataracts are due to age-related changes in the lens. A cataract is a clouding of the clear lens in the eye and is one of the leading causes of vision decline. While cataracts most commonly occur in those who are older, they can develop in younger people as well. Some people are born with a cataract. More than half of all adults over the age of 65 have cataracts in one or both eyes, eventually, everyone gets cataracts. The main cause of visually significant cataracts is ageing, and age-related cataracts are the focus of many seminars.

2.4 Color theory

2.4.1 CIE

We said earlier that seemingly identical light sources or colors can actually be composed of very different distributions of wavelengths. As we suggested, the reason we are so easily fooled by this is that the human visual system (eye plus brain) is doing its color interpretation based on just three sensors (red, green, blue). But in order to accurately control and reproduce color within an additive (or subtractive) color system, we must know exactly what combination of primaries is required to match and simulate each real-world color. This is the challenge that science of Colorimetry has set itself: to determine and map out these combinations. Each combination of red, green and blue is known as the tristimulus values for the corresponding real-world color.

The characteristics of the original, real-world color can be measured objectively using instruments to detect the wavelengths they reflect (the results are referred to as the spectral power distribution for that color). But since the tristimulus (red, green, blue) equivalents depend on human perception, they must be measured using human observers rather than instruments.

In 1931 the *International Commission on Illumination* (CIE) undertook the huge task of matching real-world colors with their tristimulus equivalents. In an approach reminiscent of Maxwell, J. and Munsell, A.H. with their spinning tops, they put each test color alongside another color created by mixing red, green and blue lights. The strengths of the red, green and blue lights were adjusted until the human observer considered the two colors were a perfect match. Lots of human observers were involved and the results were averaged and published by the CIE as the '*Standard Observer*'. In 1931 the observers were viewing the colors through small slits which gave them a 2 percent field of vision. This was later judged too limiting and the experiment was repeated in 1956 with 10 percent vision allowed and a wider selection of subjects with a more diverse ethnic background.

CIE 1931 chromaticity diagram

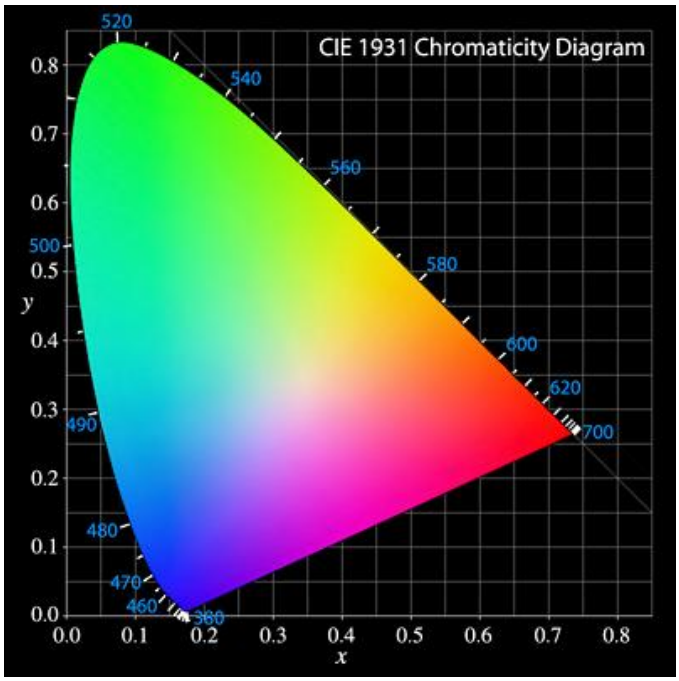

Fig. 2.14. CIE 1931 Chromaticity Diagram.

The chromaticity coordinates (Fig. 2.14) are normally specified by the x and y axis only. In general, most specifications provided by LED manufacturers do not list the chromaticity coordinates, but rather the peak and dominant wavelength (unless the LED is white). The dominant wavelength, specified in nanometers, is obtained from the color coordinates discussed above. It is essentially the color that is actually perceived by the human eye.

The peak wavelength is the wavelength at the maximum spectral intensity. The peak value is easy to obtain and is therefore the most common value specified by LED manufacturers, however, it has little practical significance for applications that are viewed with the human eye since two LEDs may have the same peak wavelength but can be perceived as different colors.

Color system and terminology

It is called color specification to display a color quantitatively, and the numerical value for a display is called a color specification value. Moreover, the system which

consists of a series of regulations and definitions for color specification is called color system. Here, it explains classification of the color system and terminology for the display.

There are a color appearance system and a color mixing system in color system. The color appearance system is based on the color appearance of the standard (for example, color chart) color for an object. Moreover, the color mixing system is based on the amount of mixtures of a light required to consider as a certain color which also stopped the color mixing experiment of light, and color matching.

The color in a color appearance system is visible and it is called color perception based on psychological impression. Moreover, although the target color is called a perceived color, generally a perceived color contains perceived, such as a situation texture, a sense of distance, and around surface. There are object color, light source color, aperture color, etc. as perceived color by the object. The object color may be distinguished in the surface color which is a perceived color belong to the object and reflects light, and the transmitted color which transmitted light. Moreover, the light source color is a color of the light which comes out of the light source. It is aperture color, for example, what it is the color which is seen from a small aperture at the time of blue sky, and the object which emits light is the color which is not known.

Now, in a color appearance system, it considers having a certain order and classifying the color chart from which 1000 sorts of chip boxes differ. First, this is called hue although it can classify according to the kind of colors, such as red, green, and blue, etc. Next, there is bright red, and the color chart of a certain hue (for example, red) also has dark red, and these color tables can be classified according to the lightness which is relative light-and-darkness feeling. The hue, lightness, and saturation which show the feature of the color of a color chart are called three attributes of a color. Although the color specification value in a color appearance system is called a color appearance value, what assigned a series of suitable numerical values for these three attributes as a color appearance value can be used. There is a Munsell color system using the color chart as a typical thing of this color specification system.

2.4.2 Color vision model

Trichromatic theory

In 1802, Young (Young, 1802) proposed trichromatic theory and it explains "Three kinds of receptors (cone) felt red, green and blue exist in retina, and the property of all colors is shown by the rate of the amount of responses of these cones". Helmholtz (Haldenwang et al., 1984) made quantification after that in 1894, he said *"Three kinds of receptors (cone) felt red, green and blue exist in retina, and the property of all colors is shown by the rate of the amount of responses of these cones*".

Trichromatic theories the numbers of receptors 3 are few, being simple to know. Fig. 2.15 (Judd and Wyszecki, 1975) shows the spectral radiant power of red, green, and blue receptor in a three-primary-colors theory. Trichromatic theory is based on the experiment which are red, green and blue suitable mixture and by which a color is reproduced mostly altogether, and was not drawn theoretically. However, since color television, a photograph, printing, etc. are altogether developed based on a trichromatic theory and the color reappearance from it can fully be satisfied, the trichromatic theory has been considered to be a very realistic and leading hypothesis.

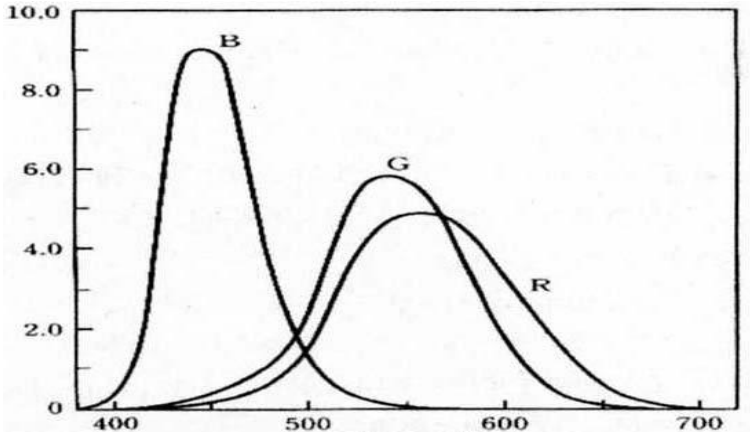

Fig. 2.15. Spectral sensitivity of the R, G, and B receptors in a trichromatic theory (Judd and Wyszecki, 1975).

Opponent color theory

On the other hand, in 1878 Hering (Hering, 1878) proposed the hypothesis “Three sorts of receptors which answer red-green, green-blue, and white-black existed in a retina, and the property of all colors was shown by the rate of the amount of responses of these receptors”. Although this has the red of the yellowish , but there is no red of the greenish, and green and red are based on the experiential experiment considered to be a opponent color, and it call opponent color theory. Although Fig. 2.16 (Judd and Wyszecki, 1975) shows the spectral radiant power of presumed opponent color receptor, a specific meaning does not have positive and the negative one of the values, for example, it means that red and green are opponent colors. Since red, green, yellow, and blue are four sorts considered as a fundamental color in a reflection theory, its call tetra chromatic theory.

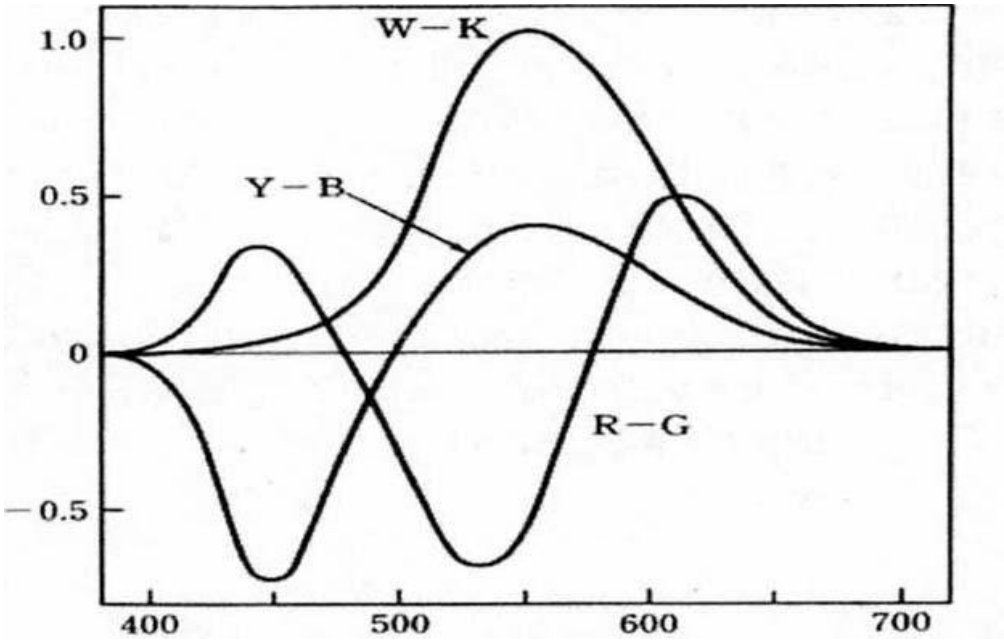

Fig. 2.16. Sensitivity of R-G, Y-B, and W-K receptors in opponent-color theory (Judd and Wyszecki, 1975).

Chapter 3

Binocular vision

3.1 Binocular vision and stereopsis

Binocular vision is a type of visual system common in many of the organisms where both eyes produce only a single image in the brain, including humans. It may be contrasted with monocular vision, which perceive the outside world with both eyes, grasping a two-dimensional retinal image which is captured by each eye as a common single image

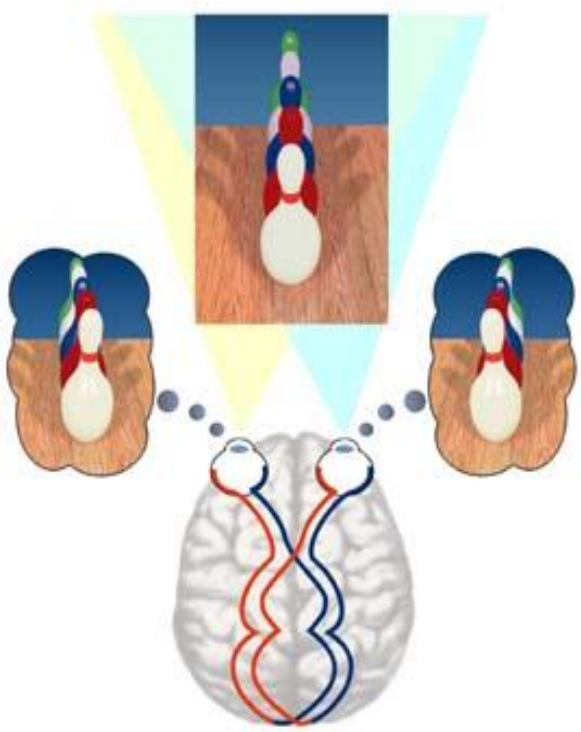

Fig. 3.1 A sample of binocular vision.

In binocular vision, the eyes are forward-facing and could not move independently of each other. Each eye thus has a slightly different perspective on a scene. This allows

the visual cortex of the brain to synthesize the two differing images into one cohesive mental image. These differences in perspective allow the brain to triangulate distance much more accurately, and thus resulting in vastly improved depth perception.

3.2 Binocular disparity

Binocular disparity is the general term that refers to the differences between retinal images created by viewing the world from two slightly different positions or vantage points. These differences can be specified and measured with respect to either the optic arrays subtended at the two vantage points or images projected on retinas or camera planes. The metric properties of an image produced by a given optical array depend on the shape of the projection surface and its position with respect to the vantage point. The nature and extent of binocular disparities also depend on the coordinate system used for measuring the images. It is important to distinguish between disparities due to viewing the world from two vantage points and those due to the coordinate system. The former disparities provide a basis for the computational theory of binocular stereopsis, which identifies the nature of information about structure and layout of the visual world. To evaluate mechanisms used for extracting this information in a visual system we must consider projection surfaces, coordinate systems, image properties, as well as the computational theory.

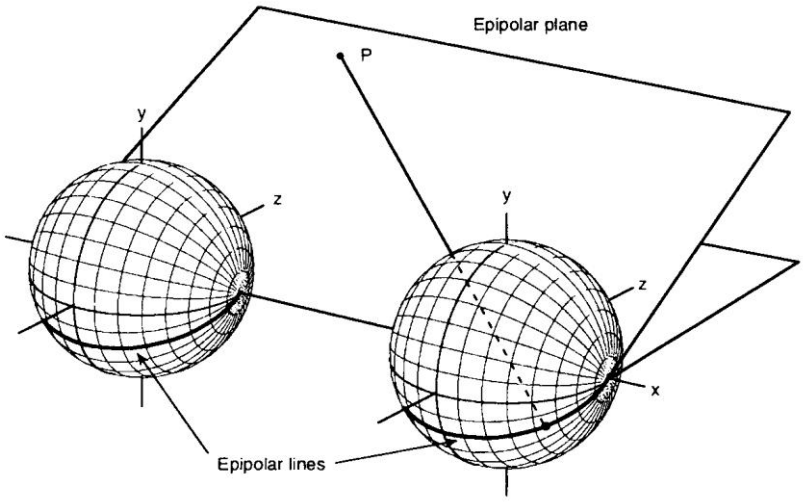

Fig. 3.2 Epipohr planes and epipolar lines (Howard, I.P., 1995).

The schematic diagram of the epipohr planes and epipolar lines are shown in Fig. 3.2. An epipolar plane passes through a point P in the visual scene and the optical centres of the two eyes. Once the visual direction of the point is established in one eye (right eye), the only possible location of the corresponding point in the other eye is along an epipolar line, which is the projection of the epipolar plane.

3.2.1 Binocular coordinate systems

To discuss the concept of binocular disparity, we need to consider how the direction of a point in space can be measured with respect to a pair of coordinate systems, which are respect to a pair of coordinate systems and separated horizontally, but not necessarily aligned with respect to each other.

(a) Aligned coordinate axes

A binocular difference in the azimuth of a point is a measurement of its absolute horizontal disparity, and a difference in its elevation is a measurement of its absolute vertical disparity.

$$Absolute\ horizontal\ disparity = \alpha_L - \alpha_R \quad (1)$$

$$Absolute\ vertical\ disparity = \beta_L - \beta_R \quad (2)$$

The information provided by the azimuth and elevation of a single point with binocular viewing is available only if (1) the coordinate frames in the two eyes or cameras are fixed and aligned, or (2) there is additional information about the precise positions of the eyes or cameras, if they are free to move. Under these circumstances, the absolute distance to a point is specified by the elevation and azimuth values, whatever coordinate system is used for measuring those values.

(b) Independent coordinate axes

Although the absolute position of a point and its distance from the observer can not be determined without knowledge of eye position, absolute disparities do provide some information about the position of the point with respect to where the eyes or cameras are

"*looking*". As long as the optic axes of the eyes or cameras intersect in a forward direction, the magnitude and sign of the absolute horizontal disparity of a single point provide information about the location of the point with respect to the Vieth-Müller circle, even if the "fixation point" is not visible. If the optic axes of the eyes or cameras do not intersect, the absolute horizontal disparity of a point can not provide the reliable information.

(c) Binocular disparity detectors

The preceding discussion is related to the physiological finding, in which some binocularly driven cells in the primate visual system have receptive fields in either the same or slightly different equivalent positions in the two retinas. These cells can be regarded as absolute disparity detectors, which are capable of specifying the disparity of a point with respect to the visual axes of the two eyes. As we have seen, absolute disparities provide information about the location of a point with respect to the Vieth-Müller circle passing through the convergence point.

(d) Shape of the retina

There are two basic types of retina or camera plane, *flat* and *spherical*. Flat retinas should remain coplanar and vergence, also should involve a horizontal, vertical, or rotary motion of the retinas, each within the flat image plane. The lens of each eye should be fixed so that each retina moves with respect to a stationary image, and the stereobase remains constant. It is usual to achieve convergence in binocular video cameras by rotating each camera like an eye. But this is not a true convergence, since each camera plane does not move within the image plane and therefore the movement changes the perspective in the image. Spherical retinas should converge by rotation about the nodal point of each eye, which is approximately what our own eyes do.

3.2.2 The concept of disparity

The vertical plane projecting to the fixation point in each eye is a plane from which the azimuth angle in that eye is measured. The relative horizontal disparity, or simply

the horizontal disparity of a pair of points, is defined as the difference between the absolute horizontal disparities of the two points:

$$Horizontal\ disparity = (\alpha 1_L - \alpha 1_R) - (\alpha 2_L - \alpha 2_R) \quad (3)$$

Alternatively, owing to the mathematically equivalent, the horizontal disparity can be expressed as the binocular difference in the horizontal separation of the points measured separately for each eye. This involves rearranging the terms in equation (3):

$$Width\ disparity = (\alpha 1_L - \alpha 2_R) - (\alpha 1_L - \alpha 2_R) \quad (4)$$

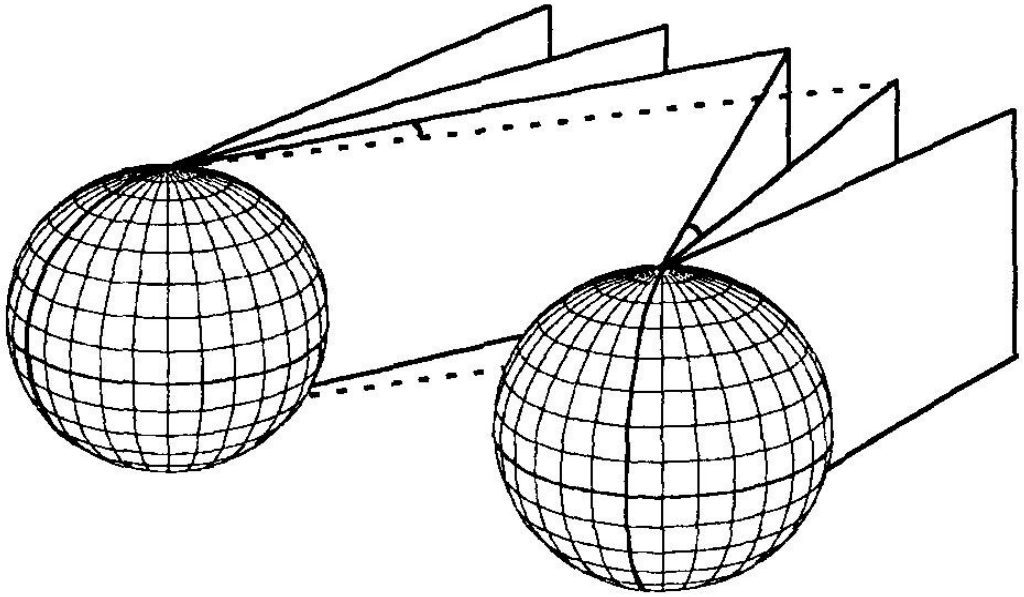

Fig. 3.3 Azimuth planes (Howard, I.P., 1995).

Equation (4) represents a difference in angular width-a horizontal width disparity (or horizontal dif-size disparity). It corresponds to the binocular difference of the separate angles between the azimuth planes containing the two points in each eye. The relative vertical disparity, or simply the vertical disparity of a pair of points, can be defined similarly as the difference in the absolute vertical disparities of the two points:

$$Vertical\ disparity = (\beta 1_L - \beta 1_R) - (\beta 2_L - \beta 2_R) \quad (5)$$

As for horizontal disparity, vertical disparity can also be expressed as the binocular difference in the vertical separation between the points measured separately in each eye.

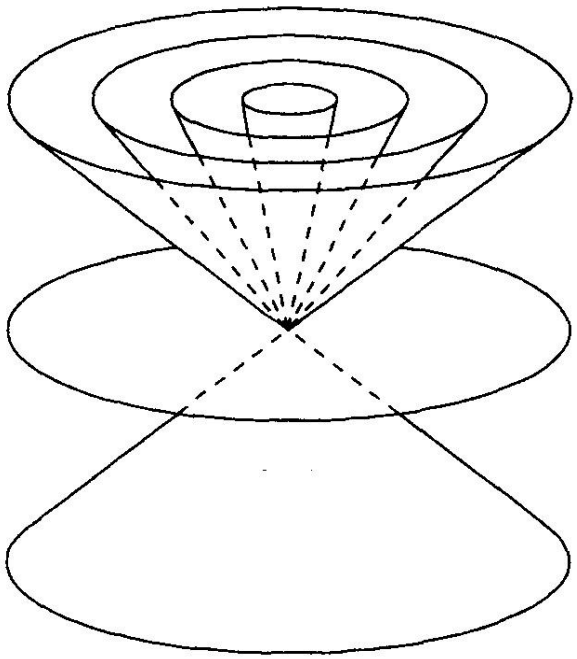

Fig. 3.4 Elevation cones (Howard, I.P., 1995).

$$Height\ disparity = (\beta 1_L - \beta 2_R) - (\beta 1_L - \beta 2_R) \quad (6)$$

The vertical height disparity (or vertical dif-size disparity) represented by equation (6) makes it clear that only the angular separation has to be measured (separately in the two eyes), rather than the absolute directions of the image points in the two eyes. In a gun-turret system, this means that the points must lie in the same vertical azimuth plane that passes through the optic centre in that eye and is orthogonal to the plane of regard (Fig 3.4). A line joining a pair of points is horizontal if the points have the same elevation. Elevation is measured within the vertical plane passing through the point, so that points are horizontal if they lie on the same cone rotated around the y-axis (Fig 3.5). Although this is not the only way to define vertical and horizontal, the gun turret system has the advantage that (1) measurements of height (elevation) and width (azimuth) differences between points and (2) what is regarded as vertical or horizontal are unaffected by changes of gaze or vergence (horizontal eye movements) within the plane

of regard. A corollary of this last statement is that the horizontal width disparities and the vertical height disparities of a pair of points typically will have different values if the eyes are elevated to a new plane of regard.

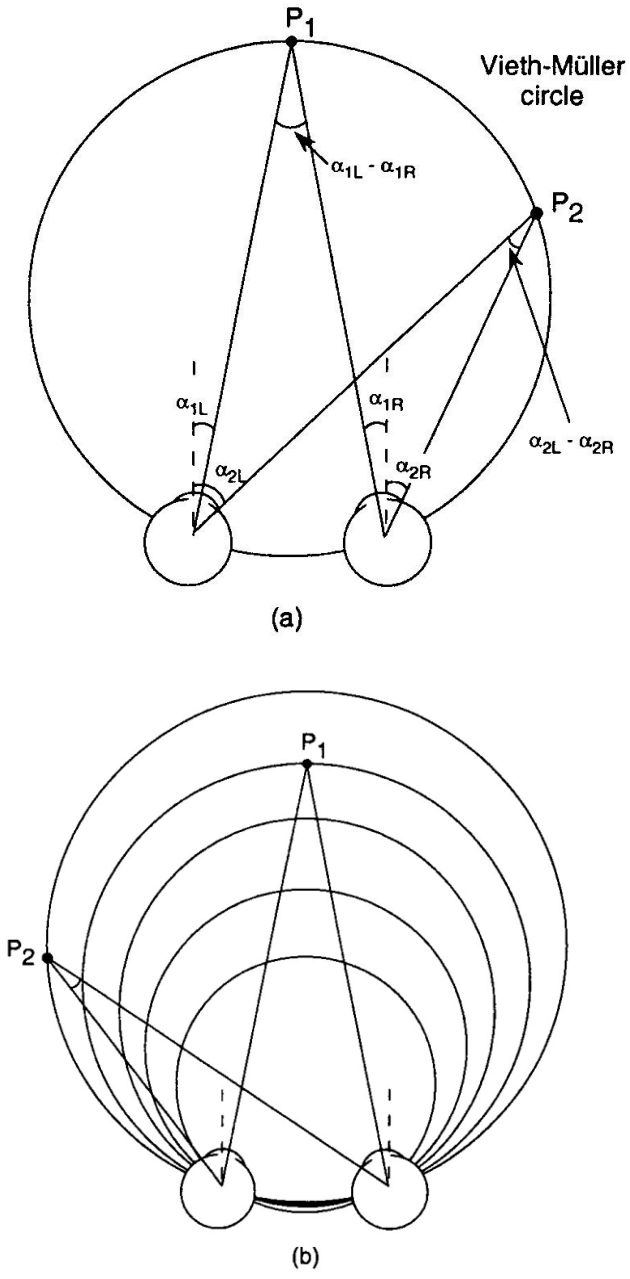

Fig. 3.5 The Vieth-Müller and isodisparity circles (Howard, I.P., 1995).

3.3 Binocular rivalry

A fundamental question in the fields of vision is psychology. The neuroscience is how the brain selects one of many competing visual signals for access to consciousness. When different monocular patterns are simultaneously presented to the two eyes, they rival for perceptual dominance. Only one monocular image is perceived at a time while the other is temporarily suppressed from awareness (Levelt, 1965; Wheatstone, 1838). This phenomenon of binocular rivalry has attracted the interest of psychologists and neuroscientists alike as a method of probing the mechanisms that determine our visual awareness.

3.3.1 Basic phenomena of binocular rivalry

If the corresponding regions of the two eyes are stimulated by very different patterns, the stimuli rival in terms of our conscious perception, rather than fuse into a composite pattern. This perceptual alternation between non-fusible dichoptic stimuli is known as *binocular rivalry*. The stimulus seen at a given time is the *dominant stimulus* and the stimulus that could not be seen is the *suppressed stimulus*. When both stimuli are small one tends to see all of one image or all of the other in alternation. This is known as *exclusive dominance*.

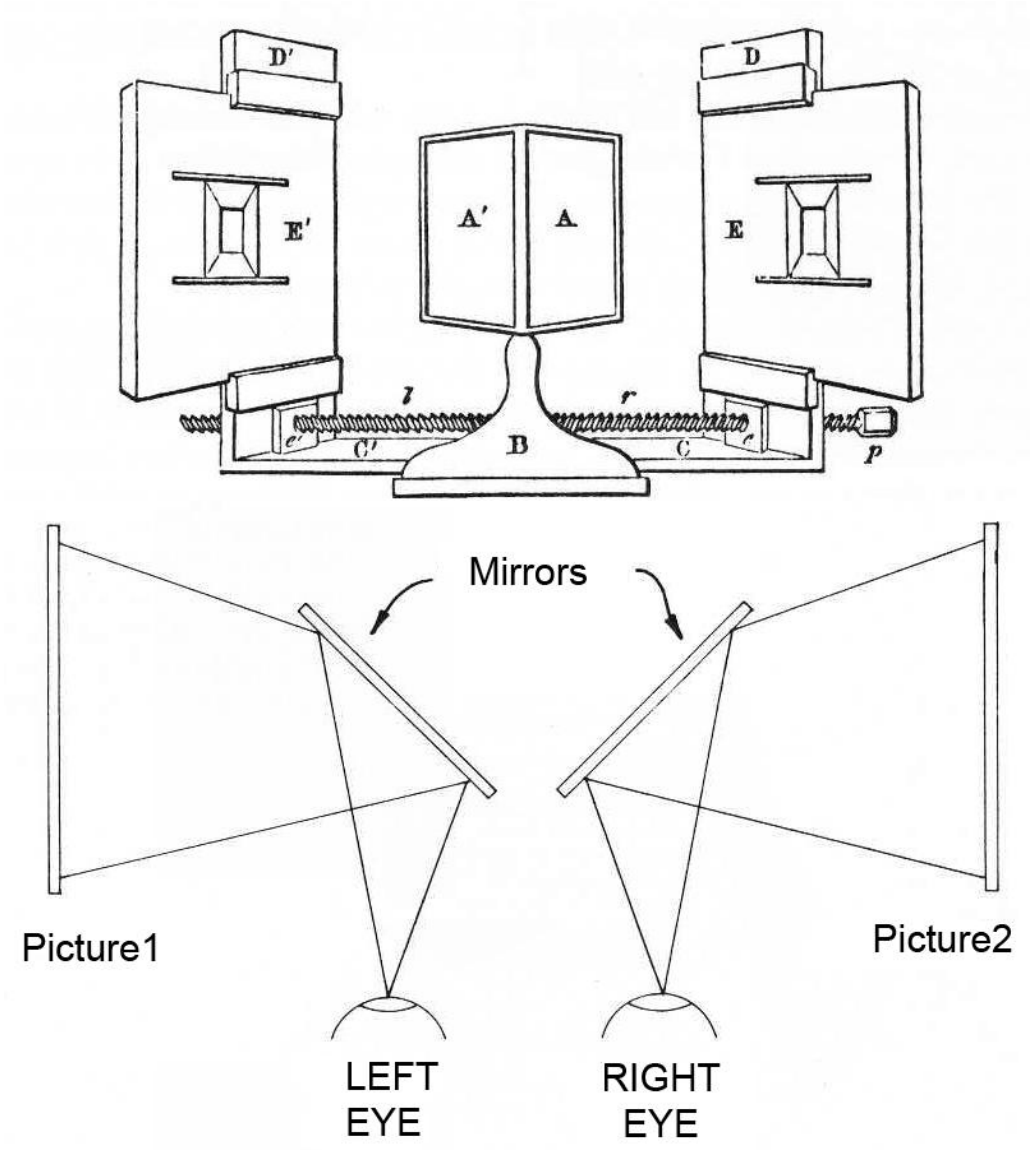

Fig. 3.6 A reproduction of Wheatstone's newly invented mirror stereoscope (Blake, R., 1989).

As for large patterns of equal area, a part of one pattern is dominant in one area and a part of the other in another area, with these areas of dominance fluctuating over time. This is known as *mosaic dominance*. A patterned stimulus is generally dominant over a blank field in the other eye. For example, a small black disc on a white ground remains visible when superimposed on a larger black disc presented to the other eye, as shown in Fig. 3.6. The edge of the small black disc suppresses the surrounding homogeneous region in the larger disc so that the edge of the small disc remains visible. The same

contour-preserving process is seen when a vertical bar in one eye is superimposed on a horizontal bar in the other eye, as shown in Fig. 3.6 (Blake, R., 1989).

3.3.2 Luminance, contrast and contour density

(a) Interocular differences in luminance and contrast

A grating near the contrast threshold can rival an orthogonal high-contrast grating in the other eye, but the low-contrast grating is visible for only short periods. The least contrast in an image that will instigate rivalry is the *rivalry contrast threshold*. The rivalry contrast threshold as a function of the spatial frequency of the rivalry gratings has been found to be similar to the contrast-sensitivity function of monocular viewed gratings (Blake 1977). The threshold for detection of a flash is elevated when the flash is presented at about the same time as a sudden change in brightness in the other eye. Presumably the change in the non-tested eye causes that eye to become dominant and this suppresses the response to the test flash. Blake and Camisa (1979) found the elevation of threshold of a test flash presented to an eye when it was suppressed by the other eye to be independent of the relative contrasts of the two stimuli (Ling and Blake, 2009). They concluded that, once a stimulus is suppressed, the degree, as opposed to the duration, of suppression is independent of its contrast. Makous and Sanders (1978) reported that dimming one of the images has no effect on the degree of suppression. Dichoptic gratings differing in color show longer periods of exclusive dominance than those of the same color. The fact that stimuli with high contrast or high spatial frequency tend to suppress stimuli with low contrast or low spatial frequency helps people who wear a contact lens for hyperopia on one eye and a lens for myopia on the other eye.

(b) Effects of the Luminance and Contrast

High-contrast orthogonal gratings alternate more rapidly than low-contrast gratings, and continuous lines alternate more rapidly than broken lines. Alternations of rivalry occur much less frequently and suppression spreads over wider areas when both images are at scotopic rather than photopic light levels (Breese 1909; Brascamp, et al., 2015; Kaplan and Metlay 1964; Attarha and Moore, 2015; Johnston et al. 1994). Two

low-contrast gratings show longer periods of exclusive dominance than do two high-contrast gratings. For a given contrast, gratings with a spatial frequency of 3 c/deg show longer periods of exclusive dominance than do gratings with higher or lower spatial frequencies (Hollins, 1980; Law et al., 2015; Roeber, 2012). Rivalry between random-dot patterns showed a similar dependence on spatial frequency (de Weert and Wade 1988; Carlson and He, 2004; Anstis and Rogers, 2012). Orthogonal dichoptic gratings with the contrast of both set just above the threshold do not begin to rival for many seconds after exposure, but appear superimposed as a plaid pattern (Tang et al., 2012; Sun et al., 2015). As the contrast of the gratings increased, the time before rivalry is experienced becomes shorter. For a given contrast, gratings with higher spatial frequency appear as plaids longer than those with lower spatial frequency probably because higher spatial-frequency gratings have higher contrast thresholds. One way to think about these effects is that when both members of a dichoptic display have low contrast, neither of them has sufficient stimulus strength to suppress the other. Liu et al. showed that a non-rivalry aperture surrounding the stimulus significantly enhanced combination of dichoptic images. It would be worthwhile to study rivalry in large low-contrast gratings in which any possible contribution of an aperture is minimized.

(c) Dominance of homogeneous fields

It is generally believed that a featureless visual field never rivals a patterned stimulus. However, a closed eye, which may be said to contain a featureless black field, can suppress a highly textured stimulus. When the dominant eye is closed while the other eye views the black and white grating, as it is oscillated up and down at about 2 Hz, a gray patch containing a diagonal meshwork pattern appears to spread out from the centre of the grating and blot it out (Howard 1959). The meshwork pattern periodically spreads and then recedes. The effect is not Troxler fading of the grating, because Troxler fading does not occur with moving stimuli. People with only one eye did not experience this effect, supporting the idea that the occluding patch is the dark field of the closed eye. When a coarse grating is held still, the dark field of the closed eye may still occlude the lines but, instead of a meshwork pattern, the occluded region contains a faint phase-reversed image of the grating that is confined to a small central patch

because not everyone sees this image. Dynamic visual noise viewed by one eye may be suppressed by a blank field in the other eye (Tyler personal communication). All these effects are strong violations of Levelt's proposition that the more highly patterned stimulus is dominant in binocular rivalry. A homogeneous luminous field (Ganzfeld) tends to fade from view after it has been inspected for some time. Bolanowski and Doty (1987) found that fading did not occur when the Ganzfeld was viewed with both eyes, and concluded that fading with a monocular stimulus is due to suppression of the luminous field by the dark field of the closed eye.

3.3.3 Characteristics of binocular rivalry

Left and right eye differences along any one of a wide range of stimulus dimensions are sufficient to instigate binocular rivalry. These include differences in color, luminance, contrast polarity, form, and size and motion velocity. Rivalry can be triggered by very simple stimulus differences (e.g., gratings differing only in orientation) and by complex differences (e.g., pictures of a human face viewed by one eye and a house viewed by the other). Rivalry can be observed over a very wide range of light levels, including scotopic, and it can be observed anywhere throughout the binocular visual field as long as the stimuli are adjusted for visibility. There appear to be only a few conditions of dichoptic stimulation that resist rivalry; these include dichoptic differences in flicker rate (O'Shea and Blake, 1986; Alais and Parker, 2012), dichoptic differences in contrast level (to be distinguished from contrast polarity), large differences in left- and right-eye spatial frequency amplitude spectra (Wu et al, 2012; Rodriguez-Fortuno et al., 2013) and large differences in speed of random-dot motion (van de Grind et al., 1986; 2002; Soon et al., 2008).

(a) Spatial Extent of Rivalry

In the literature, one often reads that binocular rivalry entails alternating periods of monocular dominance and suppression between discordant views seen by the left and right eyes (Fig. 3.7, Blake, R., 2001). Particularly for large rival stimuli, however, this characterization is not entirely correct. Rather than alternating between periods of

exclusive dominance of one eye's view and then the other eye's view, one often experiences a fluctuating patchwork consisting of intermingled portions of both eyes' views (Meenes, 1930; Hohwy et al., 2008); the incidence of "patchwork" rivalry increases with prolonged viewing of rival targets (Hollins and Hudnell, 1980; Said and Heeger, 2013). One intriguing, suggestive characteristic of rivalry concerns the spatial appearance during transitions in dominance between one stimulus and the other. However, complete monocular dominance does occur significantly more often than would be expected based on chance alone (Blake et al., 1992). In a similar vein, multiple small rival targets scattered throughout the visual field can engage in synchronized alternations, such that all targets of a given configuration (e.g. all the green circles) are dominant simultaneously. This observation, too, implies that rivalry zones are not independent.

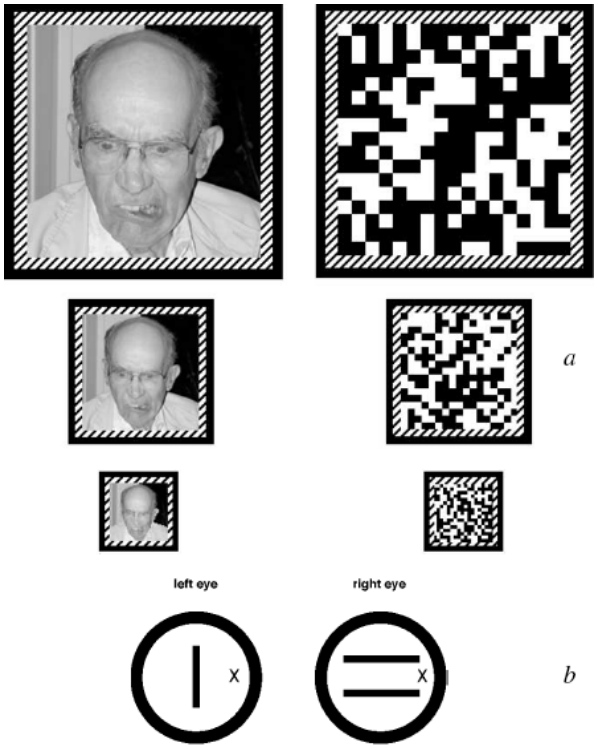

Fig. 3.7 The three pairs of rival targets to experience how to influence rivalry (Blake, R., 2001).

(b) Temporal Dynamics of Rivalry

In fact, binocular rivalry is not experienced when dissimilar monocular stimuli are very briefly exposed – instead, the perceptual result with brief exposure resembles the binocular superimposition of the two stimuli. During rivalry, a phenomenally suppressed stimulus can be readily restored to dominance by maneuvers that create transient stimulation within the eye viewing that stimulus. The most straightforward means for influencing predominance is to vary some aspect of the competing stimuli. As a generalization, a "stronger" rival target enjoys enhanced predominance, defined as the total percentage of time that a given stimulus is visible during an extended viewing period. Moreover, there is evidence that this increased predominance is produced, in large part, by decreases in the durations of suppression periods of a given stimulus – "stronger" stimuli tend to stay suppressed for shorter periods of time while not necessarily staying dominant for longer periods of time.

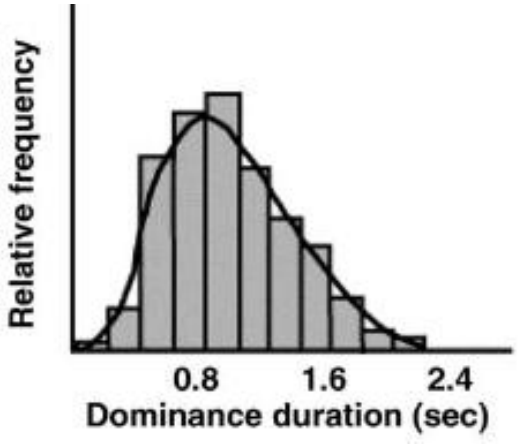

Fig. 3.8 The durations of individual periods of dominance during binocular rivalry (Blake, R., 2001).

As shown in Fig. 3.8 (Blake, R., 2001), Histogram summarizing the durations of individual periods of dominance during binocular rivalry Observers "tracked" dominance of two dissimilar patterns by pressing one of two keys, and the individual

durations were tabulated, normalized and plotted as a frequency histogram. The solid line shows the gamma function fit to the actual data.

3.3.4 Modern theories of binocular rivalry

(a) Interocular Competition Theory

Levelt (1965) described rivalry as a competitive mechanistic process involving reciprocal inhibition between the two eyes in his highly influential monograph "On binocular rivalry". Fig. 3.9 (Lehky; lehky and Sejnowski, 1988) shows an example of an interocular competition model proposed by Lehky (1988); Lehky and Sejnowski (1988). Rivalry arises from reciprocal inhibition between the left versus right monocular channel. When one monocular input is stronger than the other, it activates an inhibitory neuron that can entirely suppress input from the other eye.

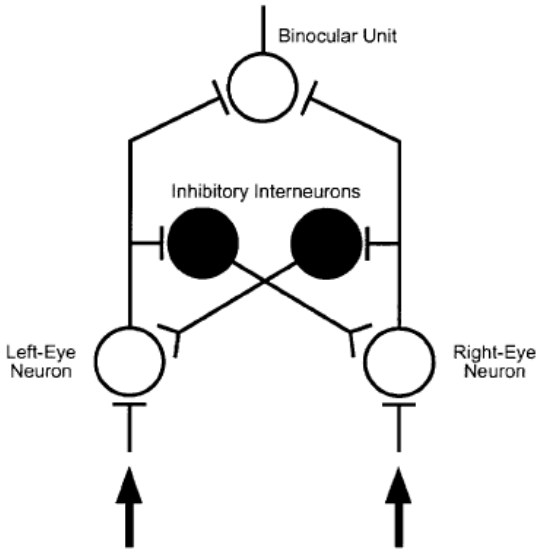

Fig. 3.9 Example of the neural network model of binocular rivalry (Lehky; lehky and Sejnowski, 1988).

Reciprocal inhibition occurs between left-eye and right-eye neurons as a result of inhibitory interneuronal connections. As a consequence, left-eye versus right-eye inputs are alternately suppressed during binocular rivalry. These competitive interactions take place prior to binocular convergence.

(b) Pattern Competition Theory

In contrast to interocular competition theory, Logothetis and colleagues (Leopold and Logothetis, 1996; Trapp and Bar, 2015; Logothetis, 1998; Logothetis et al., 1996) have proposed that binocular rivalry arises from competition among incompatible pattern representations, well after inputs from the two eyes have converged in primary visual cortex (V1). For example, rivalry between a left-eye vertical grating and a right-eye horizontal grating is assumed to reflect competition between the perceptual representations for vertical and horizontal rather than competition between left-eye and right-eye channels (Diaz-Caneja, 1928; Leopold and Logothetis, 1999; Mitchell et al., 2004). Such pattern competition can be realized using a simple competitive circuit like the model proposed by Lehky (1988) with the exception that reciprocal inhibition occurs between different pattern representations rather than between monocular channels. A more elaborate model involving multiple levels of pattern competition and feedback organizational effects has also been proposed. Although the structure of the competitive circuitry may not appear to differ greatly between interocular and pattern competition models, the latter theory holds that rivalry involves a much higher-level form of competition between equally valid perceptual interpretations of the external world. In this respect, binocular rivalry is presumed to reflect very similar or identical mechanisms as those that mediate the reversal of ambiguous figures such as the Necker Cube or Rubin's face/vase (Logothetis, 1998).

(c) Strengths and Weaknesses of Competition Theory

The strength of interocular competition theory lies in its simplicity, specificity, and testability. This theory provides a simple mechanistic account of binocular rivalry in sufficient detail to generate specific testable predictions. Further studies should be conducted to test if the same holds true for other aftereffects including those involving interocular transfer. Also, separate studies should assess whether monocular activity is enhanced during the dominance phase of rivalry as compared to monocular or dioptic viewing (Makous and Sanders, 1978; Nguyen et al., 2003). Interocular competition theory provides a compelling account of binocular rivalry but provides no explanation for why rivalry can sometimes occur in the absence of interocular competition. For example, a weaker form of perceptual alternation can occur during monocular rivalry when two low-contrast patterns are viewed by a single eye or by both eyes (Andrews

and Purves, 1997; Lumer et al., 1998; Bonneh et al., 2001; Tong et al., 2006). Such rivalry cannot be explained in terms of interocular competition and must instead reflect some form of pattern competition. Although monocular rivalry leads to weaker perceptual alternations than binocular rivalry, both phenomena share many similarities that could potentially reflect the operation of a common neural mechanism (Andrews and Purves, 1997). To summarize, interocular competition theory provides a simple, powerful explanation of binocular rivalry and leads to clear, testable predictions. It is supported by several psychophysical studies showing eye-specific effects during rivalry. However, this theory cannot generalize to related phenomena such as monocular rivalry and may have difficulty explaining the persistence of visual adaptation during binocular rivalry suppression.

(d) Other Theory of Rivalry

In addition to the theories of interocular competition and pattern competition, there are alternative proposals that rivalry may instead reflect some type of top-down selection or switching mechanism. These selection-based theories are still in development and the evidence to support them is still quite preliminary. These theories are briefly described below. Top-down selection theories forward that executive frontal-parietal brain areas are responsible for initiating rivalry alternations by sending top-down signals to steer activity in visual cortex towards one representation or another (Leopold and Logothetis, 1999; Lumer et al., 1998; Brascamp et al., 2015). Pettigrew and Miller have proposed a different theory forwarding that rivalry results from interhemispheric switching between two rivaling stimuli and that this switching arises because each stimulus is represented by a different hemisphere (see this issue for reviews). A major challenge for this theory will be to provide compelling evidence of how each hemisphere comes to adopt a different monocular image during rivalry given that corresponding regions in the two eyes are known to project to a single hemisphere in retinotopically cortex (Sereno et al., 1995; Ungerleider et al., 2000; Hopfinger et al., 2000; Haynes and Rees, 2006). A major limitation of both top-down selection and interhemispheric switching theories is that they provide no explanation for the many stimulus determinants of rivalry. Although selection mechanisms may bias the time

course of perceptual alternations to some extent, the stimulus-driven nature of binocular rivalry indicates that this phenomenon is largely determined by competitive interactions at an early stage of visual processing.

3.4 Color rivalry

Under some circumstances, an illuminated area of one color presented to one eye appears to rival a similar area of another color presented to the other eye. This is known as *color rivalry*. Under other circumstances, two different colors combine to create the impression of a third color. This is known as *binocular color mixing*. There has been some dispute about whether binocular color mixing ever occurs, and even those who believe that it occurs disagree about the necessary conditions.

3.4.1 Early research

The earliest reference to binocular color mixing seems to be a study by Haldat in which he reported that dichoptically combined images of glass prisms containing colored liquid appeared in an intermediate hue (Haldat, 1806). Later in the nineteenth century there was a controversy between those who adopted the Young-Helmholtz theory, which stipulated that all colors can be formed from mixtures of red, green, and blue light, and those who adopted the Hering or Ladd-Franklin theories, which stipulated that the sensation of yellow arises from a distinct process in the retina. It was argued that the Young-Helmholtz theory predicts a sensation of yellow arising from the dichoptic combination of red and green whereas the latter two theories do not. It is ironic that for Helmholtz binocular yellow was an artifact due to color adaptation, binocular suppression, and unconscious inference (Helmholtz, 1909), whereas Hering regarded it as due to interaction of visual inputs at a central location. Helmholtz's reluctance to regard binocular yellow as due to a central combination of inputs arose from his belief that inputs from the two eyes are not combined physiologically.

Many early investigators claimed to see binocular yellow. For instance, Hecht (1928) saw yellow when he combined a red illuminated patch with a green illuminated patch.

Murray (1939) pointed out that the Wratten filters used by Hecht extended into the yellow region of the spectrum. Dunlap (1944) argued that binocular yellow is an artifact of adaptation of the eye to the red light and claimed to see yellow when both eyes looked at red patches for some time. He concluded that binocular color mixture can be laid away in the museum of curious superstitions. But the problem lives on. Prentice (1948) claimed to have overcome Murray's objection by using narrowband Farrand interference filters centred on 530 mμ (green) and 680 mμ (red), neither of which extends into the yellow region of the spectrum. He obtained good binocular yellow even with short exposure, and the fused image became more yellow with longer exposure. Others have also reported binocular yellow with narrow-band filters and appropriate controls for color adaptation. However, Hurvich and Jameson (1951) pointed out that the spectral purity of the red and green filters is irrelevant. The crucial factor is the chromatic bandwidth of the receptors, since a receptor cannot distinguish between one wavelength and another within its tuning range-the principle of univariance. The wave-lengths selected by Prentice and others evoked sensations of yellowish red and yellowish green and it was therefore not surprising that they produced binocular yellow. When Hurvich and Jameson used unique red and green, which evoke the purest sensations of red and green, the dichoptic mixture was not yellow but white. This still represents a form of binocular color mixing that needs to be explained. The colors used by Hurvich and Jameson were close to being opponent colors that produce white when mixed monocularly. As ordinarily understood, the opponent mechanism resides in the retina, so that the occurrence of binocular white must depend on a distinct cortical process.

Effects of color matches

Color matches obtained under dichoptic viewing differ from those obtained with monocular viewing. Lights combined monocularly obey Abney's law; that is, the luminances of differently colored lights add linearly. Lights combined dichoptically, whether of the same or different colors, do not obey Abney's law of linear luminanceummation but produce an intermediate brightness, especially when they are similar in luminance. Dichoptic color matches are less saturated and more variable than

similar matches made monocularly. The proportion of green to red required to match a spectral yellow and the proportion of yellow required to cancel blue were found to be less with dichoptic than with monocular viewing (Hoffman 1962; Hovis and Guth 1989) De Weert and Levelt (1976) presented a dichoptic mixture of equiluminous lights of different wavelength in a small area and asked subjects to adjust the relative luminance of two lights of the same two wavelengths presented to both eyes in an adjacent small area until the two areas appeared most similar in hue. They did this for many pairs of wavelengths and derived a set of hue-efficiency functions for the dichoptic mixtures. Reasonably good matches of hue were obtained between the dichoptic and dioptic stimuli with the same wavelength components. In general, a smaller amount of the wavelength component nearer the middle of the spectrum was required in the dichoptic mixture than in the dioptic mixture. When a grid of black lines was superimposed on a colored patch in one eye the color in that eye became strongly dominant over the untextured colored patch in the other eye. A colored patch presented to an amblyopic eye contributed less to the dichoptic color than a patch presented to the non-amblyopic eye (Lange-Malecki et al. 1985).

Effects of stimuli size

Hering observed that dichoptic color mixtures are more stable with small than with large stimuli and this has been confirmed more recently (Thomas et al., 1961; Ikeda and Sagawa, 1979; Qin et al., 2009) With large stimuli, people experience color rivalry rather than color mixture. With stimuli subtending less than 2º, most subjects reported stable color mixture (Grimsley 1943; Gunter 1951; Morgan and Tromborg, 2007; Anstis and Rogers, 2012). With a display subtending 3.5º, the impression of binocular color mixture was unstable but became stable when a fusible micro-pattern was superimposed on the display, (de Weert and Wade, 1998). One could think of the textured pattern as breaking up the display into small regions and thus preventing rivalry. Binocular color mixture is difficult to see in the presence of rivalrous patterns (Dawson, 1915; Rivers et al., 2014).

Effects of stimuli duration

Hering (1861) observed that prolonged inspection of a dichoptic mixture produces more stable color mixtures. Johannsen (1930) suggested that prolonged inspection causes the color in each eye to become desaturated through adaptation and this, rather than duration, is responsible for the increased stability of color mixtures. However, dichoptic color mixtures also seen be more stable with very short exposure times. Thus, synchronous flicker of red and green dichoptic stimuli increased the apparent saturation and stability of binocular yellow and the best results were obtained with flash durations of less than 100 ms and interflash durations of more than 100 ms (Gunter, 1951). We will see that binocular rivalry of contours does not occur with brief stimuli. Stimulus asynchrony of more than 25 ms disrupts the impression of binocular yellow.

Effects of stimuli luminance

Dichoptic color mixtures are more stable at lower than at higher luminance levels and (2) when the luminance in the two eyes is the same. These effects were observed by Hering and confirmed by Dawson and Johannsen. Color mixtures become more stable as the saturation of the colors decreases. Matches between dichoptic and dioptic mixtures are most stable when the components of the dichoptic mixture are presented on a dark rather than a light background.

Effects of visual field

The periods of color rivalry that occur with larger visual fields are more pronounced the greater the color difference presented to the two eyes. Ikeda and Nakashima gradually increased the dichoptic difference in the wavelength of a 10º test patch until the subject reported color rivalry. The threshold difference for the occurrence of rivalry varied as a function of wavelength in a manner closely resembling the hue-discrimination curve. In other words, threshold color differences for the production of rivalry were equally discriminable. Sagawa asked whether the threshold for discriminating between two patches of wavelength λ and $\lambda + \Delta\lambda$ presented to one eye was affected when patches of wavelength λ were superimposed in the other eye. The idea was that if color processing is independent in the two eyes, the addition of the

dichoptic masking patches would not affect the discrimination threshold. Wavelength discrimination deteriorated in the presence of the masking stimulus, but the extent of the deterioration was largely independent of the luminance of the masking stimuli. This suggests that dichoptic masking between chromatic signals is independent of the luminance component of the visual stimulus.

3.4.2 EEG studies of color rivalry

Early EEG studies in humans provided the first evidence that neural activity correlates with conscious perception during binocular rivalry. Lansing monitored electrical activity from the occipital scalp and found that EEG responses to a monocular flickering light were significantly reduced when a rivaling static pattern was presented to the other eye (Lansing 1964). The extent of physiological suppression corresponded well to the subject's report of rivalry suppression. Cobb et al. investigated binocular rivalry between two oscillating gratings that evoked EEG modulations that were 180 º out of phase (Cobb et al., 1967). The phase of the EEG response tightly corresponded to the subject's report regarding which grating pattern appeared to be dominant. Remarkably, the magnitude of these rivalry-related responses were as large as those observed when either grating pattern was presented alone, suggesting that the physiological suppression during rivalry was essentially complete. These powerful EEG modulations found in humans differ from the weak rivalry effects subsequently found in early visual areas of the monkey (Leopold and Logothetis, 1996; Logothetis and Schall, 1989; Siegel et al., 2015).

More recent EEG studies have demonstrated that two rivaling stimuli can be uniquely tagged using different flickering frequencies to reveal real-time response modulations that correspond to the subject's perception (Brown and Norcia, 1997; Jamison et al., 2015; Norcia et al, 2015; Sandberg et al., 2013). Magneto-encephalography (MEG) has also been used to investigate the neural correlates of binocular rivalry. Compared to the poor spatial resolution of EEG, MEG provides somewhat better source localization by measuring neurally induced changes in local magnetic-field potentials from multiple sites on the human scalp. Tononi and colleagues compared MEG responses during

rivalry alternations to those evoked by actual stimulus alternations between the two frequency-tagged stimuli (Tononi and Edelman, 1998; Tononi et al., 1998a; 1998b). They found strong rivalry-related responses throughout occipital cortex and also from some anterior temporal and frontal sites. These MEG responses during rivalry were about 50–85% of the magnitude of those observed during stimulus alternation. Although the origin of these rivalry-related responses could not be localized, their widespread nature may indicate that rivalry interactions occur quite early in the processing stream and that the result of this competition is propagated throughout the rest of the brain.

Chapter 4

Experimental apparatus

4.1 Hardware

3D display

In our experiments we employed a special device of 3D display (SANYO, THD-10P3) shown on Fig. 4.1.

Illustrated as Fig. 4.2, a 3D display requiring no special viewing glasses is generated by controlling the path of travel of light from the display so that slightly different images reach the left and right eyes; in other words, the right eye sees only the image intended for it, and the left eye only the image intended for it. This Switching LCD establishes an optical parallax barrier, and by controlling the path of travel of light, makes it possible to separate the display images so that slightly different images reach the left and right eyes. By displaying the image intended for the left eye and the image for the right eye as a stereographic pair on a TFT LCD, each eye sees only the image intended for it and the brain combines the images and perceives them as a 3D representation. In addition, the Switching LCD electrically controls the parallax barrier to make it transparent, eliminating its ability to separate light paths. This way, the right and left eyes can see the same image when viewing ordinary 2D content. In other words, the display can also function as a conventional standard imaging device. Therefore, we could arbitrarily and accurately control the stimulus targets of left or right eye by a program, which was installed in a computer connected with the 3D display. Fig. 4.3(2) is the real photo of 3D display.

Fig. 4.1. A sketch map of 3D display (SANYO, THD-10P3).

Trestle to fix the head

In this experiment, we used a trestle to fix the subject's head in order to create a fixed view. The trestle is fixed on a side of table showed on Fig. 4.3. The high of trestle can be adjusted manually.

A computer to control the 3D display device

In this experiment, we used a note computer with a software system operated by an experimenter to control the display of 3D display device, which is shown in Fig 4.2.

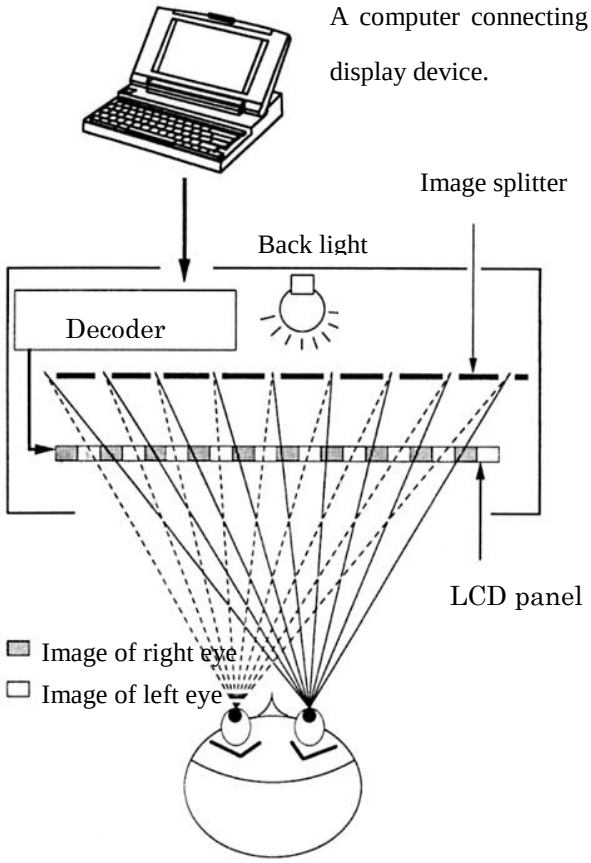

Fig. 4.2. Principle figure of a 3D display device.

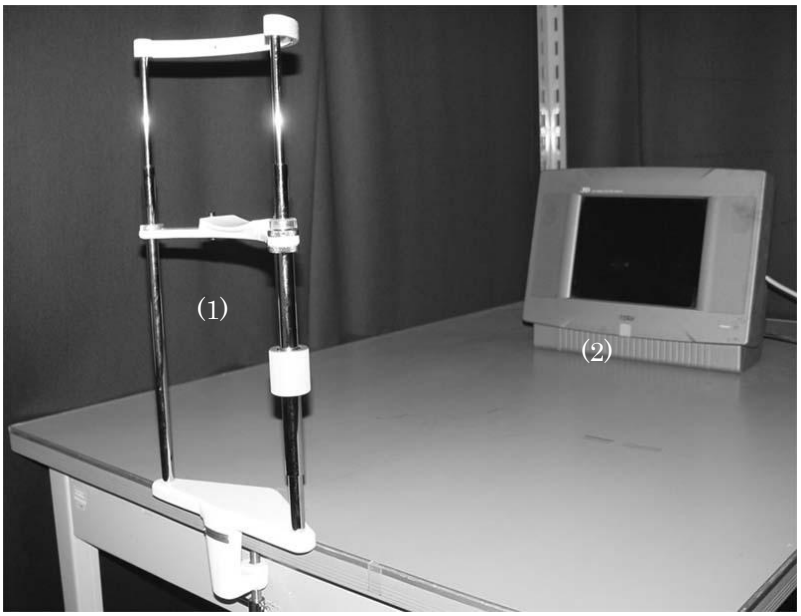

Fig. 4.3. (1) A trestle to fix the subject's head. (2) A 3D display device.

Cataract experiencing goggle

In this study, a specialized goggle (Fig. 4.4) produced by the government of Ontario in Canada for instant senior program was used for provide the vision as close appearance of age-related (senile) cataract as possible. The spectral transmittance of goggle is 20% in blue, 45% in green, 70% in red, which that reproduced a severely age-related cataract.

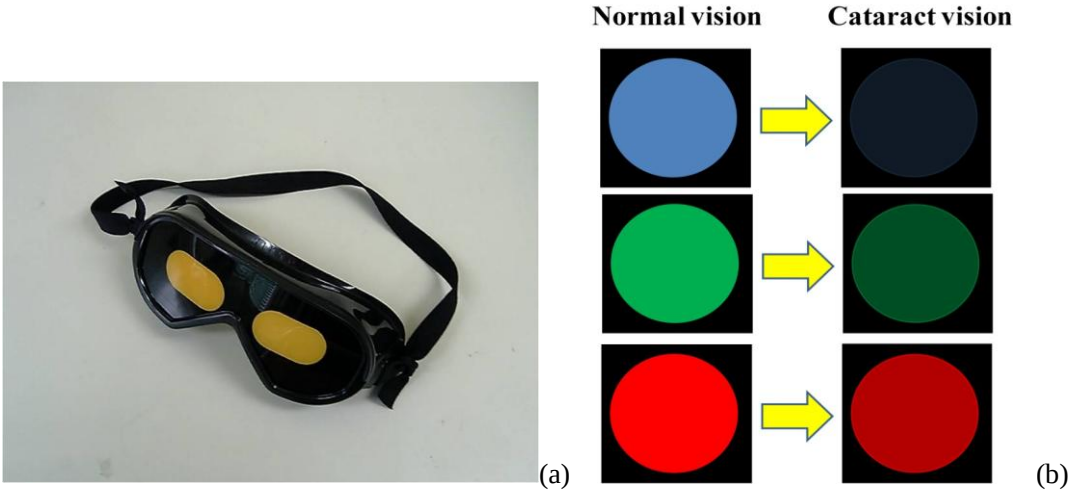

(a) (b)

Fig. 4.4. (a) Cataract experiencing goggle, (b) The viewing effects of the cataract experiencing goggle where the left subfigure denotes the normal vision, while the left one represents the cataract vision.

Active Two system

In this experiment, the Active Two System produced by BioSemi Inc. (Fig.4.5) with event-related EEG using independent component analysis (ICA), time/frequency 64 channels were employed to acquire the signals of the brain activity. The original data is analyzed by the EEGlab which is the toolbox for processing continuous and analysis, artifice rejection, and several modes of data visualization. The Active Two system sets new standards for multi channel, high resolution biopotential measurement systems for research applications.

Fig. 4.5. The active two system (BioSemi Inc.).

4.2 The software system

A software system was developed by author using Visual Basic.net. This software system was developed in order to control the subject's view so that the left view would reach the left eye and the right view would reach only the right eye.

The principle of creating a 3-D view from 2-D views is shown as Fig.3.4. Firstly, two 320 pixel *460 pixel images are made in a computer with a software system, and then send the images to the 3D display device. In the 3D display device the two 320 pixel * 480 pixel images become two 640 pixel * 480 pixel images, and separated by an optical parallax barrier, so that each eye sees only the image intended for it and the brain combines the images and perceives them as a 3D representation.

In order to expediently control the display of 3D display device, we made a program software system using Visual Basic.net.

XYZ color match function

In the file ColorMatch. vb, we can define a class ColorMatch by which we can get all values of all points in CIE 1931 or 1976 by reading the text files 1931.txt and 1976.txt which are located at a root directory "./seeting/".In fact, the data of CIE 1931 or 1976 is open, so we can get the data easily from internet .For example, the Color and Vision

Research Laboratories' web which is a primarily scientific and technical web site provides the data of CIE 1931 which is shown at the page "http://cvision.ucsd.edu/database/data/cmfs/ciexyz31_1.txt" and data of 1976 at "http://cvision.ucsd.edu/database/data/cmfs/ciexyz64_1.txt".After getting the values of CIE Graph, we can analyze any values of random point by a file WaveLengthMatch. vb, in which we can define another class WaveLengthMatch to analyze the values of XY axis if we know the purity of one color and to get the wavelength of one color if we know the values of XY axis. The principle of calculation is shown as Fig.4.6.

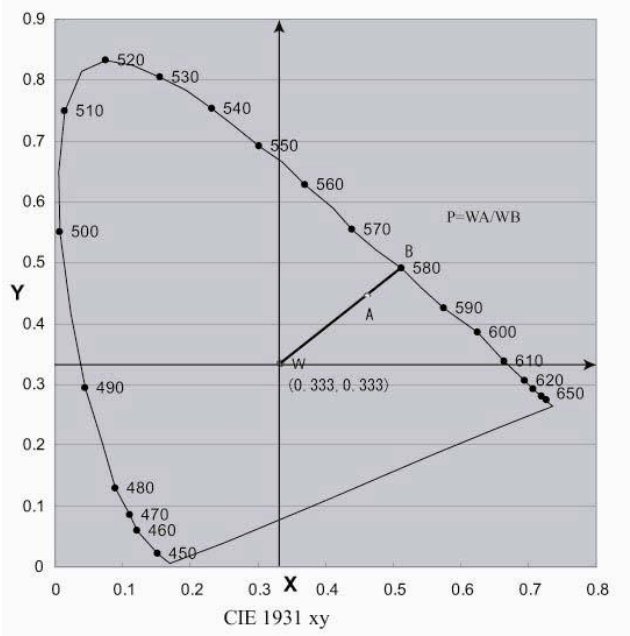

Fig. 4.6. The principles view about how to match xyz color.

XW=0.333.YW=0.333.By file ColourMatch.vb, we can get the values of B (XB, YB). If we know the purity of one colour, by the expression p=wa/wb (p<=1), we can analyze the values of XY axis (XA=p*(XB-XW) +XW, YA=p*(YB-YW) +YW). And by calculating more complexly, we can get the wavelength of one colour if we have known the XY values of one point.

Console platform

The software system mainly is divided into two parts: remote terminal software system and console terminal software system. The remote terminal software system is a

display window for subjects in the 3D display. The console terminal software system is control program by experimenter running in a computer.

The console terminal connects the remote terminal through a Winsock (Fig. 4.7). WinSock is short for Windows Sockets. Today's most popular Internet applications for Microsoft Windows and IBM OS/2 are developed according to the WinSock standard. In actual experiment the two programs run on a same note computer. The note computer has two video card, one is connected the outer display device, 3D display device, and the other one is for the inner display, the LCD display screen of note computer. Thought the console terminal software we can control the size, angle, position and color of the left and right eye's image. The console terminal sends a command to the remote terminal, which is listening on the Winsock port (in this system it is 8000). After the remote terminal software got a command from console terminal, a certain pattern will be shown on the 3D display.

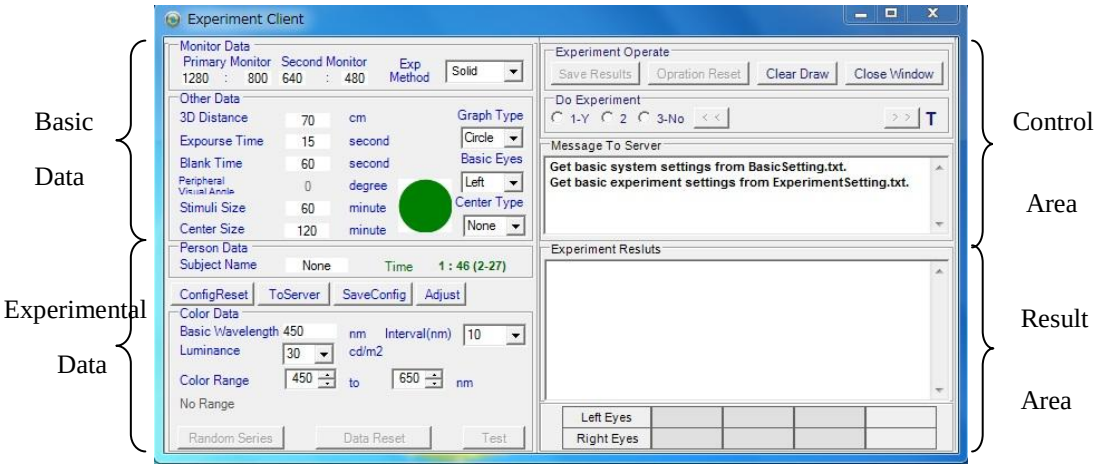

Fig. 4.7. Screen print of the console terminal software system.

Screen print of the console terminal software system including the basic data area, experimental data area, experimental control area and result-show area.

Screen print of the console terminal software system including the basic data area, experimental data area, experimental control area and result-show area. The basic data and experimental data will be described later. In the control area, there are all kinds of

operations about experimental control. And in the result area, there are messages shown as errors or graph locations or RGB color mixture.

EEGlab

In this study, we analyzed the EEG signal with EEGlab. EEGLAB is an interactive Matlab toolbox for processing continuous and event-related EEG, MEG and other electrophysiological data incorporating independent component analysis, time/frequency analysis, artifact rejection, event-related statistics, and several useful modes of visualization of the averaged and single-trial data (Fig.4.8).

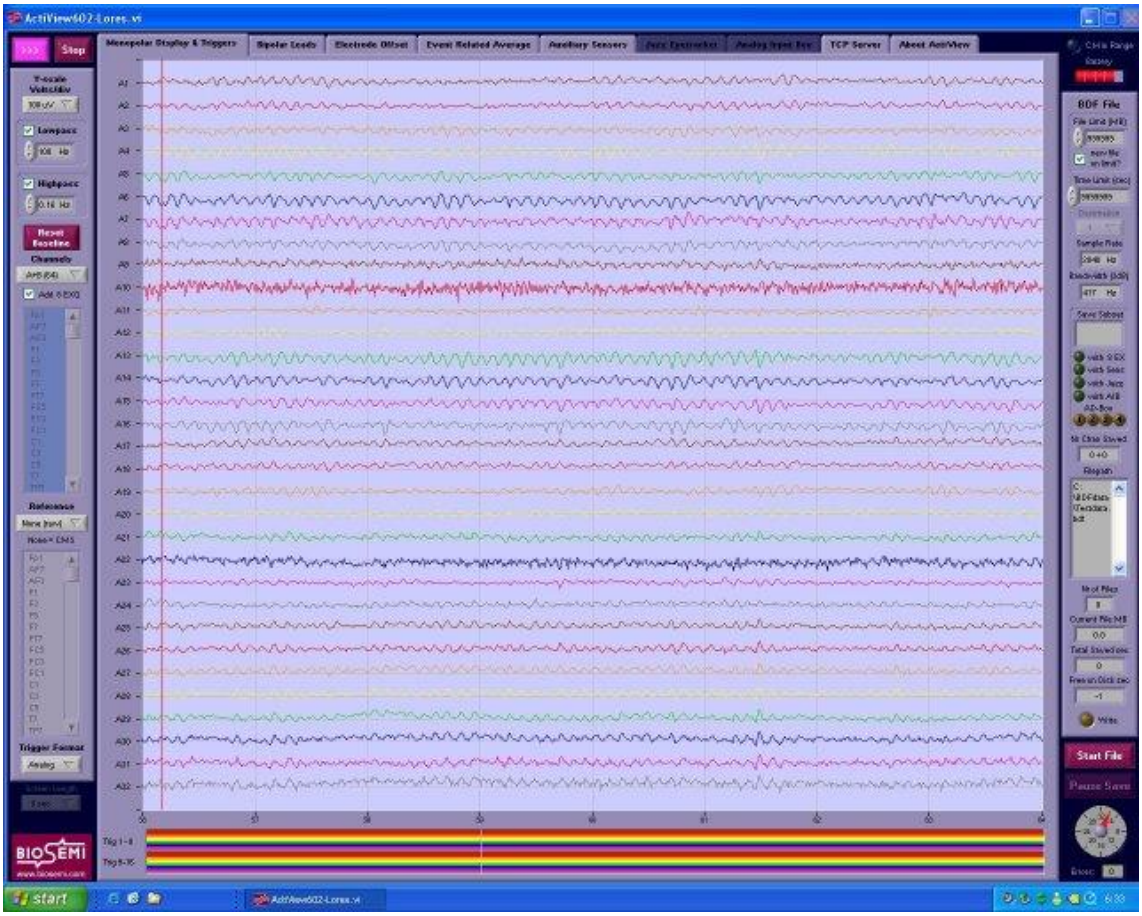

Fig.4.8. The example shows the acquisition program called ActiView.

Chapter 5

Binocular color fusion limit in experiencing cataract

5.1 Stimulus targets

The stimulus is very important. The shape, size and color of stimuli deeply influence the result of the wavelength difference limit for binocular color fusion.

A random-dot stereogram, colorful circular stereogram and pot stereogram are classical stimuli frequently employed in previous experimental works. For example, a colorful circular stimulus was by Ikeda (1978) and Nakajima (1979); two retinal stabilized dark bars subtending 60 min arc vertically and 13 min arc horizontally was used by D. Fender (1988); the random-dot patterns consisting of 50 % grey dots were used by M.M. Weert (1988); Rivalrous stimuli for the left and right eyes consisting of horizontal and vertical gratings respectively were used by P. Dayan (1997); Stereogram depicting a rectangle which contains two rivalrous, achromatic patches placed on a fusible pattern or a rivalrous pattern were used by C. J. Erkelens (2002); Rivalrous dot arrays in which the arrays overlap in visual space but the individual dot elements do not were used by M.A. Silver (2004);A grey central disk surrounded by a colored inner ring and a grey outer ring which colors were blue, green, yellow, and red, whereas the other stimulus parts were grey were used by K. Hamburger (2006).

In central vision, the circular patches for the left eye view and the right eye view on a black background. As shown in Fig.5.1, the diameter of circular stimuli is approximately 2.5 cm, subtending the visual angle 2°. During the experiment, stimuli are presented to both eyes dichoptically with the same luminance and different dominant wavelengths (λ_{dl} and λ_{dr}), in peripheral vision, the experimental stimuli

consist of a pair of cross fixation and the same circular patches. The cross fixation subtending a visual angle of 1° arc is used to stabilize the eyes.

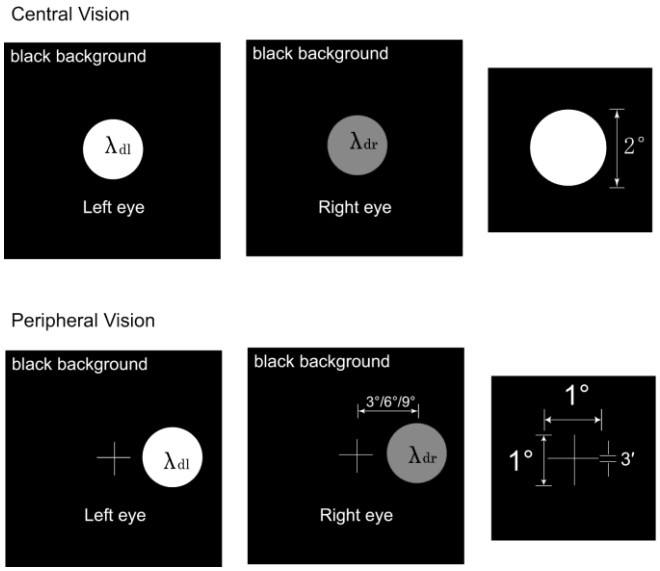

Fig. 5.1. Experimental stimulus for each eye comprising a pair of circular patches and cross fixation.

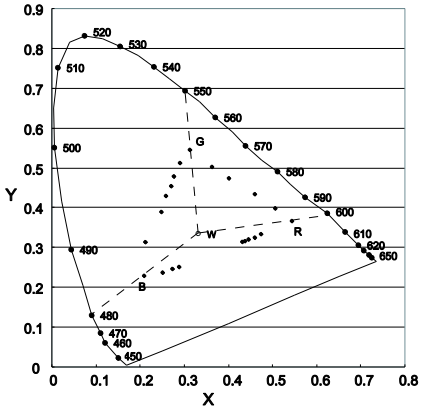

Fig. 5.2. Chromaticity coordinates of 21 experimental stimuli; the data of Points R, G and B, such as wavelength, purity and the value of x and y axes, are shown in Table 5.1.

Table 5.1: The basic data of points R, G and B.

	Wavelength(nm)	Purity	x	y
R	600	72%	0.532	0.361
G	550	67%	0.312	0.545
B	480	53%	0.192	0.262

In this study, the dominant wavelength range of stimuli was set from 450 to 650 nm with intervals of about 10 nm. We obtained 21 experimental points, of which chromaticity coordinates are plotted in the chromaticity diagram as shown in Fig. 5.2. The excitation purities of all 21 dominant wavelengths are between 27 and 72%. The data of Points R, G, and B in Fig. 5.2, such as dominant wavelength, purity, are shown in Table 5.1.

5.2 Experimental procedure

Design of Experiment

The experiment is spatially divided into two parts; one is for experimenter and the other part is for the subjects shown as Fig. 5.4. In the part one, it is a dark room for the subjects, in which there is a table, on which a 3D display device is placed. A trestle to fix the subject's head is placed on the nearer side of the table. The distance from the 3D display device to the trestle is about 70 cm, because only at this distance subjects can get best present from the 3D display which decided by the product of 3D display device, also, cannot be changed later. The subject was seated in front of the table and set his chin and forehead on the trestle to fix his head. In the other part, a console computer connected with the 3D display device through a video cable in dark room is used.

The Criterion of Judging Fusion or Non-fusion

Table 5.2: Three phases of color appearance in visual fields.

Category	Percept	Response
A	Completely fused color	Fusion
B	Inhomogeneous color	Non-fusion
C	Color alternation	Non-fusion

In the experiments, after the stimulus targets were appeared, the subject would report his view response, whether the line target is seen as single or double. In actual view, it

is difficult to clearly judge the response. If the subject clearly saw the targets as fused (when two different colors combine to create the impression of a third color), response "1" should be gotten; except it, when any trace of inhomogeneity or alternation was seen, then he should respond response "2". In fact, there are two kinds of phenomena of binocular non-fusion. One is color mixture unstable, which means subjects can see two or more than two colors in the visual filed; the other one is color rivalry, which means an illuminated area of one color presented to one eye appears to rival a similar area of another color presented to the other eye.

Procedure

On the central vision, a left stimulus with dominant wavelength λ_{dl} was observed only in the left eye and a right stimulus with dominant wavelength λ_{dr} was observed only in the right eye. The exposure time of the stimuli was 15 s, which was long enough to recognize that the perception was either "fusion" or "non-fusion". After the response, a new λ_{dr} was selected randomly from 21 experimental points and used for the next exposure, while the dominant wavelength λ_{dl} was kept constant. About one minute interval was required between the two exposures. This duration was long enough to remove the chromatic adaption caused by the previous exposure. Each point was exposed 10 times to complete one session. Then, some other dominant wavelength λ_{dl} ware selected and the next session was started. This procedure continued until all wavelengths were employed as λ_{dl} from 450 nm through 650 nm with 10 nm steps. Each subject was required to adapt to the dark environment for about 30 min. before the experiment, which has shown to be long enough to remove the chromatic adaptation.

On the peripheral vision, a pair of white cross fixations, which were simultaneously projected on the central fovea of the left and right eye retina, was presented for 3 sec.. The fixation cross was kept constant. Thereafter, the stimulus targets with different dominant wavelength appeared at the retinal eccentricity of 3^o, 6^o or 9^o. Then, the same procedure as on the central vision was carried out.

Two steps were carried out repeatedly in this experiment.In first step, the stimuli were presented to subjects with normal vision. In secend step, the stimuli were

presented to subjects with cataract experiencing vision. To find out the difference of the fusion limit of two eyes between the normal vision and the cataract vision, where each subject wearing the cataract experiencing goggle for simulating the elderly vision. There subjects were also requested to adapt to the dark environment by about 30 min. in the darkroom.

The subjects included 5 students aged average of 23 years old with normal or corrected to normal visual acuities. Meanwhile, they were either experienced with viewing dichoptic stimuli, or were trained beforehand. Subjects were recruited from the Visual and Auditory Information Processing Lab of the Faculty of Engineering in the University of Toyama. Each subject performed a number of trails with the stimuli before manipulating the actual experiment to be familiar with the experimental situation and to insure that they could recognize the stimulus clearly.

5.3 Experimental results of central vision

The results about central vision were shown from Fig. 5.3.1 to Fig. 5.3.21. The curves' data are obtained from the average values of five subjects. The probability of binocular fusion becomes lower with λ_{dr} far from λ_{dl}, whether towards a shorter or longer wavelength. The relation is quite evident in the date shown in the fllowing figures.

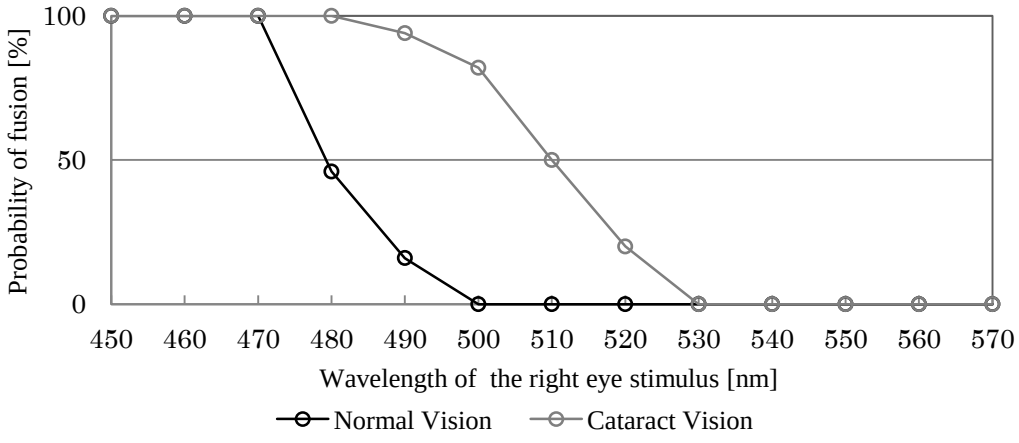

Fig. 5.3.1. Fusion probability curve in central vision when λ_{dl} = 450 nm.

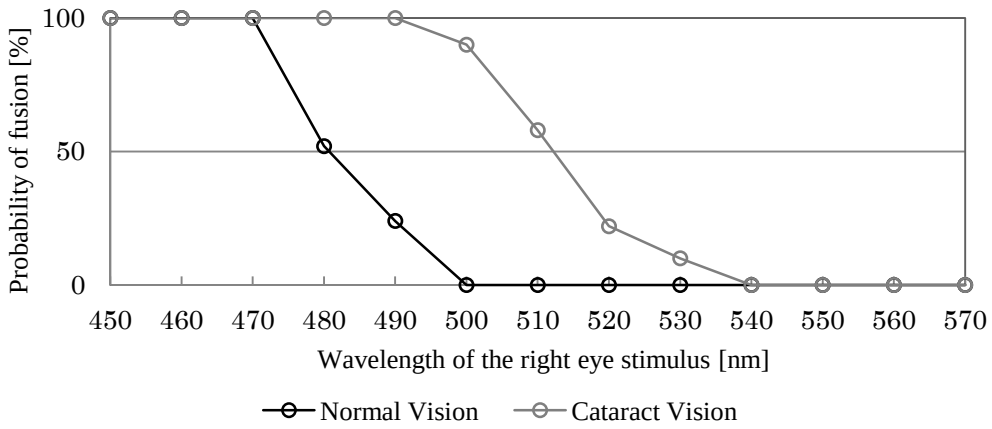

Fig. 5.3.2. Fusion probability curve in central vision when λdl = 460 nm.

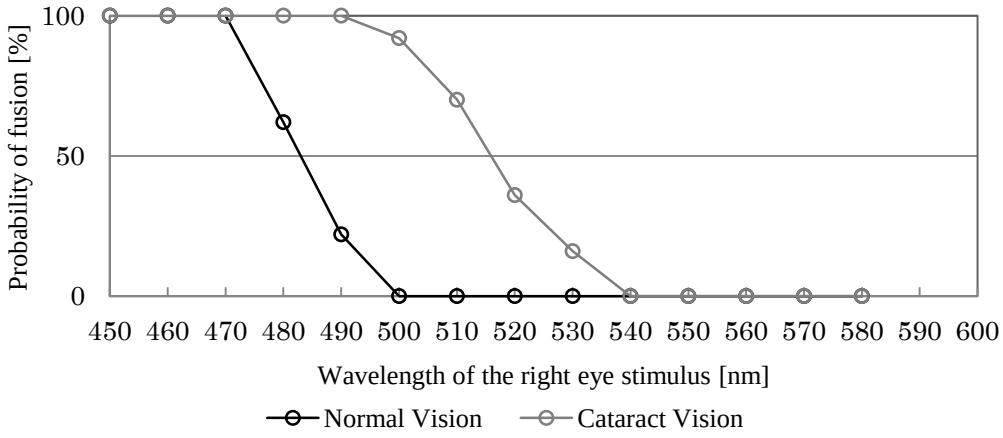

Fig. 5.3.3. Fusion probability curve in central vision when λ_{dl} = 470 nm.

In Fig. 5.3.1, Fig. 5.3.2 and Fig. 5.3.3, we plot the fusion probability curve in central vision when λ_{dl} is 450 nm, 460 nm and 470 nm respectively, where the horizontal axis denotes the wavelength of the right eye stimulus, while the vertical axis represents the probability of fusion. Normal vision and cataract vision are illustrated by using a black line and a grey line respectively. From these figures, we can find that, from 450 nm to 470 nm, both visions are fusional. From 470 nm, the fusion probability of normal vision decreases more sharply than that of cataract vision, suggesting that the width of the fusion of cataract vision is larger than that of normal vision.

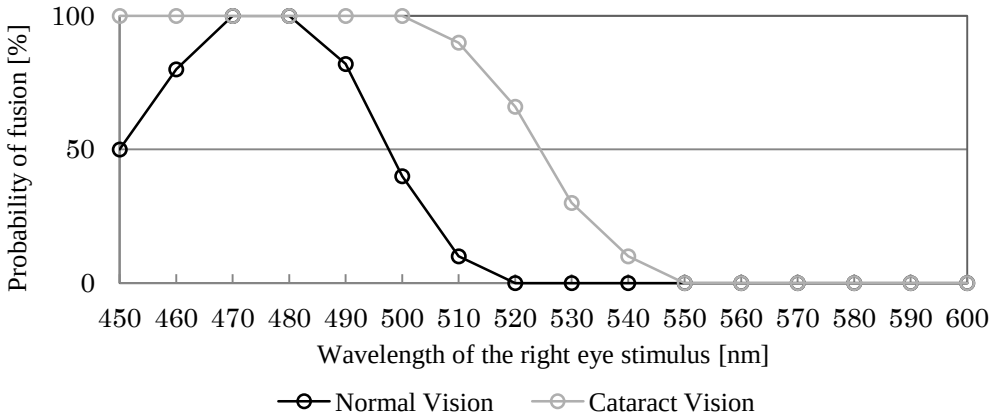

Fig. 5.3.4. Fusion probability curve in central vision when λ_{dl} = 480 nm.

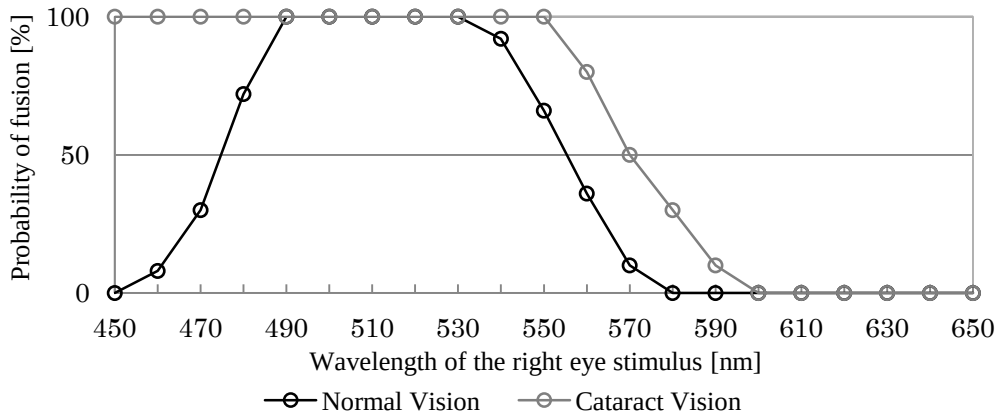

Fig. 5.3.5. Fusion probability curve in central vision when λ_{dl} = 490 nm.

The Fig. 5.3.4 and Fig. 5.3.5 show the fusion probability curve in central vision when λ_{dl} is 480 nm and 490 nm respectively, where the horizontal axis indicates the wavelength of the right eye stimulus and the vertical axis represents the probability of fusion. Normal vision and cataract vision are expressed by a black line and a grey line respectively. According to these figures, we can see that both visions are fusional from 470 nm to 480 nm and from 490 nm to 530 nm respectively, and the fusion probability of cataract vision keeps 100% from 450nm to 500 nm and 550 nm respectively, which is equal or higher than that of normal vision, indicating that the expanding domain of the fusion of cataract vision is still larger than that of normal vision.

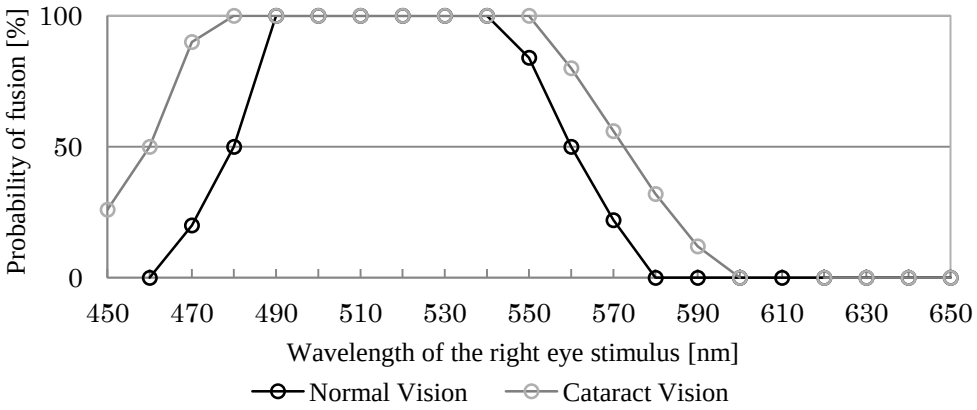

Fig. 5.3.6. Fusion probability curve in central vision when λ_{dl} = 500 nm.

The fusion probability curve in central vision when λ_{dl} = 500 nm where the horizontal axis is the wavelength of the right eye stimulus and the vertical axis denotes the probability of fusion is shown in Fig. 5.3.6. A black line indicates normal vision and a grey line represents cataract vision. From this figure, it can be observed that the fusion probability of cataract vision decreases from 450 nm to 480 nm and both visions are fusional from 490 nm to 540 nm, denoting that the performance of the fusion of cataract vision reduces.

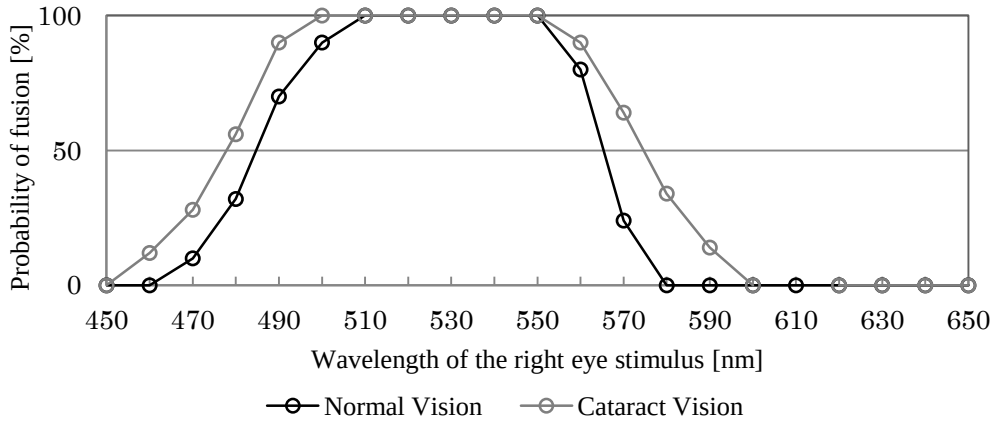

Fig. 5.3.7. Fusion probability curve in central vision when λ_{dl} = 510 nm.

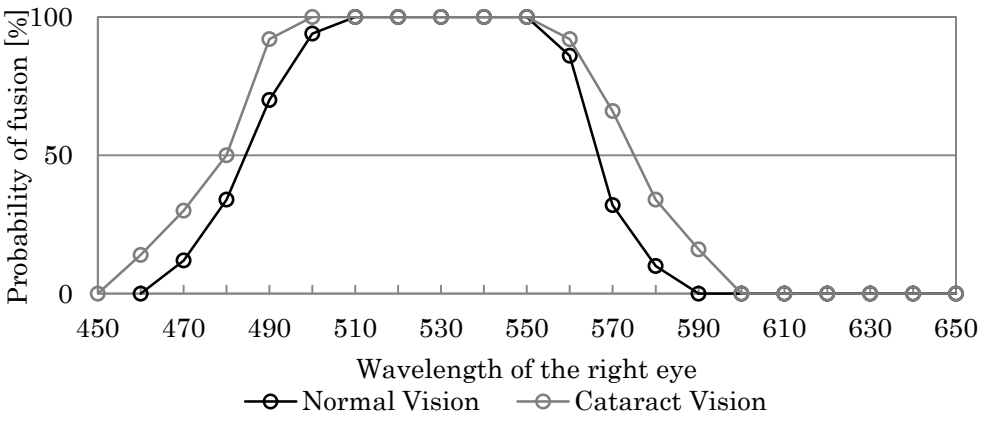

Fig. 5.3.8. Fusion probability curve in central vision when λ_{dl} = 520 nm.

Fig. 5.3.7 and Fig. 5.3.8 describe the fusion probability curve in central vision when λ_{dl} = 510 nm and 520 nm where the horizontal axis denotes the wavelength of the right eye stimulus, while the vertical axis represents the probability of fusion. Normal vision is illustrated using a black line and cataract vision using a grey line. In terms of two figures, we can notice that the fusion probability of cataract vision decreases quickly from 450 nm to 500 nm and both visions are fusional from 510 nm to 550 nm, meaning that the difference of fusion between normal vision and cataract vision reduces sharply.

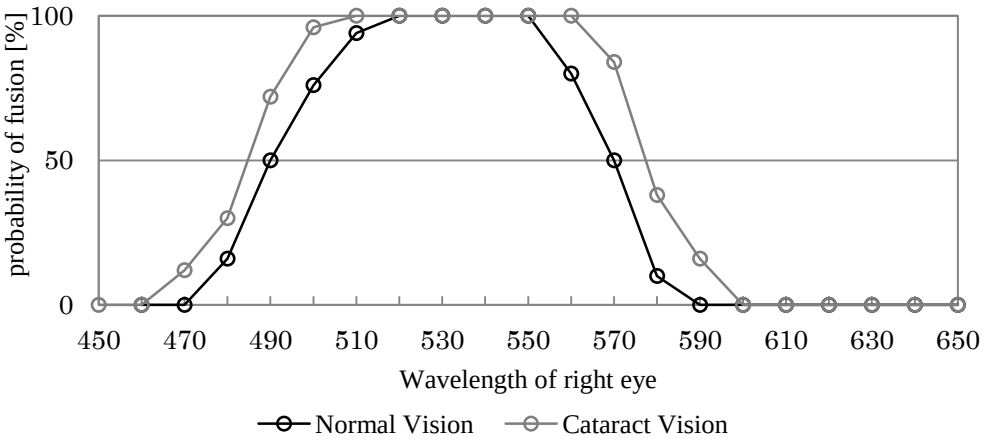

Fig. 5.3.9. Fusion probability curve in central vision when λ_{dl} = 530 nm.

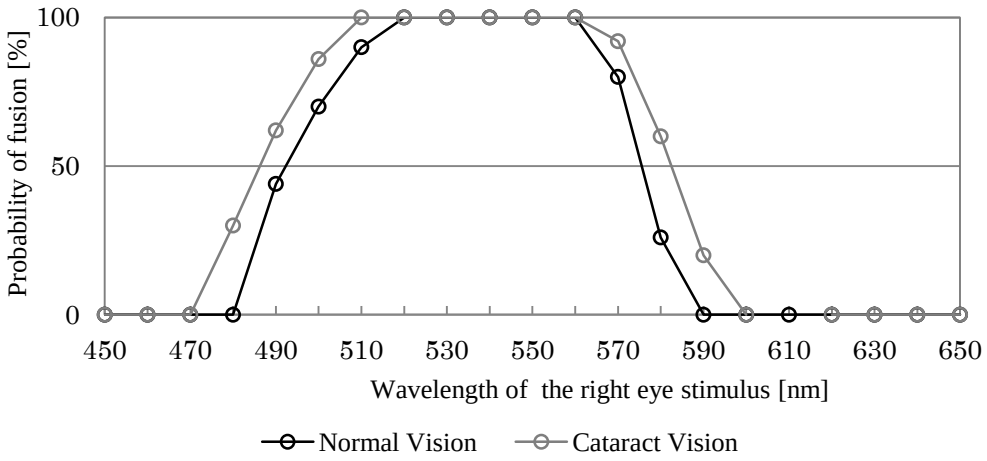

Fig. 5.3.10. Fusion probability curve in central vision when λ_{dl} = 540 nm.

In Fig. 5.3.9 and Fig. 5.3.10, we can observe the fusion probability curve in central vision when λ_{dl} = 530 nm and 540 nm where the wavelength of the right eye stimulus is denoted by the horizontal axis and the probability of fusion is represented by the vertical axis. Normal vision and cataract vision are represented by a black line and a grey line respectively. These figures show that the fusion probability of both visions becomes 0 on the left wavelengths such as 450 nm, 460 nm and 470 nm, and the complete fusion is from 520 nm to 550 nm and 560 nm respectively. It implies that the range of the fusion of both visions narrows.

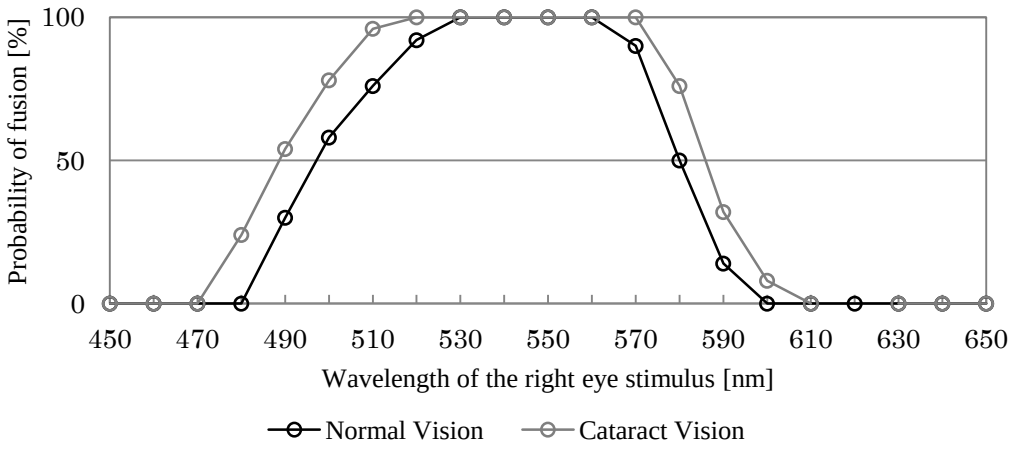

Fig. 5.3.11. Fusion probability curve in central vision when λ_{dl} = 550 nm.

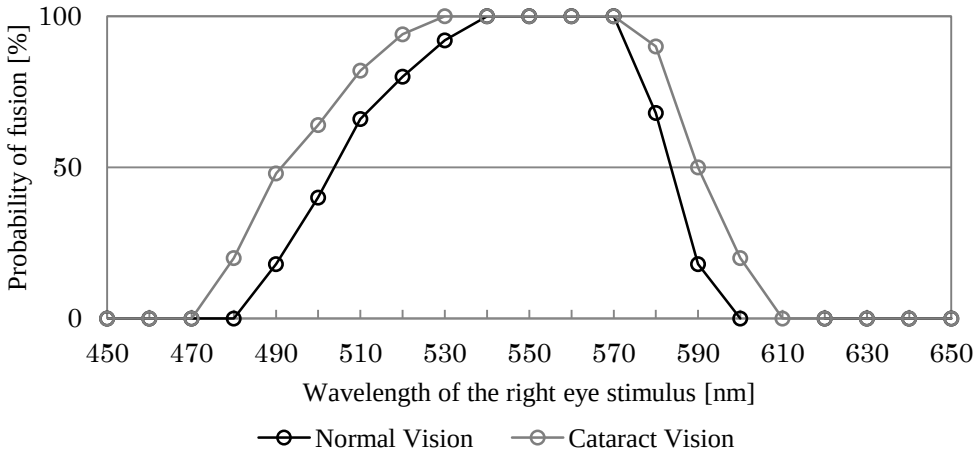

Fig. 5.3.12. Fusion probability curve in central vision when λ_{dl} = 560 nm.

The Fig. 5.3.11 and Fig. 5.3.12 display the fusion probability curve in central vision when λ_{dl} = 550 nm and 560 nm where the horizontal axis and the vertical axis indicate the wavelength of the right eye stimulus and the probability of fusion respectively. Cataract vision is plot by a grey line and normal vision is plot by a black line. On the basis of two figures, both visions are fusional from 530 nm to 560 nm and from 540 nm to 570 nm respectively, and the gradients of the fusion probability of both visions in Fig. 5.3.11 are larger than that in Fig. 5.3.12. It suggests that the performances of the fusion of both visions in Fig. 5.1.11 are better than that in Fig. 5.3.12.

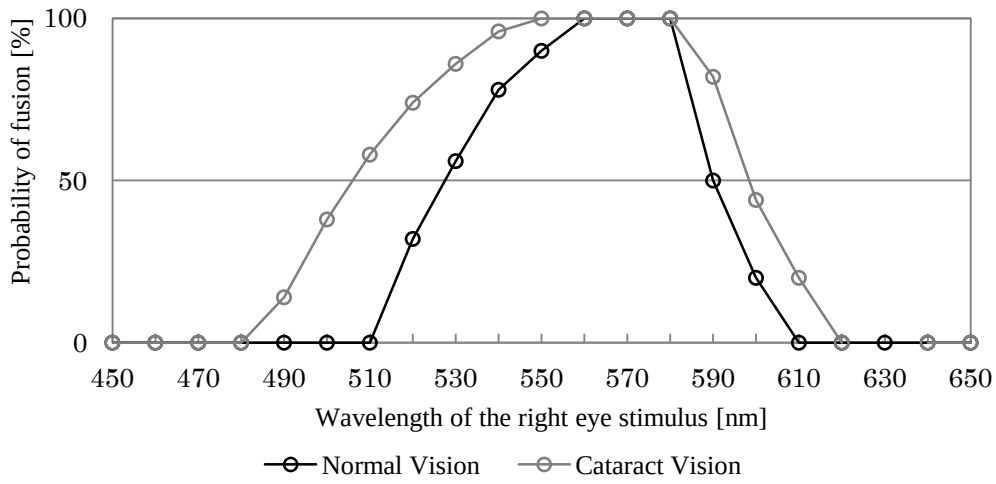

Fig. 5.3.13. Fusion probability curve in central vision when λ_{dl} = 570 nm.

In Fig. 5.3.13, we draw the fusion probability curve in central vision when λ_{dl} = 570 nm where the horizontal axis is the wavelength of the right eye stimulus and the vertical axis is the probability of fusion. A grey line and a black line represent cataract vision and normal vision respectively. This figure reveals that there are more 0 values on the left wavelengths and the range of the complete fusion between normal vision and cataract vision becomes short, illustrating that the difference of both visions increases.

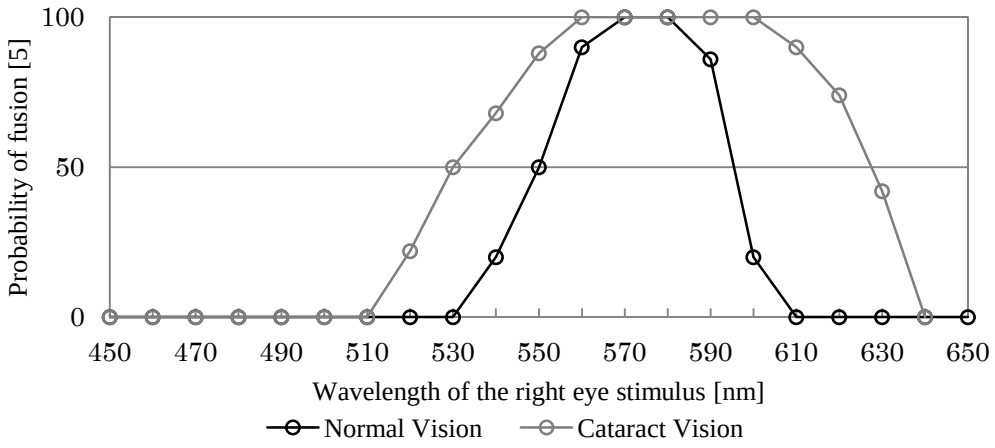

Fig. 5.3.14. Fusion probability curve in central vision when λ_{dl} = 580 nm.

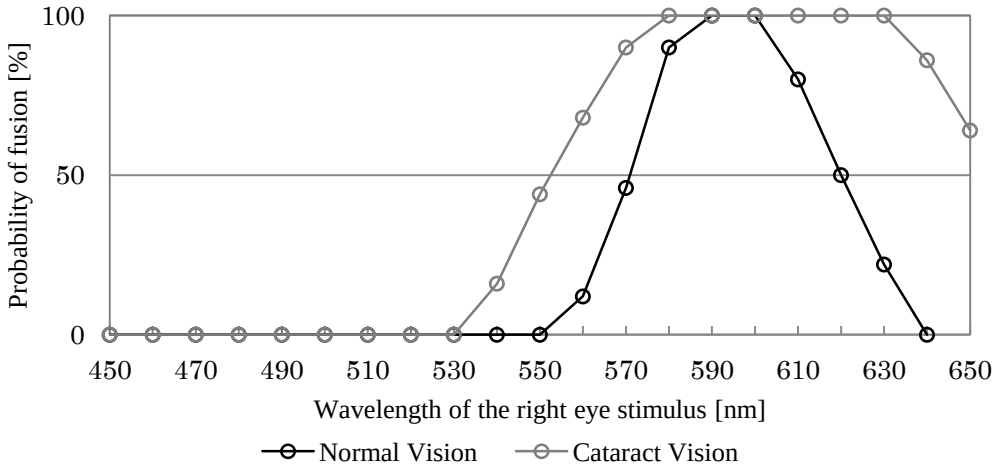

Fig. 5.3.15. Fusion probability curve in central vision when λ_{dl} = 590 nm.

When λ_{dl} = 580 nm and 590 nm, the fusion probability curve in central vision is shown in Fig. 5.3.14 and Fig. 5.3.15, where the vertical axis indicates the probability of fusion and the horizontal axis denotes the wavelength of the right eye stimulus. And normal vision is shown with a black line and cataract vision with a grey line. Compared

with above figures, there is the obvious difference where the range of the complete fusion between normal vision and cataract vision is only 10nm (i.e., 570-580 nm in Fig. 5.3.14 and 590-600 nm in Fig. 5.3.15). Meanwhile, the width of the fusion probability of normal vision further narrows and is much lower than that of cataract vision.

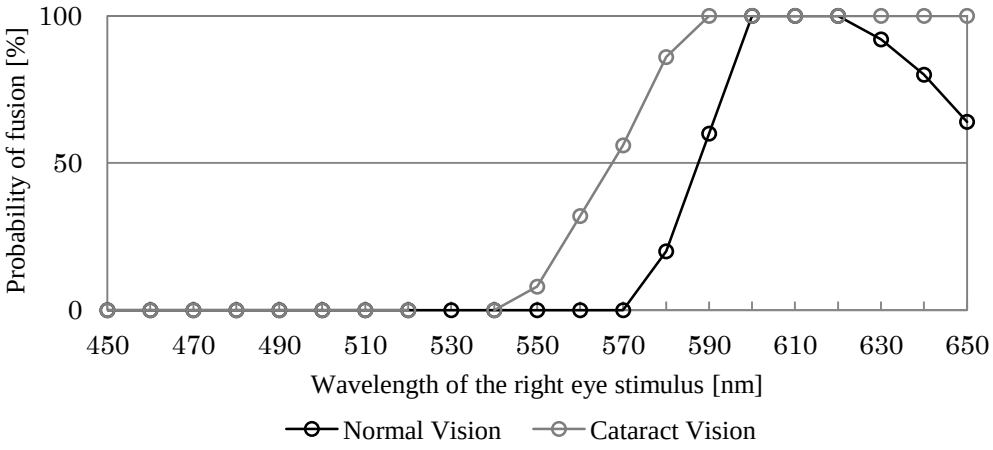

Fig. 5.3.16. Fusion probability curve in central vision when λ_{dl} = 600 nm.

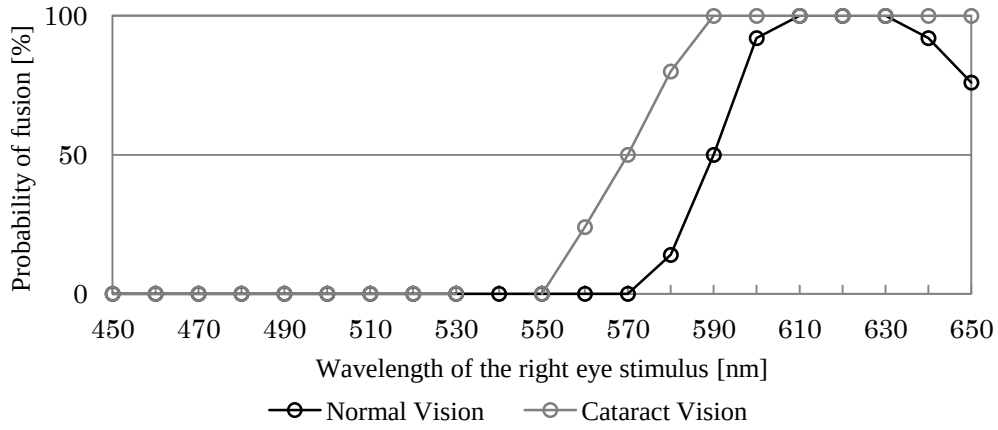

Fig. 5.3.17. Fusion probability curve in central vision when λ_{dl} = 610 nm.

Fig. 5.3.16 and Fig. 5.3.17 depict the fusion probability curve in central vision when λ_{dl} = 600 nm and 610 nm where the horizontal axis denotes the wavelength of the right eye stimulus, while the vertical axis represents the probability of fusion. Normal vision and cataract vision are described by a black line and a grey line respectively. These figures illustrate that the fusion probability of cataract vision maintains 100 % from 590 nm to 650 nm and the right curve of normal vision rises quickly to reduce the gap

between normal vision and cataract vision, where the range of the complete fusion is expanded to 20 nm (i.e., 600-620 nm in Fig. 5.3.16 and 610-630 nm in Fig. 5.3.17).

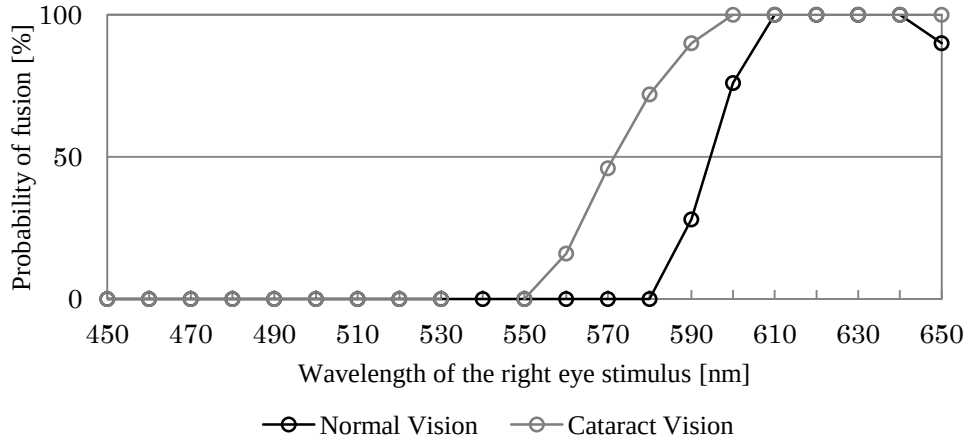

Fig. 5.3.18. Fusion probability curve in central vision when λ_{dl} = 620 nm.

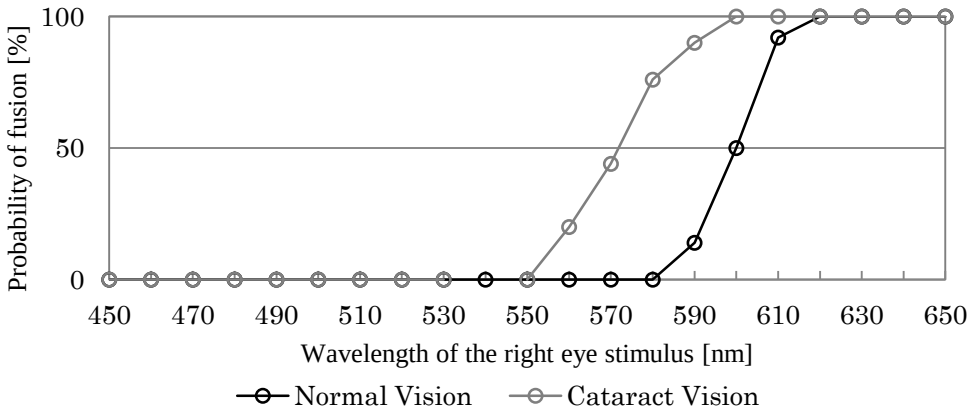

Fig. 5.3.19. Fusion probability curve in central vision when λ_{dl} = 630 nm.

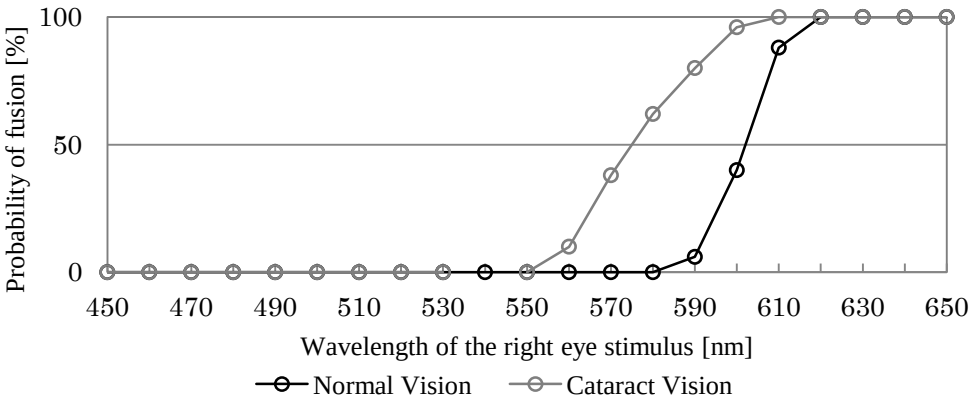

Fig. 5.3.20. Fusion probability curve in central vision when λ_{dl} = 640 nm.

In Fig. 5.3.18, Fig. 5.3.19 and Fig. 5.3.20, the fusion probability curve in central vision is plot when λ_{dl} = 620 nm, 630 nm and 640 nm where the horizontal axis represents the wavelength of the right eye stimulus and the vertical axis indicates the probability of fusion. To plot normal vision and cataract vision, a black line and a grey line are used respectively. It should be noted that the range of the complete fusion is further expanded to 30 nm, and the right curves of normal vision and cataract vision are fusional from 620 nm to 650 nm in Fig. 5.3.19 and Fig. 5.3.20, suggesting that the width of the fusion of cataract vision is larger than that of normal vision due to the different start points of two curves.

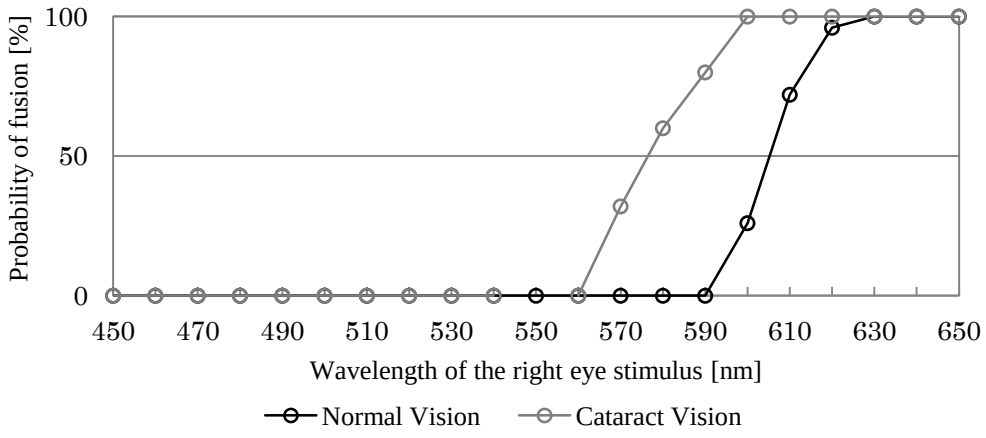

Fig. 5.3.21. Fusion probability curve in central vision when λ_{dl} = 650 nm.

Finally, the Fig. 5.3.21 shows the fusion probability curve in central vision when λ_{dl} = 650 nm where the wavelength of the right eye stimulus is illustrated by the horizontal axis and the vertical axis is to indicate the probability of fusion. From the figure, there is the similar situation compared with Fig. 5.3.20 and two curves are almost parallel.

5.4 Experimental results of peripheral vision

The results about peripheral vision 3°, 6°, 9° were shown from Fig. 5.4.1 to Fig. 5.4.21. The curves' data are obtained from the average values of five subjects. The probability of binocular fusion becomes lower with λ_{dr} far from λ_{dl}, whether towards a shorter or longer wavelength. The relation is quite evident in the date shown in the fllowing figures.

In Fig. 5.4.1, Fig. 5.4.2 and Fig. 5.4.3, we plot the fusion probability curve in peripheral vision when λ_{dl} = 450 nm, 460 nm and 470 nm respectively, where the horizontal axis denotes the wavelength of the right eye stimulus, while the vertical axis represents the probability of fusion. Normal vision 3°, 6° and 9° are illustrated by using a black line with triangle, diamond and starlike mark, and cataract vision 3°, 6° and 9° using a grey line with triangle, diamond and starlike mark, respectively. In Fig. 5.4.2, all the visions are fusional from 450 nm to 460 nm. The other figures show fusional visions are from 450 nm to 470 nm. From these figures, we can see that the fusion probability of normal visions decrease early, suggesting that the width of the fusion of cataract visions are larger than that of normal visions. Furthermore, the fusion range of both visions 9° are larger than that of both visions 6° and both visions 3° have the least fusion width.

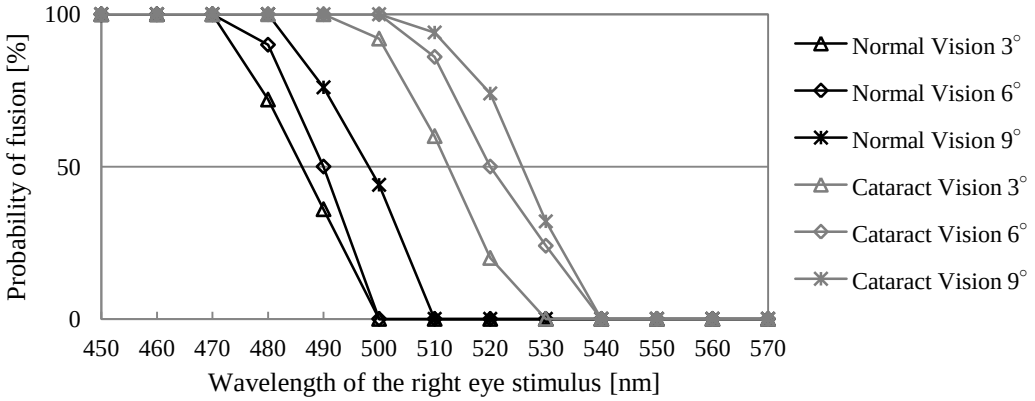

Fig. 5.4.1. Fusion probability curve in peripheral vision when λ_{dl} = 450 nm.

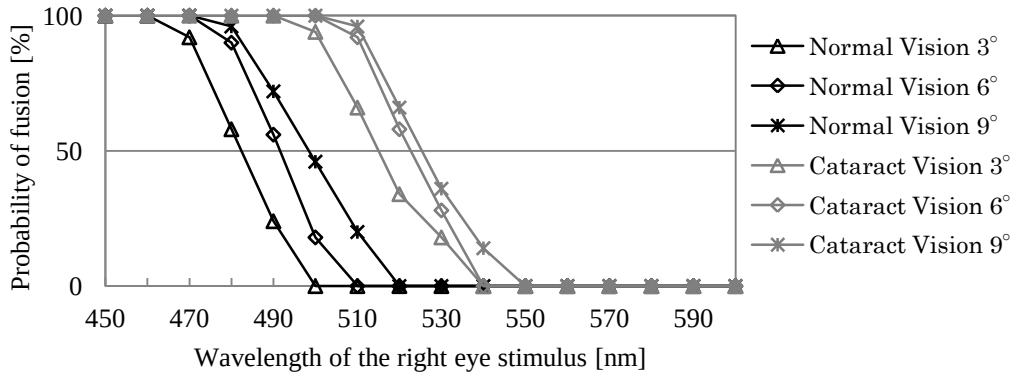

Fig. 5.4.2. Fusion probability curve in peripheral vision when λ_{dl} = 460 nm.

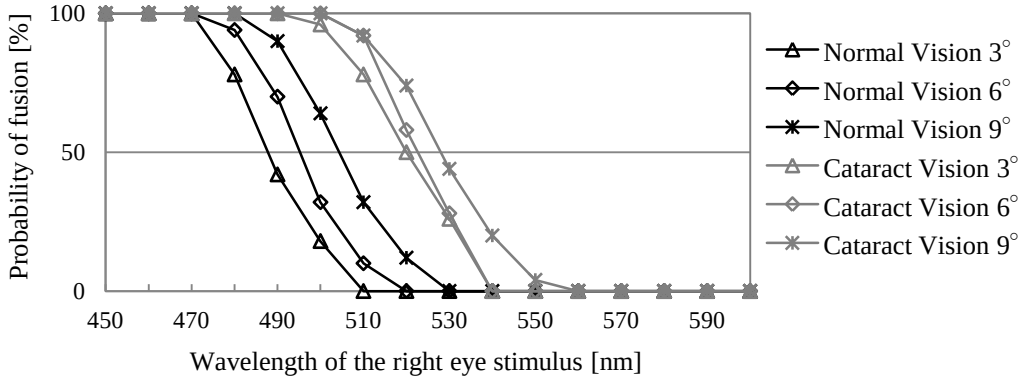

Fig. 5.4.3. Fusion probability curve in peripheral vision when λ_{dl} = 470 nm.

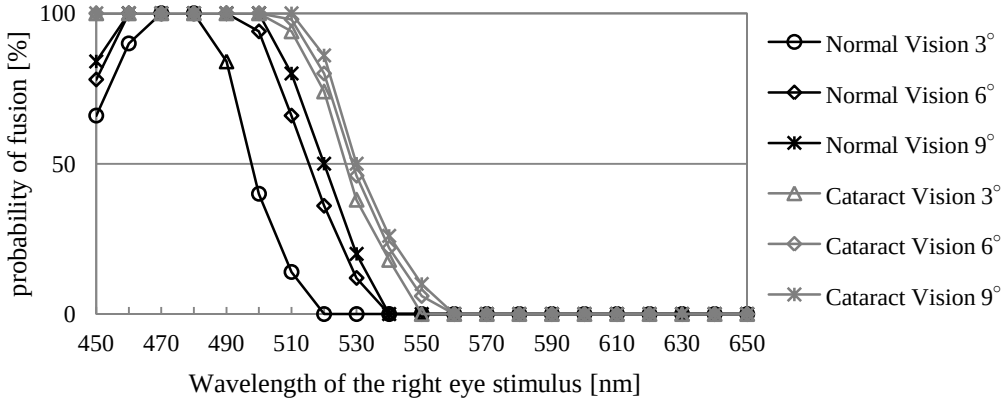

Fig. 5.4.4. Fusion probability curve in peripheral vision when λ_{dl} = 480 nm.

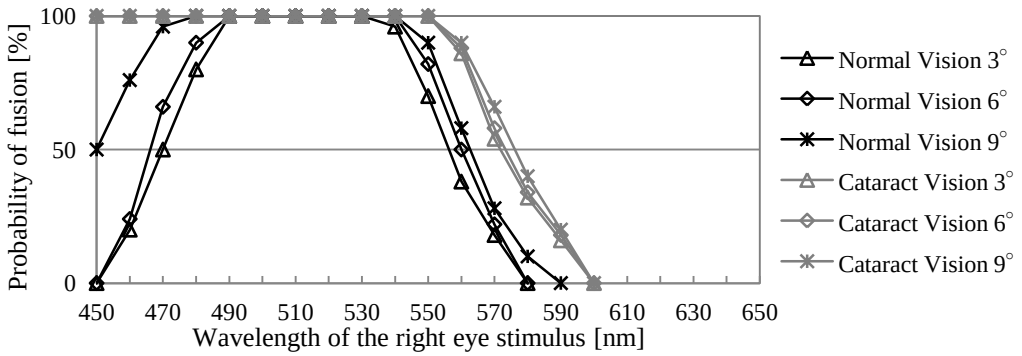

Fig. 5.4.5. Fusion probability curve in peripheral vision when λ_{dl} = 490 nm.

The Fig. 5.4.4 and Fig. 5.4.5 show the fusion probability curve in peripheral vision when λ_{dl} is 480 nm and 490 nm respectively, where the horizontal axis indicates the wavelength of the right eye stimulus and the vertical axis represents the probability of fusion. Normal vision 3°, 6°, 9° and cataract vision 3°, 6°, 9° are expressed by a black line and a grey line with triangle, diamond and starlike mark respectively in Fig. 5.4.5. And in Fig. 5.4.4, normal vision 3° uses a black line with circle mark. According to these figures, we can find that all the visions are fusional from 470 nm to 480 nm and from 490 nm to 530 nm respectively, and the fusion probability of all the cataract visions keep 100 % from 450 nm to 500 nm and 550 nm respectively, whereas left curves of normal visions decrease, where normal vision 3° decreases the most, indicating that the width of the fusion of all the visions are expanded and the gaps between normal visions and cataract visions are still large.

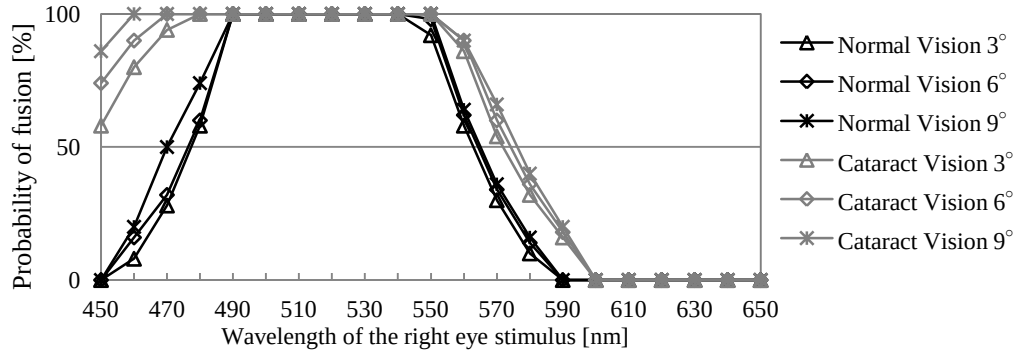

Fig. 5.4.6. Fusion probability curve in peripheral vision when λ_{dl} = 500 nm.

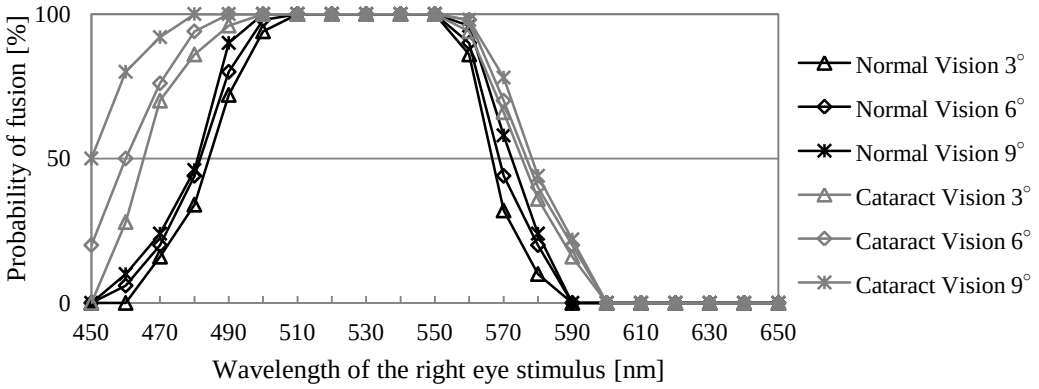

Fig. 5.4.7. Fusion probability curve in peripheral vision when λ_{dl} = 510 nm.

The fusion probability curve in peripheral vision when λ_{dl} = 500 nm and 510 nm where the horizontal axis is the wavelength of the right eye stimulus and the vertical axis denotes the probability of fusion is shown in Fig. 5.4.6 and Fig. 5.4.7. A black line with triangle, diamond and starlike mark indicates normal vision 3°, 6°, 9° and a grey line with triangle, diamond and starlike mark represents cataract vision 3°, 6°, 9°. From two figures, it can be observed that the fusion probability of cataract visions decrease on the left wavelength where cataract vision 3° decreases the most and cataract vision 6° takes second place, and all the visions are fusional from 490 nm to 540 nm and from 510 nm to 550 nm respectively, denoting that the difference of the fusion between cataract visions and normal visions reduces.

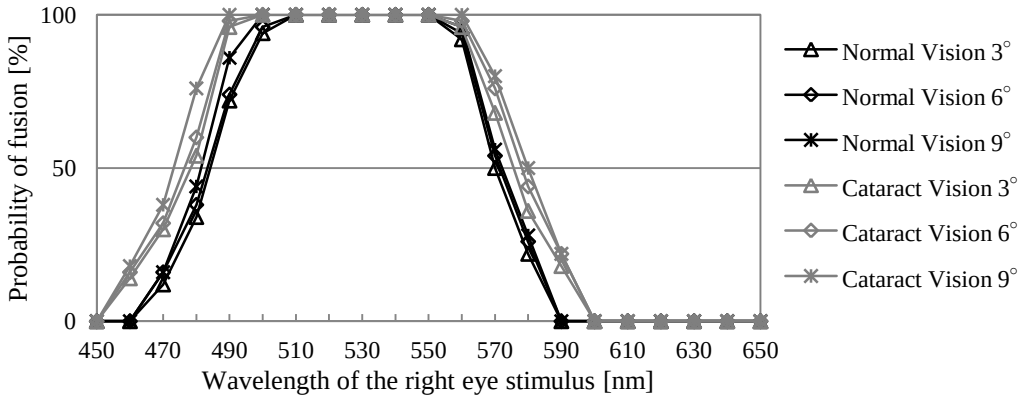

Fig. 5.4.8. Fusion probability curve in peripheral vision when λ_{dl} = 520 nm.

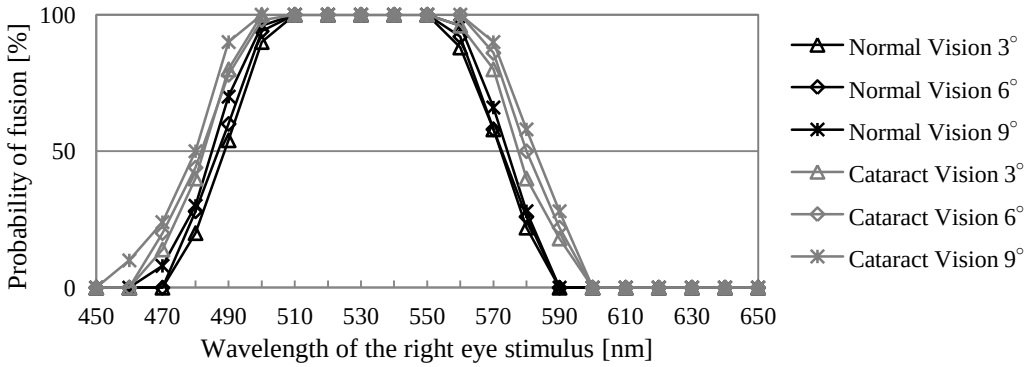

Fig. 5.4.9. Fusion probability curve in peripheral vision when λ_{dl} = 530 nm.

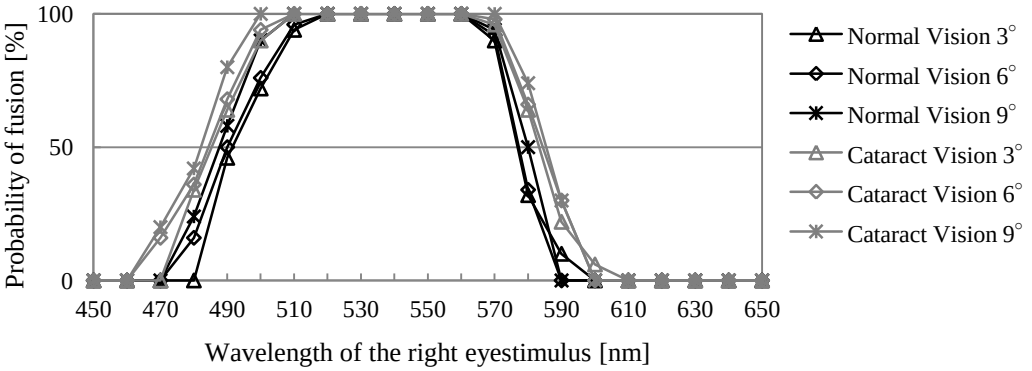

Fig. 5.4.10. Fusion probability curve in peripheral vision when λ_{dl} = 540 nm.

Fig. 5.4.8, Fig. 5.4.9 and Fig. 5.4.10 describe the fusion probability curve in peripheral vision when λ_{dl} = 520 nm, 530 nm and 540 nm respectively, where the horizontal axis denotes the wavelength of the right eye stimulus, while the vertical axis represents the probability of fusion. Normal vision 3°, 6°, 9° are illustrated using a black line with triangle, diamond and starlike mark, and cataract vision 3°, 6°, 9° using a grey line with triangle, diamond and starlike mark. In terms of these figures, we can notice that the fusion probability of cataract visions decrease quickly from 450 nm to 500nm and all the visions are fusional from 510 nm to 550 nm in Fig. 5.4.8 and Fig. 5.4.9, meanwhile, the fusion probability of all the visions are 0 on the left wavelength and the fusional range is from 520 nm to 560 nm in Fig. 5.4.10, meaning that the difference of fusion between normal visions and cataract visions reduce sharply and the range of the fusion of all the visions narrow.

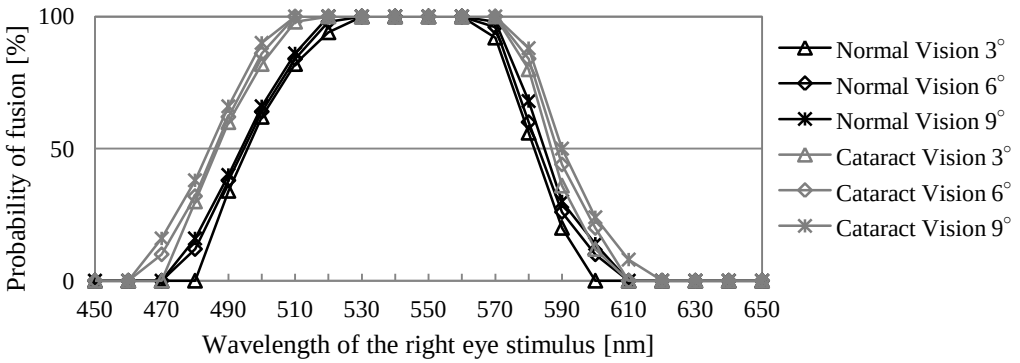

Fig. 5.4.11. Fusion probability curve in peripheral vision when λ_{dl} = 550 nm.

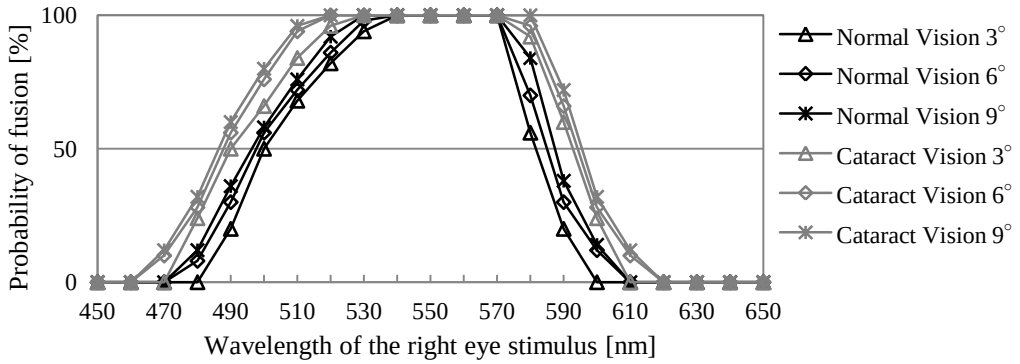

Fig. 5.4.12. Fusion probability curve in peripheral vision when λ_{dl} = 560 nm.

The Fig. 5.4.11 and Fig. 5.4.12 display the fusion probability curve in peripheral vision when λ_{dl} = 550 nm and 560 nm where the horizontal axis and the vertical axis indicate the wavelength of the right eye stimulus and the probability of fusion respectively. Cataract vision 3°, 6°, 9° are plot by a grey line with triangle, diamond and starlike mark and normal vision 3°, 6°, 9° are plot by a black line with triangle, diamond and starlike mark in Fig. 5.4.12, while a grey dashed is used to represent cataract visions in Fig. 5.4.11. On the basis of two figures, all the visions are fusional from 530 nm to 560 nm and from 540 nm to 570 nm respectively. In Fig. 5.4.11, the fusion probability curves of normal visions and cataract visions gather together respectively. It suggests that the difference of the fusion between normal visions and cataract visions still exist, whereas respective vision in each type has the similar performance (i.e., normal vision 3°, 6°, 9° and cataract vision 3°, 6°, 9°). However, in Fig. 5.4.12, the curve of each vision separates in normal visions and cataract visions.

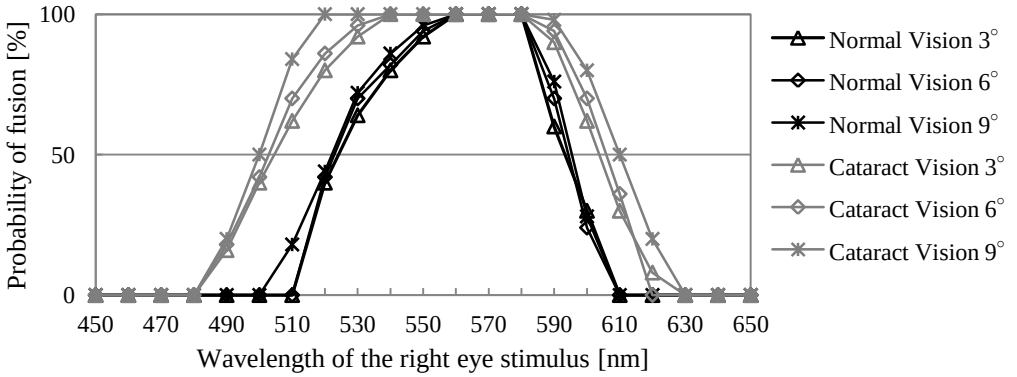

Fig. 5.4.13. Fusion probability curve in peripheral vision when λ_{dl} = 570 nm.

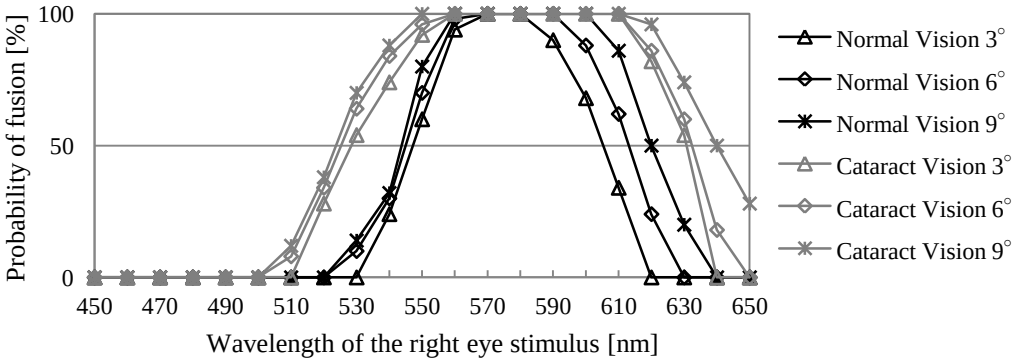

Fig. 5.4.14. Fusion probability curve in peripheral vision when λ_{dl} = 580 nm.

When λ_{dl} = 570 nm and 580 nm, the fusion probability curve in peripheral vision is shown in Fig. 5.4.13 and Fig. 5.4.14, where the vertical axis indicates the probability of fusion and the horizontal axis denotes the wavelength of the right eye stimulus. A grey line and a black line with triangle, diamond and starlike mark represent cataract vision 3°, 6°, 9° and normal vision 3°, 6°, 9° respectively. From Fig. 5.4.13, we can observe that all the visions are fusional from 560 nm to 580 nm and the width of the fusion of all the visions reduce. Meanwhile, the difference of both visions increases. In Fig. 5.4.14, the range of the complete fusion is from 570 nm to 580 nm and there are more 0 values on the left wavelength. The right curves of the fusion of both visions separate obviously, indicating that the performances of the declined curves are different from those of the ascending curves.

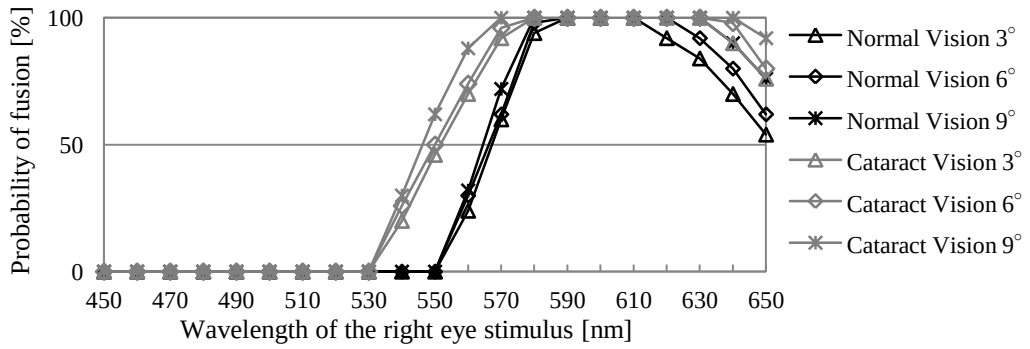

Fig. 5.4.15. Fusion probability curve in peripheral vision when λ_{dl} = 590 nm.

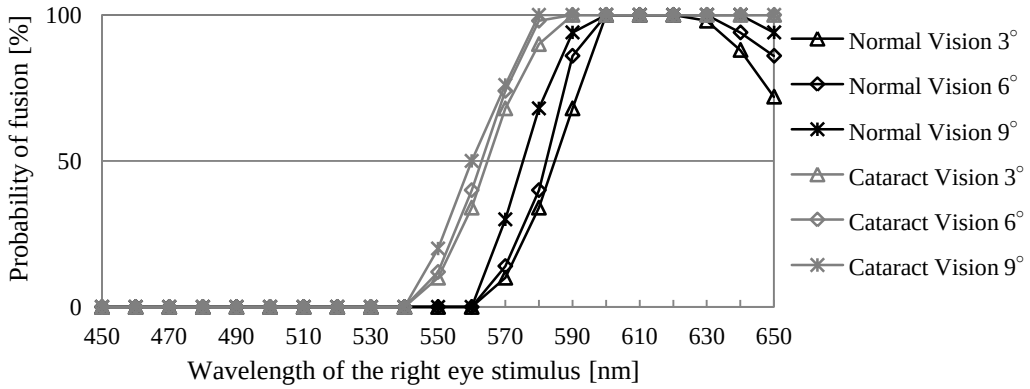

Fig. 5.4.16. Fusion probability curve in peripheral vision when λ_{dl} = 600 nm.

Fig. 5.4.15 and Fig. 5.4.16 present the fusion probability curve in peripheral vision when λ_{dl} = 590 nm and 600 nm where the horizontal axis denotes the wavelength of the right eye stimulus, while the vertical axis represents the probability of fusion. Normal vision 3°, 6°, 9° and cataract vision 3°, 6°, 9° are described by a black line and a grey line with triangle, diamond and starlike mark respectively. From these figures, the observation that the right curves of the whole visions rise quickly to reduce their gaps can be obtained, and the whole visions are fusional from 590 nm to 610 nm and from 600 nm to 620 nm respectively. Furthermore, the fusion probability of cataract visions maintains 100 % on the right wavelength in Fig. 5.4.16.

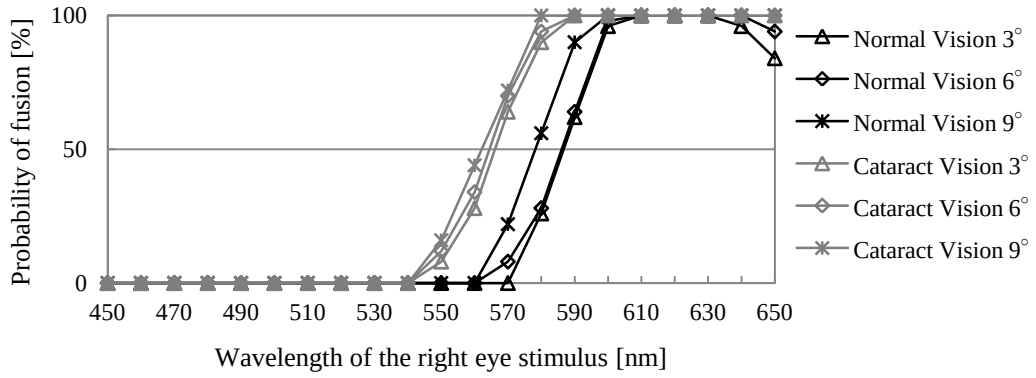

Fig. 5.4.17. Fusion probability curve in peripheral vision when λ_{dl} = 610 nm.

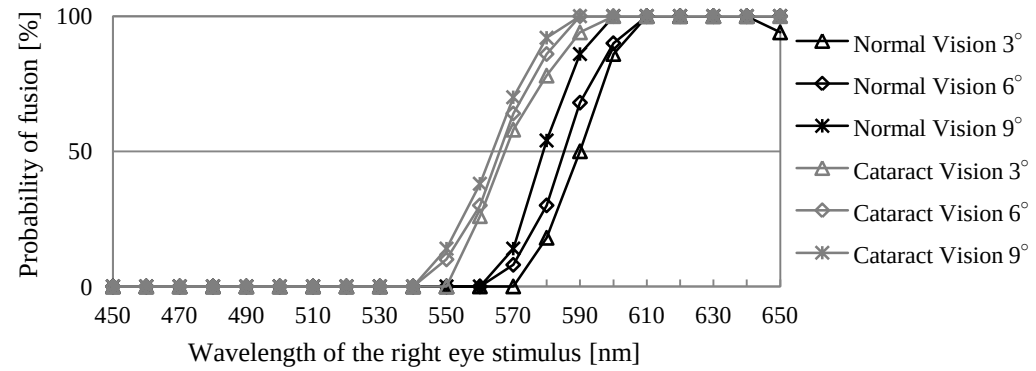

Fig. 5.4.18. Fusion probability curve in peripheral vision when λ_{dl} = 620 nm.

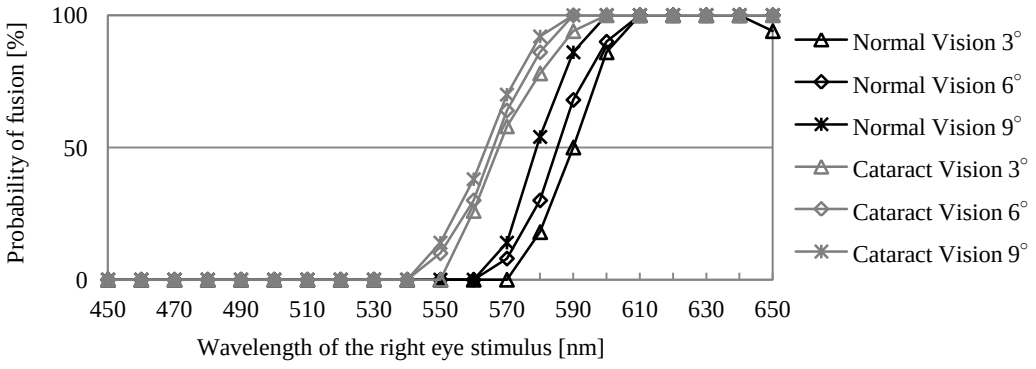

Fig. 5.4.19. Fusion probability curve in peripheral vision when λ_{dl} = 630 nm.

In Fig. 5.4.17, Fig. 5.4.18 and Fig. 5.4.19, the fusion probability curve in peripheral vision is plot when λ_{dl} = 610 nm, 620 nm and 630 nm where the horizontal axis represents the wavelength of the right eye stimulus and the vertical axis indicates the probability of fusion. To show normal vision 3°, 6°, 9° and cataract vision 3°, 6°, 9°, a black line and a grey line with triangle, diamond and starlike mark are used respectively.

These figures reveal that the right curves of normal visions further rise according to above figures and the width of the complete fusion is expanded from 20 nm to 30 nm (i.e., 610-630 nm in Fig. 5.4.17 and 610-640 nm in Fig. 5.4.18 and Fig. 5.4.19). It means that the gaps between normal visions and cataract visions further reduce.

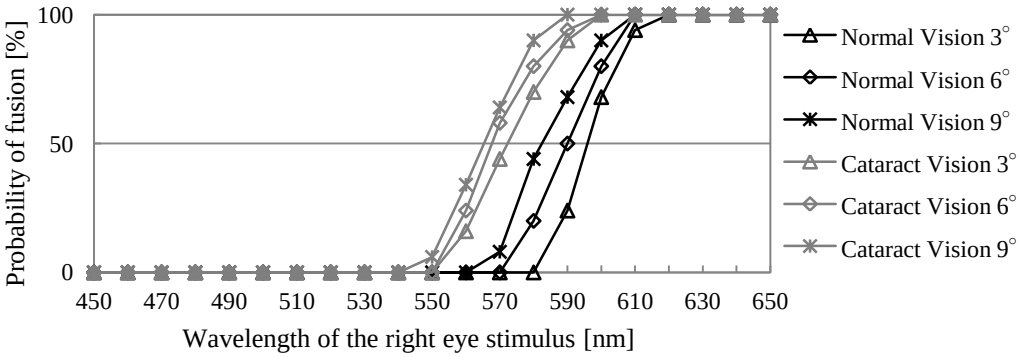

Fig. 5.4.20. Fusion probability curve in peripheral vision when λ_{dl} = 640 nm.

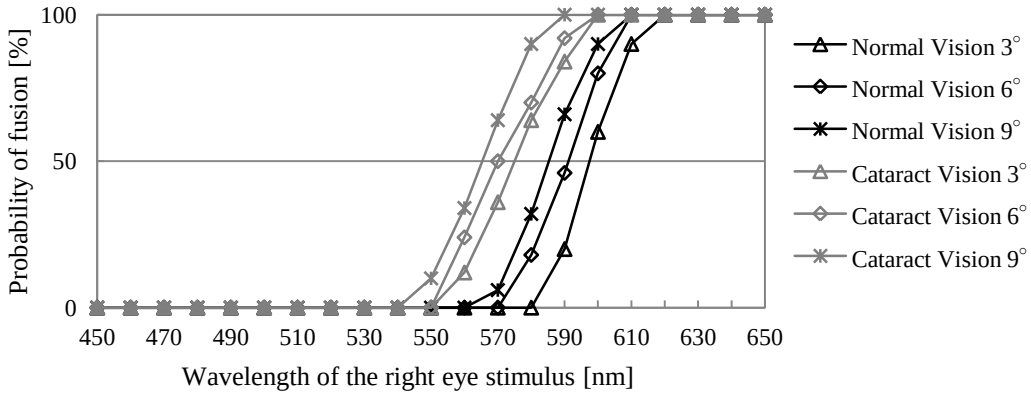

Fig. 5.4.21. Fusion probability curve in peripheral vision when λ_{dl} = 650 nm.

Fig. 5.4.20 and Fig. 5.4.21 show the fusion probability curve in peripheral vision when λ_{dl} = 640 nm and 650 nm. The horizontal axis indicates the wavelength of the right eye stimulus and the vertical axis denotes the probability of fusion. Normal vision 3°, 6°, 9° and cataract vision 3°, 6°, 9° are shown by a black line and a grey line with triangle, diamond and starlike mark respectively. In these figures, we can find that the right curves of normal visions and cataract visions are fusional from 620 nm to 650 nm and each curve is similarly parallel, suggesting that the width of the fusion of cataract visions are larger than that of normal visions due to the different start points and both visions 9° and 3° have the largest and the least width respectively.

5.5 Discussion and conclusions

5.5.1 Discussions

The results were obtained from five subjects. Three examples of the percentage P_d of the uniform homogeneous appearance versus λ_{dr} were shown in Fig. 5.5.1, where the results were illustrated for the wavelength of left eye stimulus λ_{dl} = 450 nm (a), 550 nm (b) and 650 nm (c).

$$p_d = \frac{\text{Total number of the stable homogeneity color view reports}}{\text{Total number of the inhomogeneus and alternant color view reports}} \quad (1)$$

The results show that, with λdr far from λdl, whether towards a shorter or longer wavelength, the probability of color fusion decreases and finally became 0 % either in normal vision or in cataract experiencing vision. In other words, the visual view of the subject became inhomogeneous or alternate along with the value of the difference between λdr and λdl being larger. On the contrary, when λdr was close to λdl, the color fusion probability Pd approached to 100 %, suggesting that the subject perceived a uniform homogeneity color view. Similar results had been reported in many previous studies. The result in Fig. 5.5.1 was quite illuminating to illustrate the characteristics of P_d. In Fig. 5.5.1 (a), when the stimuli whose wavelength of left eye was 450 nm and right eye was 460 nm were displayed to both eyes in central vision, all the subjects respond that they could receive the same one single color image. However, when the wavelength of left eye was kept constant and the wavelength of right eye was increased to 470 nm, someone began to create one impression with multiple colors rather than only one color, and the color rivalry started to take place once differences increased. Moreover, we also found that the color fusion probability increased with the increment of the retinal eccentricity in cataract experiencing vision.

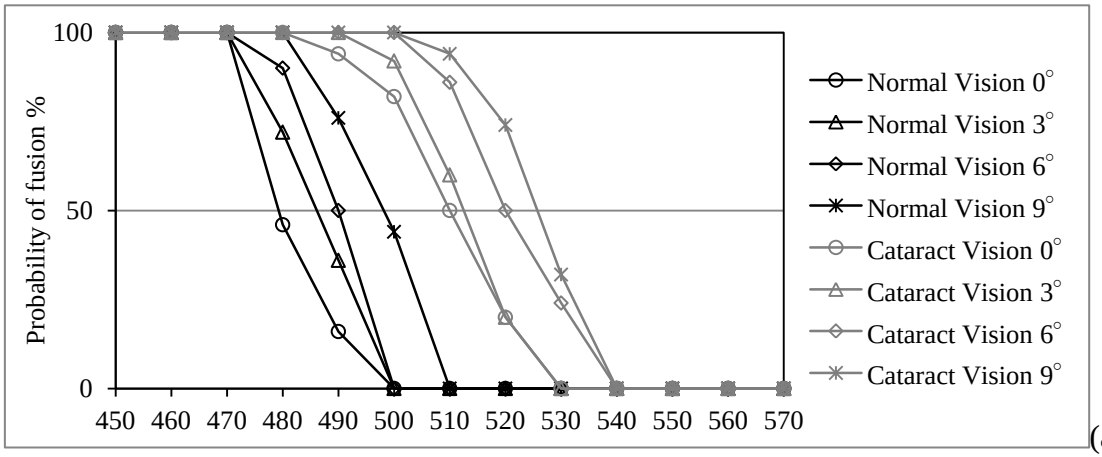

(a)

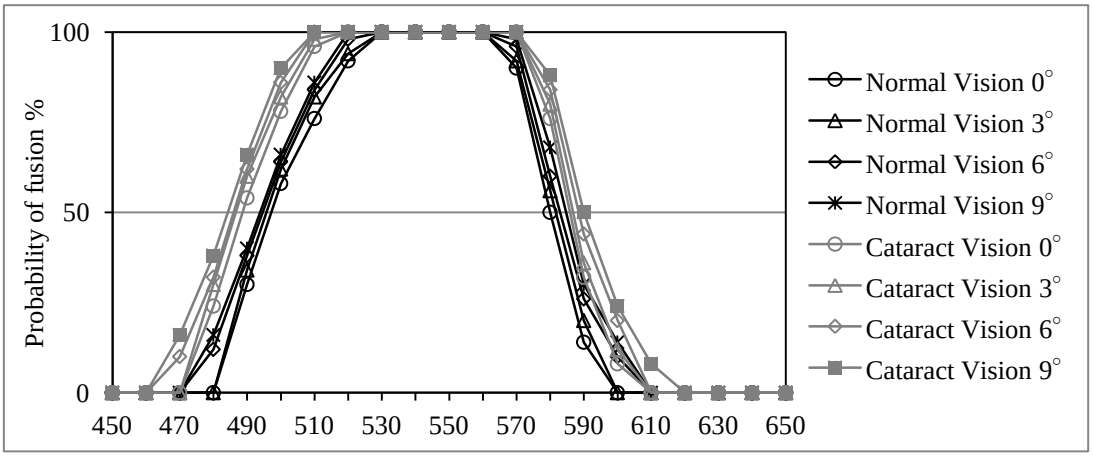

(b)

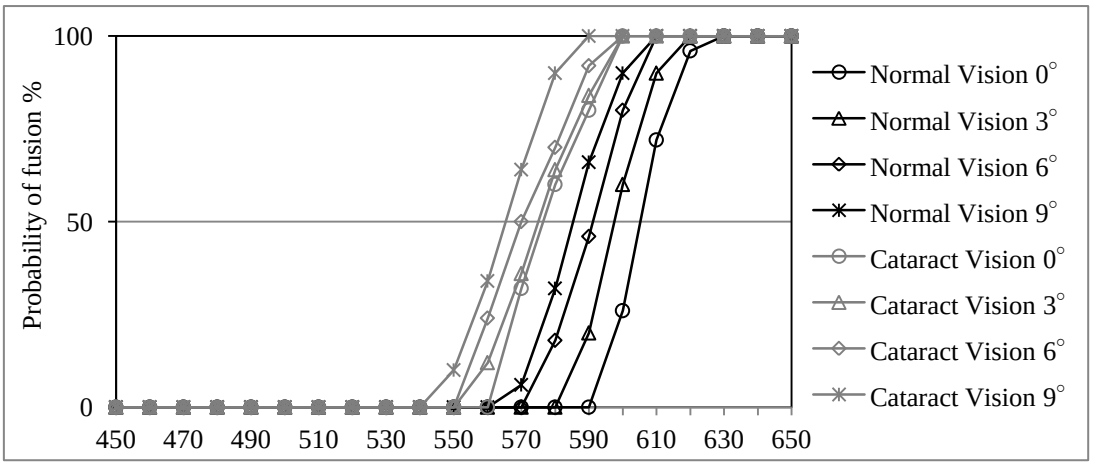

(c)

Fig.5.5.1. Fusion probability curve in peripheral vision for normal vision and cataract vision respectively when λ_{dl} = (a) 450, (b) 550, and (c) 650 nm.

In order to find out the relationship between fusion limits at each dominant wavelength with the retinal eccentricity, the same calculation used in many previous experiments was adopted. The calculation with a 50 % fusion criterion was used as the usual specifying threshold. By defining $\Delta\lambda_d = \lambda_{dr} - \lambda_{dl}$, two binocular color fusion limits, i.e., $\Delta\lambda_d+$ and $\Delta\lambda_d-$ were measurable. It should be note that, while λ_{dl} locates at the ends of the spectrum, only one $\Delta\lambda_d+$ or one $\Delta\lambda_d-$ could be obtained. For example, when λ_{dl} = 450 nm, any dominant wavelength λ_R below 450 nm could fuse with λ_{dl}, therefore, only one $\Delta\lambda_d+$ was obtained. Similarly, when λ_{dl} = 650 nm, only one $\Delta\lambda_d-$ was obtained. Color fusion limit curves $\Delta\lambda_d+$ and $\Delta\lambda_d-$ with the retinal eccentricity of 0° (central vision), 3°, 6° and 9° were plotted against λ_{dl} in the normal vision and the cataract experiencing vision respectively in Fig. 5.5.2.

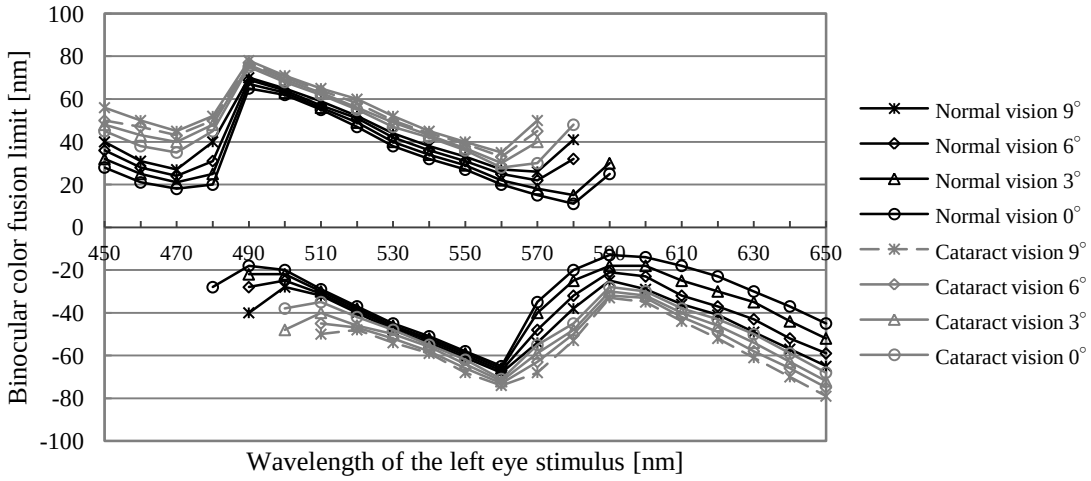

Fig. 5.5.2. Binocular color fusion limits in normal vision and that in cataract experiencing vision on each visual fields as a function of λ with the fusion probability above 50 %.

The data were summarized based on the average values from five subjects. The shapes of the $\Delta\lambda_d/\lambda_d$ function indicated very similar treadlines with the results of Ikeda and Qin et al. The results revealed that, in the normal vision, the color fusion limit $\Delta\lambda_{dn}$ was within a range about 11~65 nm on the central vision, 15~67 nm on the retinal eccentricity of 3°, 21~69 nm on the retinal eccentricity of 6°, and 25~70 nm on the retinal eccentricity of 9° as shown in Table 1. In the cataract experiencing vision, the color fusion limit $\Delta\lambda_{dc}$ was within a range about 28~75 nm on the central vision, 30~76

nm on the retinal eccentricity of 3°, 32~77 nm on the retinal eccentricity of 6°, and 33~79 nm on the retinal eccentricity of 9° as shown in Table 2.

The above results also appeared to suggest that, the binocular color fusion limit was increased along with the retinal eccentricity increasing, and the binocular color fusion limit in the cataract experiencing vision $\Delta\lambda_{dc}$ was wider than that in the normal vision $\Delta\lambda_{dn}$ or the cataract experiencing vision at each retinal eccentricity. In addition, we found the minimum value of the binocular color fusion limit existing in 590 nm both in the normal vision and the cataract experiencing vision. This result was very similar with the pointview that the minimum value of the monocular wavelength discrimination curve was in the range of 580~600 nm found by Wright & Pitt.

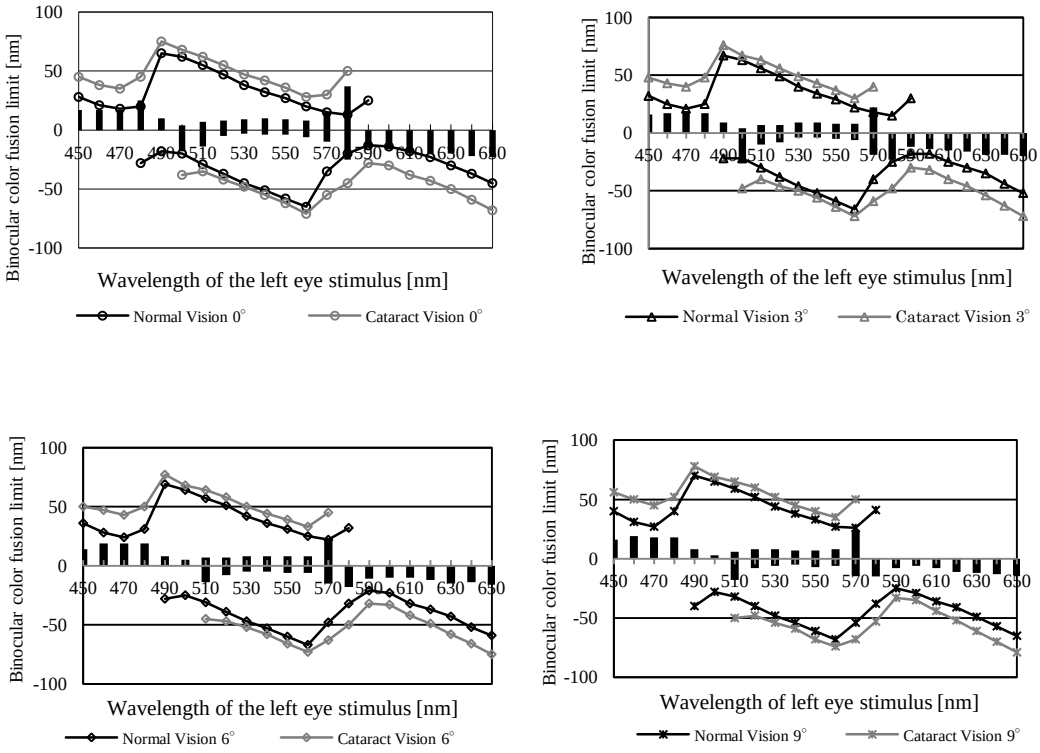

Fig. 5.5.3. The wavelength difference of the binocular color fusion limit between the normal vision and the experiencing cataract vision at each retinal eccentricity.

On the contrary, we tried to find the relationship between $\Delta\lambda_{dn}$ and $\Delta\lambda_{dc}$ with the multiples of retinal eccentricity which was set linearly increasing. The results revealed that there was no relevance arithmetic progression and binocular color fusion limit. Then, we plotted the wavelength difference of the binocular color fusion limit between

the normal vision and the cataract experiencing vision at each retinal eccentricity in Fig. 5.5.3. We noticed that the growth of $\Delta\lambda_d$ at the two ends of spectrum was faster than that at the middle section of spectrum with the increment of the retinal eccentricity both in the normal vision and the cataract experiencing vision. The columns show the wavelength difference between the normal vision and the cataract experiencing vision. Moreover, several experiments were conducted to make a qualitative investigation. Compared with the binocular color fusion limit of the normal vision $\Delta\lambda_{dn}$, the binocular color fusion limit in cataract experiencing vision $\Delta\lambda_{dc}$ was approximately 3~39 nm increased on the central vision, 4~22 nm on the retinal eccentricity of 3°, 5~23 nm on the retinal eccentricity of 6°, and 5~24 nm on the retinal eccentricity of 9°. We noticed that the $\Delta\lambda_d$ increased steadily with the decrease of the retinal eccentricity of stimuli.

Table 5.1 Binocular color fusion limit in normal vision.

	Δλmin-	Δλmax-	Δλmin+	Δλmax+
Central vision	13 nm	65 nm	11 nm	65 nm
peripheral vision 3°	18 nm	66 nm	15 nm	67 nm
peripheral vision 6°	21 nm	67 nm	22 nm	69 nm
peripheral vision 9°	25 nm	68 nm	26 nm	70 nm

Table 5.2 Binocular color fusion limit in cataract experiencing vision.

	Δλmin-	Δλmax-	Δλmin+	Δλmax+
Central vision	28 nm	71 nm	28 nm	75 nm
peripheral vision 3°	30 nm	72 nm	30 nm	76 nm
peripheral vision 6°	32 nm	75 nm	33 nm	77 nm
peripheral vision 9°	33 nm	79 nm	35 nm	79 nm

5.5.2 Conclusions

In this study, we propose a method to measure the binocular color fusion limit using a three-dimensional display. The quantitative data $\Delta\lambda$ for each λ on peripheral vision were seldom measured perhaps because of the difficulty in displaying the correct stimuli at the correct location. Hence, to simplify the experimental procedure and control the stimuli such as shape, size, position and color of both eyes accurately, we used a three-dimensional display connected to a computer to present experimental stimuli conveniently, although, in general, a LCD shutter has a limited range of reduction of the cross-talk, and this cross-talk causes a certain amount of artifact. The experimental results reveal the fundamental data which lead us to further understand the factors influencing the color fusion limits $\Delta\lambda_d$ for each dominant wavelength λ_d at different peripheral visual fields. The results revealed that, in the normal vision, the color fusion limit $\Delta\lambda_{dn}$ was within a range about 11~65 nm on the central vision, 15~67 nm on the retinal eccentricity of 3°, 21~69 nm on the retinal eccentricity of 6°, and 25~70 nm on the retinal eccentricity of 9°. In the cataract experiencing vision, the color fusion limit $\Delta\lambda_{dc}$ was within a range about 28~75 nm on the central vision, 30~76 nm on the retinal eccentricity of 3°, 32~77 nm on the retinal eccentricity of 6°, and 33~79 nm on the retinal eccentricity of 9°. We noticed that the $\Delta\lambda_d$ increases steadily with the decrease of the retinal eccentricity of stimuli. We plan to measure the binocular color limit under much higher retinal eccentricity, so that we can further determine the relation of the ratio of retinal eccentricity with the change of $\Delta\lambda_d$. Also it is planned to measure the binocular color limit, not only for horizontal meridian, but also for all other directions.

Generally, the study of the binocular color fusion limits between the normal vision and the cataract experiencing vision revealed that, the value of such fusion limits in cataract experiencing vision was wider than those in the normal vision. To the best of our knowledge, this was the first report to find out such revelation. It is worth emphasizing that, although the subjects were not the actual elderly, the equipment was able to simulate the conditions as likely as possible. It reveals that similar limit values are observed in the range of 520~560 nm both in normal and cataract experiencing

visions, which might give some potential evidences for designing three-dimensional equipment.

Ikeda and Nakashima hypothesized that rivalry occurred when antagonistic (opponent) chromatic responses from each eye exceeded a threshold value. For example, if the wavelength presented to one eye appeared reddish yellow, then rivalry would occur when either the green or blue chromatic response from the other eye surpassed the critical threshold value. Their model worked well in prediction rivalry between wavelengths in the mid-spectral region. However, it predicted that dichoptic mixtures of violet lights or red lights would be stable, whereas the data showed that rivalry occurred. Discrepancies for these mixtures may have resulted from using previously published color opponent functions instead of their subjects' opponent functions to compute the antagonistic chromatic responses, rather than a basic failure in their model.

Chapter 6

Empirical and EEG evidences of binocular color fusion

6.1 EEG rhythms

At the root of all our thoughts, emotions and behaviors is the communication between neurons within our brains. Brainwaves are produced by synchronised electrical pulses from masses of neurons communicating with each other. Brainwaves are detected using sensors placed on the scalp. They are divided into bandwidths to describe their functions (below), but are best thought of as a continuous spectrum of consciousness; Delta being slow, loud and functional - to Gamma being fast, subtle, and complex. It is a handy analogy to think of Brainwaves as musical notes - the low frequency waves like a deeply penetrating drum beat, while the higher frequency brainwaves are like a subtle high pitched flute. Brain waves are divided into five different bandwidths that are believed to create a spectrum of human consciousness. Our brain waves change throughout the day and are part of a feedback loop that is influenced by what we're doing, thinking, and feeling emotionally at any given time—or while we sleep.

Delta waves (0.5 to 3 Hz)

Delta brainwaves are the slowest but loudest brainwaves (low frequency and deeply penetrating, like a drum beat). They are generated in deepest meditation and dreamless sleep. Delta waves suspend external awareness and are the source of empathy. Healing and regeneration are stimulated in this state, and that is why deep restorative sleep is so essential to the healing process.

Theta waves (3 to 8 Hz)

Theta brainwaves occur often in sleep mostly, and also dominant in deep meditation. It acts as our gateway to learning and memory. In theta, our senses are withdrawn from the external world and focused on signals originating from within. It is that twilight state which we normally only experience fleetingly as we wake or drift off to sleep. In theta we are in a dream; vivid imagery, intuition and information beyond our normal conscious awareness. It's where we hold our 'stuff', our fears, troubled history, and nightmares.

Alpha waves (8 to 13 Hz)

Alpha brainwaves are dominant during quietly flowing thoughts, and in some meditative states. Alpha is 'the power of now', being here, in the present. Alpha is the resting state for the brain. Alpha waves aid overall mental coordination, calmness, alertness, mind/body integration and learning.

In 1924, a Germany physiologist and psychiatrist named Hans Berger recorded the first human EEG. Berger also invented the electroencephalogram and gave the device its name. This invention has been described as, "one of the most surprising, remarkable, and momentous developments in the history of clinical neurology". EEG oscillations that occur during arousal, sleep and absence seizures are generated in the thalamic and cortical networks that are mutually connected (Steriade et al., 1993; McCormick and Bal, 1997). The alpha rhythms (8-13 Hz) are seen in the EEG mainly during relaxed wakefulness. It is well known that when a subject focuses attention on a particular sensory modality the corresponding alpha EEG activity decreases, as was classically demonstrated for the alpha activity of the posterior regions of the brain by Berger and thereafter studied in detail (see review inNiedermeyer and Lopes da Silva, 1999). The EEG varies with activity, both in humans and other animals, and particularly with the sleep-wakefulness cycle. Classically, because alpha power was larger with eyes closed than with eyes open, it was thought that alpha reflected a relaxed, unoccupied brain. An overall decrease in alpha power, has been linked to increasing demands of attention, alertness and task load in general.

They were the first brain waves ever detected, hence named after the first letter in the Greek alphabet – Alpha. Alpha brain waves have electrical frequencies between 8-13 hertz. They are generated in the Thalamus (the brain within the brain). Alpha brain waves are most present in a wakeful state that is characterized by a relaxed and effortless alertness. Alpha states have been described variously as sublime, flying, floating, lightness, peace, and tranquility. Alpha brain waves are not always present. For example, if someone is in deep sleep or in intense anger there are almost no Alpha brain wave.

Beta waves (13 to 38 Hz)

Beta brainwaves dominate our normal waking state of consciousness when attention is directed towards cognitive tasks and the outside world. Beta is a 'fast' activity, present when we are alert, attentive, engaged in problem solving, judgment, decision making, and engaged in focused mental activity.

Gamma waves (13 to 38 Hz)

Gamma brainwaves are the fastest of brain waves (high frequency, like a flute), and relate to simultaneous processing of information from different brain areas. It passes information rapidly, and as the most subtle of the brainwave frequencies, the mind has to be quiet to access it. Gamma was traditionally dismissed as 'spare brain noise' until researchers discovered it was highly active when in states of universal love, altruism, and the 'higher virtues'. Gamma rhythms modulate perception and consciousness, disappearing under anaesthesia. Gamma is also above the frequency of neuronal firing, so how it is generated remains a mystery. The presence of Gamma relates to expanded consciousness and spiritual emergence.

Generally, our brainwaves change according to what we're doing and feeling. When slower brainwaves are dominant we can feel tired, slow, sluggish, or dreamy. The higher frequencies are dominant when we feel wired, or hyper-alert. The descriptions that follow are only broadly descriptions - in practice things are far more complex, and brainwaves reflect different aspects when they occur in different locations in the

brain. Brainwave speed is measured in Hertz (cycles per second) and they are divided into bands delineating slow, moderate, and fast waves.

Our brainwave profile and our daily experience of the world are inseparable. When our brainwaves are out of balance, there will be corresponding problems in our emotional or neuro-physical health. Research has identified brainwave patterns associated with all sorts of emotional and neurological conditions. The brain mediates our perception every wave of emotion, every thought, every sensation you have corresponds to activity in your brain. The brain drives our ability to pay attention, our emotional balance, central nervous system tone, autoimmune function and more.

6.2 Experimental method and procedure

In this study, we also carried out EEG based experiments to further find out the relationship between the fusion limit and the brainwave rhythm. EEG was recorded at all 64 scalp sites to acquire the signals of the brain activity show in Fig. 6.2.1.

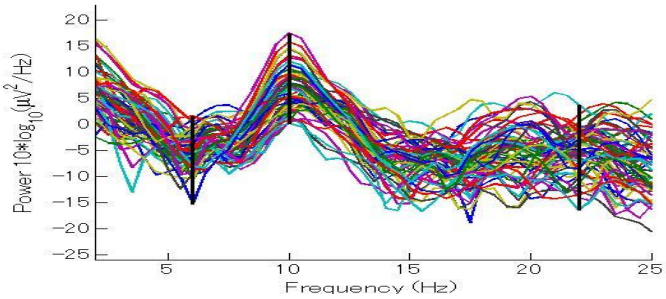

Fig.6.2.1. The values of energy variation diagram of EEG recorded on 64 channels.

In EEG based experiments, the fast and middle alpha-variant rhythms (Markand 1990) on the front of the brain (locations Fp1, Fpz and Fp2) were recorded and analyzed. The fast alpha-variant rhythm (11~13 Hz) is reported to be related with the state of conscious concentration, while the middle alpha-variant rhythm (9~11 Hz) appears when the subject is under relaxation. The original data is analyzed by the EEGlab which is the toolbox for processing continuous and event-related EEG using independent component analysis (ICA), time/frequency analysis, artifice rejection and several modes

of data visualization. To remove the residual gradient artifacts, a 8-18 Hz hand-pass filter was applied to the data. ICA was carried out in the Fieldtrip toolbox for EEG/Meg-analysis, using the runica algorithm (Makeig et al., 1997; Delorme and Makeig, 2004; Hu et al., 2015; Cong et al., 2015) implemented in EEGLAB version 5.03 (Delorme and Makeig, 2004; Slagter et al., 2016; Voytek et al., 2015). Both Fieldtrip and EEGLAB run under matlab (MathWorks, Natick, Ma). The experimental environment was design as the same as the experimental of the binocular color fusion limit, where the subject seated in front of the display device and was presented dichoptically a binocular view through the optical polarization action of the image splitter installed behind the liquid crystal display panel. A chin-rest and head-rest system was utilized to fix the head of the subject against sliding. All experiments were carried out in a darkroom and each subject was required to adapt for the dark environment about 15 min. within the darkroom. A left eye stimulus with wavelength of λ_L and a right eye stimulus with wavelength of λ_R were set respectively. The subject gradually increases the disparity in fused dischoptic stimuli until the subject reports diplopia. Then starting with the stimuli well separated, disparity is decreased until the subject reports fusion. In the EEG based experiments, the fast and middle alpha-variant rhythms (Markand, 1990) on the front of the brain (locations Fp1, Fpz and Fp2) were recorded and analyzed. The fast alpha-variant rhythm (11~13 Hz) is reported to be related with the state of conscious concentration, while the middle alpha-variant rhythm (9~11 Hz) appears when the subject is under relaxation. In the experiment of normal vision, the wavelength of the stimuli for the left eye was set to be blue, green, yellow and red, and that for the right eye was set to be 450~650 nm with the equal intervals of 10 nm. In the experiment of experiencing cataract vision, a specialized goggle (produced by the government of Ontario, Canada) was used for simulating the cataract. Considering brightness reduction caused by the spectral transmittance of the crystalline lens of the elderly (Van Den Berg and Tan 1994), the intensity of the simulation light was set to 30cd / m^2, the wavelength of the stimuli for the left eye was also set to be blue, green, yellow and red, and that for the right eye was set to be 450~650 nm with the equal intervals of 10 nm. About 10s interval was required between the two exposures. The subjects included 3 students aged average of 23 years old with normal or

corrected to normal visual acuities. Subjects were also recruited from the Visual and Auditory Information Processing Lab of the Faculty of Engineering in the University of Toyama.

6.3 Experimental results of normal vision

Fig. 6.3.1- Fig. 6.3.3 showed the EEG based energy variation diagram obtained by EEGlab and the locations Fp1, Fpz and Fp2 used in the experiment for each subject on binocular color fusion (BF) with the normal vision, which the stimuli ware set as blue to blue, or red to red (Opponent, Hering, 1892).

In Fig. 6.3.1, the values of energy variation diagram of EEG for the subject A when the binocular color fusion occurs were depicted, where the horizontal axis denotes the rhythms of the EEG in hertz, and the vertical axis represents the value of the energy calculated by EEGlab. Fp1, Fp2, Fpz represent three locations where EEG was recorded. From this figure, it is apparent that three curves exhibit almost the same trend lines, increasing from 8 Hz to 11 Hz, and thereafter decreasing from 12 Hz to 16 Hz. From 16 Hz to 18 Hz, the energy obtained showed disordered. However, only small values were acquired within these hertz. The peaks of three curves (i.e. the middle alpha-variant rhythm) were located at 9 Hz ~11 Hz, suggesting that the subject was under relaxation.

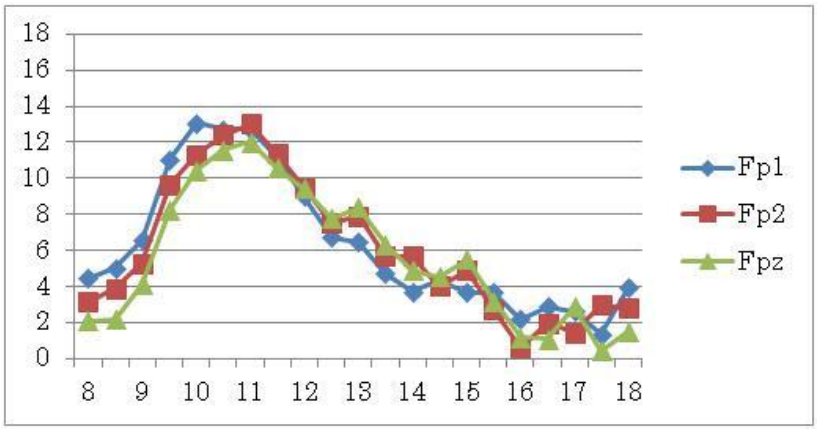

Fig. 6.3.1. The values of energy variation diagram of EEG for subject A on binocular fusion.

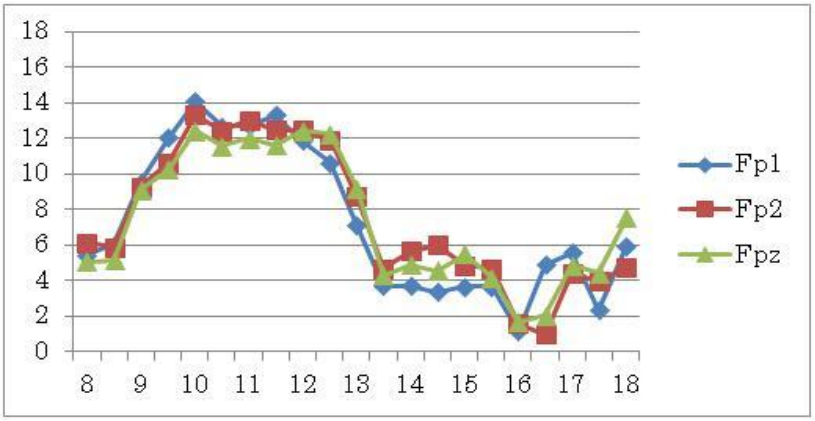

Fig. 6.3.2. The values of energy variation diagram of EEG for subject B on binocular fusion.

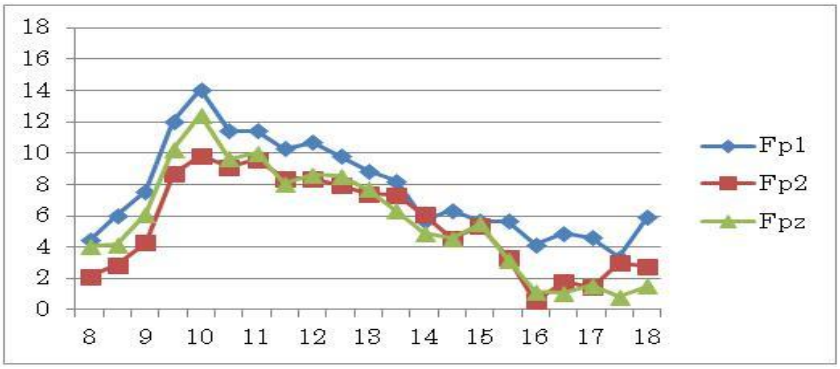

Fig. 6.3.3. The values of energy variation diagram of EEG for subject C on binocular fusion.

The results in Fig. 6.3.2 and Fig. 6.3.3 were illustrated based on the other two subjects B and C. It was clear that similar results and trend lines were obtained in the two figures, which consistently suggested that the subjects under relaxation were easier to view 3D objects.

On the other hand, the EEG based energy variation diagram on binocular color rivalry (BR), which the stimuli ware set as blue to yellow, or green to red was shown in Fig. 6.3.4-Fig. 6.3.6. In Fig. 6.3.4, the values of energy variation diagram of EEG for the subject A when the binocular color rivalry occurs were depicted, where the horizontal axis denotes the rhythms of the EEG in hertz, and the vertical axis represents the value of the energy calculated by EEGlab. Fp1, Fp2, Fpz represent three locations where EEG was recorded. From this figure, it is apparent that three curves exhibit almost the same trend lines, increasing from 8 Hz to 13 Hz, and thereafter decreasing from 13 Hz to 18

Hz. The peaks of three curves (i.e. the middle alpha-variant rhythm) were located at 11 Hz ~13 Hz, suggesting that the subject was nearly with the state of conscious concentration.

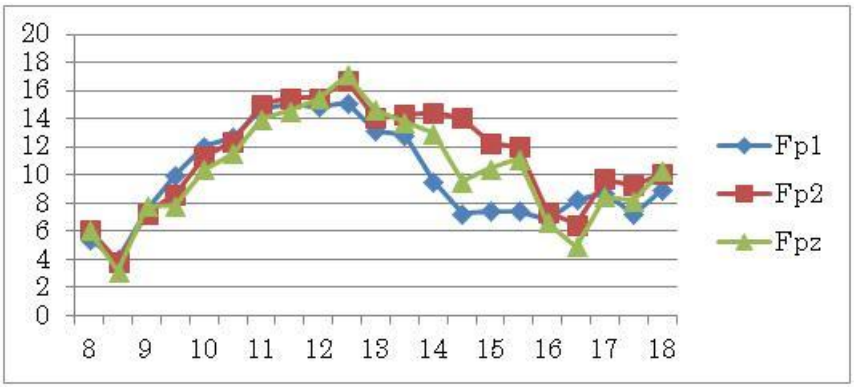

Fig. 6.3.4. The values of energy variation diagram of EEG for subject A on binocular rivalry.

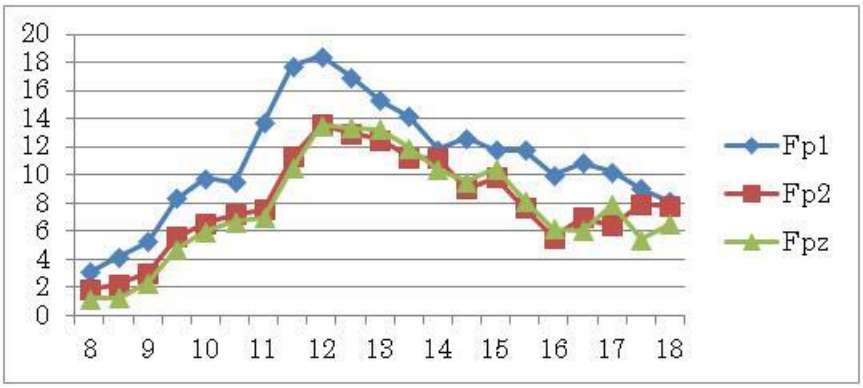

Fig. 6.3.5. The values of energy variation diagram of EEG for subject B on binocular rivalry.

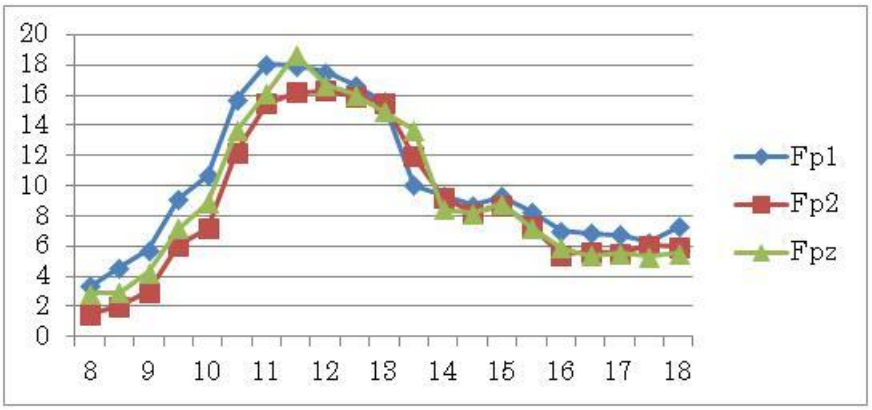

Fig. 6.3.6. The values of energy variation diagram of EEG for subject C on binocular rivalry.

Moreover, the results in Fig. 6.3.5 and Fig. 6.3.5 were depicted based on the other two subjects B and C when the binocular color rivalry occurs. It was clear that similar results and trend lines were obtained in all obtained three figures, which consistently suggested that the subjects under the state of conscious concentration were difficult to obtain fusional images.

6.4 Experimental results of experiencing cataract vision

Fig. 6.4.1- Fig. 6.4.3 showed the EEG based energy variation diagram obtained by EEGlab and the locations Fp1, Fpz and Fp2 used in the experiment for each subject on binocular color fusion (BF) with the experiencing cataract vision, which the stimuli ware set as blue to blue, or red to red (Opponent, Hering, 1892).

In Fig. 6.4.1, the values of energy variation diagram of EEG for the subject A with simulated cataract vision when the binocular color fusion occurs were illustrated, where the horizontal axis denotes the rhythms of the EEG in hertz, and the vertical axis represents the value of the energy calculated by EEGlab. Fp1, Fp2, Fpz represent three locations where EEG was recorded. From this figure, it is apparent that three curves exhibit almost the same trend lines, increasing from 8 Hz to 11 Hz, and thereafter decreasing from 11 Hz to 18 Hz. The peaks of three curves (i.e. the middle alpha-variant rhythm) were located at 9 Hz ~10 Hz, suggesting that the subject was nearly with the state of conscious concentration. Moreover, the results in Fig. 6.4.2 and Fig. 6.4.3 were depicted based on the other two subjects B and C when the subject viewed binocular color fusional images.

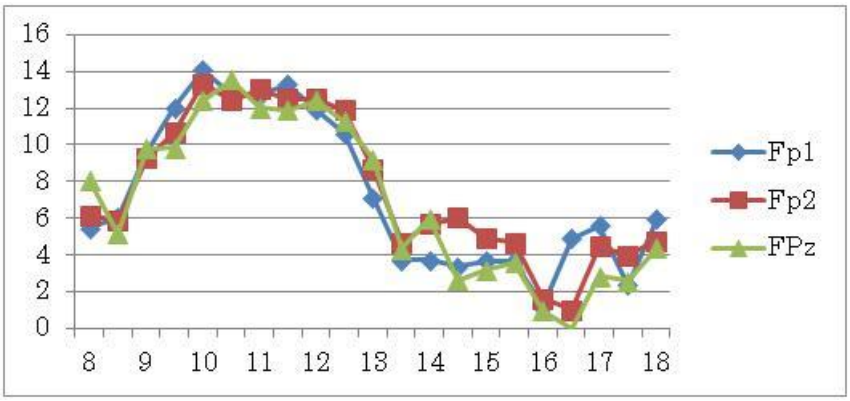

Fig. 6.4.1. The values of energy variation diagram of EEG for subject A on binocular fusion.

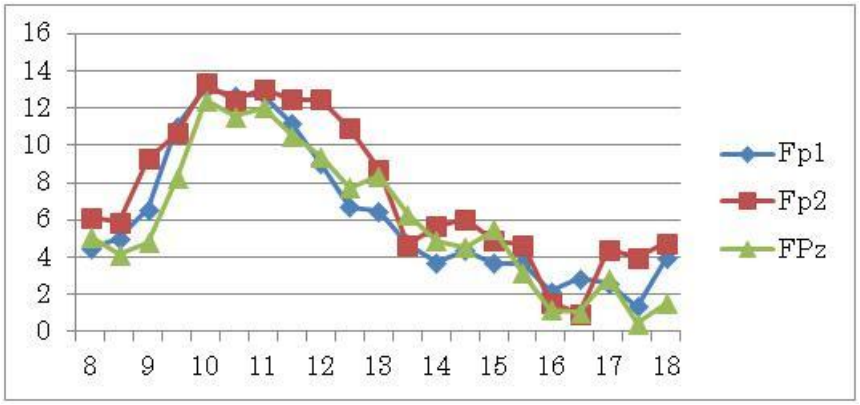

Fig. 6.4.2. The values of energy variation diagram of EEG for subject B binocular fusion.

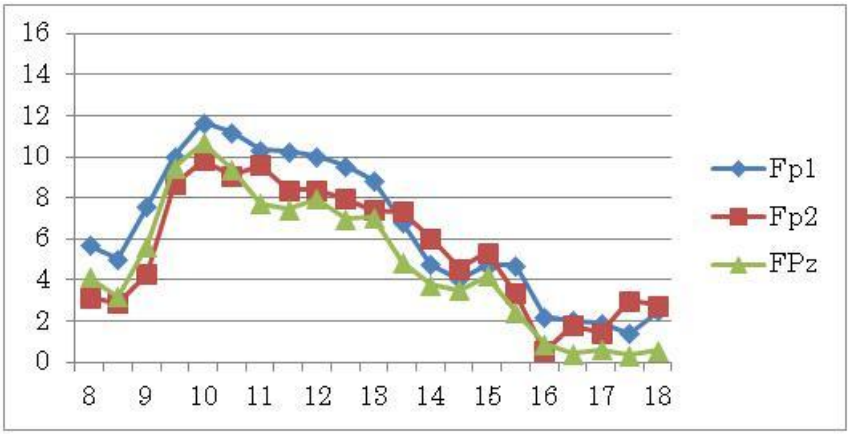

Fig. 6.4.3. The values of energy variation diagram of EEG for subject C on binocular fusion.

Fig. 6.4.2 and Fig. 6.4.3 showed the results of the energy variation diagram of EEG for the remaining two subjects in the experiment. The trend lines in these two figures exhibited similar changing results when compared with those in Fig. 6.4.1. The common results in the obtained three graphs were that the peaks were located at 9 Hz ~ 11 Hz, indicating that subjects with cataract visions still were capable of viewing fusional images when they were under relaxation, no matter the type of visions, either normal vision or experiencing cataract visions.

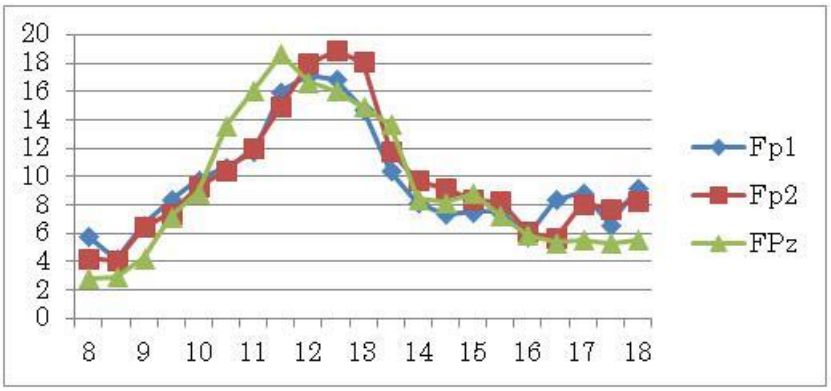

Fig. 6.4.4. The values of energy variation diagram of EEG for subject A on binocular rivalry.

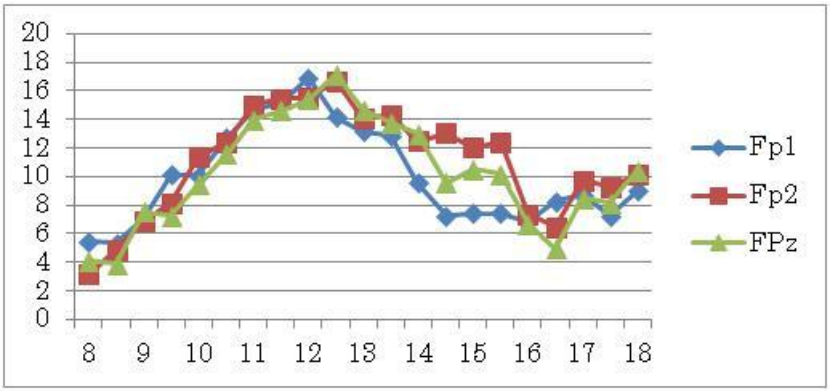

Fig. 6.4.5. The values of energy variation diagram of EEG for subject B on binocular rivalry.

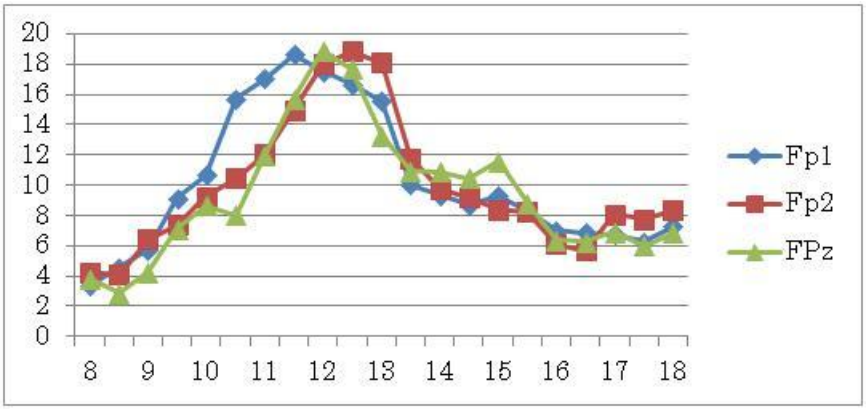

Fig. 6.4.6. The values of energy variation diagram of EEG for subject C on binocular rivalry.

The EEG based energy variation diagram on binocular color rivalry (BR), which the stimuli ware set as blue to yellow, or green to red was shown in Fig. 6.4.4 - Fig.6.4.6. From these figures, we quickly found that similar results were acquired with those subjects with normal visions. As a result, it can be said that no matter in normal vision or in cataract experiencing vision, the middle alpha-variant rhythm (9~11 Hz) was bigger than the fast alpha-variant rhythm (11~13 Hz) when binocular fusion appeared, while became smaller when binocular rivalry appears on all tested electrodes. To elaborate more about this observation, Fig. 6.4.4 was illumining to be explained, where the peaks were found to be located at 11 Hz~ 13 Hz, and all three electrodes showed the same results.

6.5 Discussion and conclusions

To give more certification on the fusion limit, EEG based experiments were carried with the above experiments. The fast and middle alpha-variant rhythms on the front of the brain (locations Fp1, Fpz and Fp2) were recorded and analyzed. Fig. 6.5.1 showed the EEG based energy variation diagram obtained by EEGlab (left figure) and the locations Fp1, Fpz and Fp2 (right figure) used in the experiment. From this figure, it is clear that the binocular fusion shows strongly correlation with the EEG.

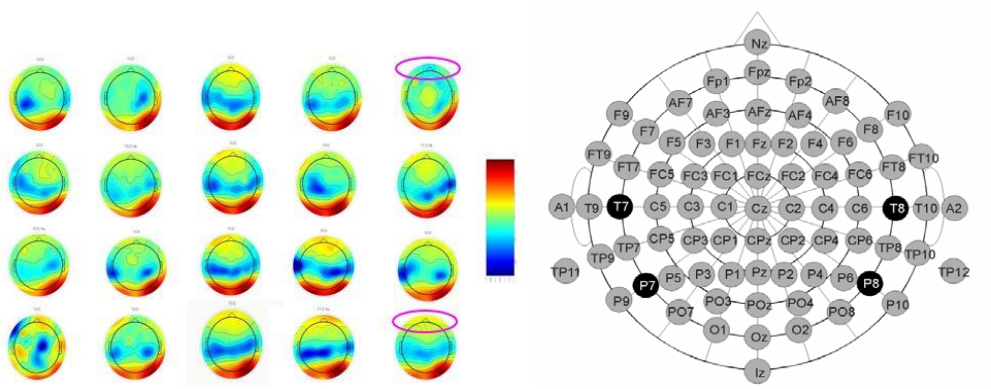

Fig. 6.5.1 The EEG based energy variation diagram obtained by EEGlab (left) and the locations Fp1, Fpz and Fp2 used in the experiment (right).

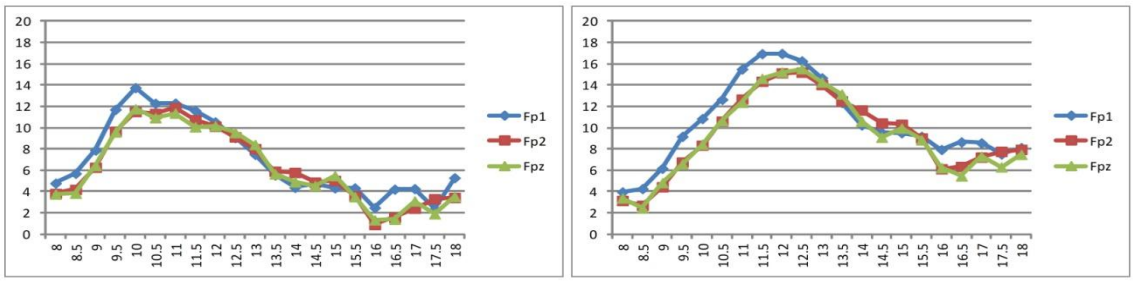

Fig. 6.5.2. The values of energy variation diagram of EEG recorded on Fp1, Fp2 and Fpz in normal vision. (left): binocular fusion; (right): binocular rivalry.

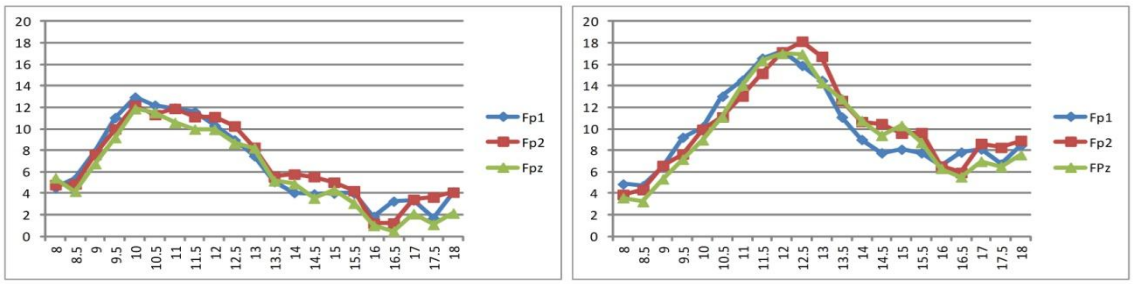

Fig. 6.5.3 The values of energy variation diagram of EEG recorded on Fp1, Fp2 and Fpz in cataract experiencing vision. (left): binocular fusion; (right): binocular rivalry.

To be specific, the averaged data of three subjects were depicted in Fig. 6.5.2 - Fig. 6.5.3 where the horizontal axis denotes the rhythms of the EEG in hertz, and the vertical axis represents the value of the energy calculated by EEGlab. The left subfigure in Fig. 6.5.2 - Fig. 6.5.3 illustrates the diagram obtained when binocular fusion appears, while

the right one shows the diagram of the binocular rivalry (i.e. when the subjects respond "non-fusion").

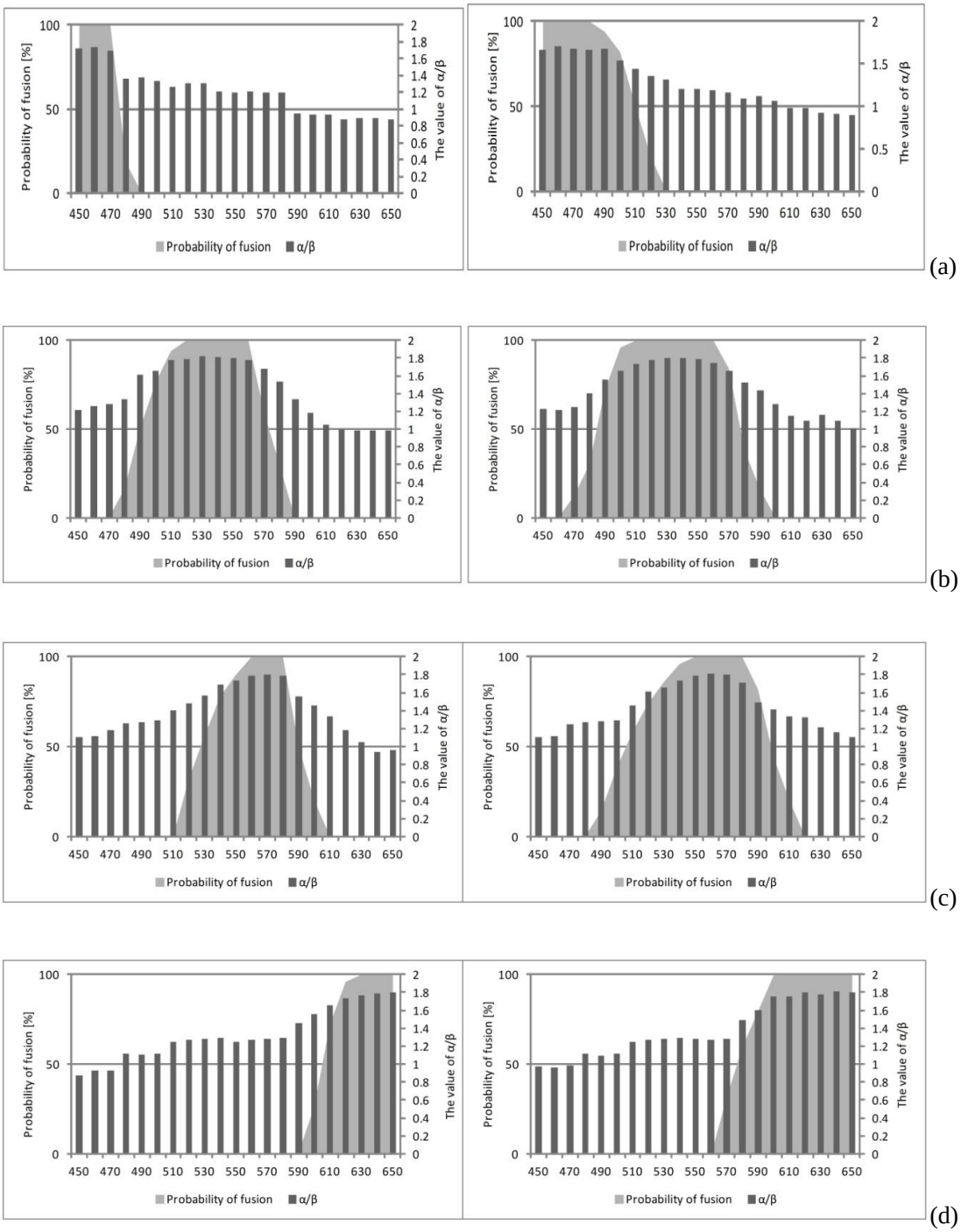

Fig. 6.5.4 The probability of fusion vs. the ratio of α/ β. The grey bars are the probability of fusion. Four colors were tested: (a) blue; (b) green; (c) yellow; and (d) red.

Fig. 6.5.2 - Fig. 6.5.3 clearly indicates that whether in normal vision or in cataract experiencing vision, the middle alpha-variant rhythm (9~11 Hz) is bigger than the fast alpha-variant rhythm (11~13 Hz) when binocular fusion appears, while becomes smaller when binocular rivalry appears on all tested electrodes.

In addition, EEG-based experimental results show that the middle alpha-variant rhythm is bigger than the fast alpha-variant rhythm when binocular fusion appears, while becomes smaller when binocular rivalry appears.

Finally, we analyzed our results using the ratio of α/ β to derivate the changing of EEG in the brain, as shown in Fig. 6.5.4. In this figure, the horizontal axis represents the ratio of α/ β, which was calculated based on the following equation.

$$\frac{\alpha}{\beta} = \frac{\text{The power of } \alpha \text{ in Fp1} + \text{The power of } \alpha \text{ inFp2} + \text{The power of } \alpha \text{ inFpz}}{\text{The power of } \beta \text{ in Fp1} + \text{The power of } \beta \text{ in Fp2} + \text{The power of } \beta \text{ inFpz}} \qquad (1)$$

The above equation calculated the ratio of the α wave to the β wave on three tested EEG locations. Since the energy value of α wave represents the degree of relaxation, and the energy value of β wave indicates the degree of the state of concentration, their ratio thus reflects the influence of the comfortable. That is to say, if the subject feels comfortable, the ratio increases, and vice verse. In Fig. 6.5.4, the vertical axis shows the probability of fusion, and four basic colors are tested in the experiment. The grey bars are the probability of fusion. From this figure, it can be found that the difference of the wave length between two eyes becomes larger, the ratio decreases, suggesting that it is more difficult to view fusional images.

Chapter 7

Conclusion

It has been known that the different views projected to our two eyes contain information that is used to recover depth. It also has been realized that the two eyes have slightly different views of the world contribute to the perception of depth. Many of the organisms, including humans, perceive the outside world with both eyes, grasping a two-dimensional retinal image that is captured by each eye as a common single image. This phenomenon is known as binocular fusion which means that similar images presented to the two eyes appear as one and are processed simultaneously rather than successively. Fusion limit (i.e. diplopia threshold) denotes the largest retinal disparity between two images for which the impression of a single fused image can be maintained. It has pronounced influence on the generation of the percepts of 3D because goods are sterically recognized by the deviation of the retinal image generated in the position of the two eyes (i.e. binocular parallax).

In this study, we measured the binocular color fusion limit in normal and experiencing cataract visions. The experimental results reveal the fundamental data which lead us to further understand the factors influencing the color fusion limits $\Delta\lambda_d$ for each dominant wavelength λ_d at different peripheral visual fields. The results revealed that, in the normal vision, the color fusion limit $\Delta\lambda_{dn}$ was within a range about 11~65 nm on the central vision, 15~67 nm on the retinal eccentricity of 3°, 21~69nm on the retinal eccentricity of 6°, and 25~70 nm on the retinal eccentricity of 9°. In the cataract experiencing vision, the color fusion limit $\Delta\lambda_{dc}$ was within a range about 28~75 nm on the central vision, 30~76 nm on the retinal eccentricity of 3°, 32~77 nm on the retinal eccentricity of 6°, and 33~79 nm on the retinal eccentricity of 9°. We noticed that the $\Delta\lambda_d$ increases steadily with the decrease of the retinal eccentricity of stimuli. We plan to measure the binocular color limit under much higher retinal eccentricity, so that we can further determine the relation of the ratio of retinal eccentricity with the change

of $\Delta\lambda_d$. Also it is planned to measure the binocular color limit, not only for horizontal meridian, but also for all other directions.

To conclude this thesis, the study of the binocular color fusion limits between the normal vision and the cataract experiencing vision revealed that, the value of such fusion limits in cataract experiencing vision was wider than those in the normal vision. To the best of our knowledge, this was the first report to find out such revelation. It is worth emphasizing that, although the subjects were not the actual elderly, the equipment was able to simulate the conditions as likely as possible. It reveals that similar limit values are observed in the range of 520~560 nm both in normal and cataract experiencing visions, which might give some potential evidences for designing three-dimensional equipment.

The above results also appeared to suggest that, the binocular color fusion limit was increased along with the retinal eccentricity increasing, and the binocular color fusion limit in the cataract experiencing vision $\Delta\lambda_{dc}$ was wider than that in the normal vision $\Delta\lambda_{dn}$ or the cataract experiencing vision at each retinal eccentricity. In addition, we found the minimum value of the binocular color fusion limit existing in 590 nm both in the normal vision and the cataract experiencing vision. This result was very similar with the pointview that the minimum value of the monocular wavelength discrimination curve was in the range of 580~600 nm found by Wright & Pitt.

To give more certification on the fusion limit, EEG based experiments were carried with the above experiments. The fast and middle alpha-variant rhythms on the front of the brain (locations Fp1, Fpz and Fp2) were recorded and analyzed. The fast alpha-variant rhythm (11~13 Hz) is reported to be related with the state of conscious concentration, while the middle alpha-variant rhythm (9~11 Hz) appears when the subject is under relaxation. The results clearly indicates that either in normal vision or in cataract experiencing vision, the middle alpha-variant rhythm (9~11 Hz) is bigger than the fast alpha-variant rhythm (11~13 Hz) when binocular fusion appears, while becomes smaller when binocular rivalry appears on all tested electrodes. The values of energy variation diagram of EEG when the binocular color fusion occurs were depicted, which

the peaks (i.e. the middle alpha-variant rhythm) were located at 9 Hz ~11 Hz, suggesting that the subject was under relaxation.

Acknowledgement

I would like to deeply thank the various people who, during my study and research, gave me with useful and helpful assistance. Without their care and consideration, this thesis would likely not have finished.

To my supervisor Prof. Mamoru Takamatsu at University of Toyama, who introduced me to the significant and fascinating world of Vision Research, for his support and continuous encouragement. Without his kind guidance and encouragement, I would never have completed this degree. Furthermore, his help and support are not limited in my study career, but also extended to my living life in Japan. Numerous stimulating discussions and supports make me go ahead during the past times since I came to Japan. Thanks to him, I could accomplish this thesis within three years.

I would like to thank my thesis referees, Prof. Hideyuki Hasegawa, Prof. Takahashi Ooji from University of Toyama for a review and qualification of my thesis and giving various valuable comments and suggestions. To all the members of the Visual and Kansei Information Processing Lab in University of Toyama, for all their help and friendship that made this time much more enjoyable.

I would like to thank all the members of my family, for their unconditional love, support, and encouragement through this process, through all my study process. In particular, I would like to offer thanks to my wife Ai Chen, who endured my seemingly endless hours of absorption in this effort without complaint, who gave me her unwavering support, and who took care of many of those “nuisance” items usually referred to as “Real Life” when I was off in my other world, that of completing this endeavor.

References

Alais, D., and Parker, A., 2012. Binocular rivalry produced by temporal frequency differences. Frontiers in human neuroscience, 6, 227.

Anderson, B. L., and Nakayama, K., 1989. Toward a general theory of stereopsis: binocular matching, occluding contours, and fusion. Psychological Review, 101(3), 414-445.

Andrews, T.J. and Purves, D., 1997. Similarities in normal and binocularly rivalrous viewing. Proceedings of the National Academy of Sciences, 94(18), 9905-9908.

Anstis, S. and Rogers, B., 2012. Binocular fusion of luminance, color, motion and flicker--Two eyes are worse than one. Vision research, 53(1), 47-53.

Artigas, JM., Felipe, A., Navea, A., Fandiño, A. and Artigas, C., 2012. Spectral transmission of the human crystalline lens in adult and elderly persons: color and total transmission of visible light, Invest Ophthalmol Vis.Sci. 53(7).

Asbell PA., 2005. Age-related cataract. The Lencet, 365, 599-609.

Attarha, M., and Moore, C., 2015. Onset rivalry: factors that succeed and fail to bias selection. Attention, Perception, & Psychophysics, 77(2), 520-535.

Blake, R., and Camisa, J., 1979. On the inhibitory nature of binocular rivalry suppression. J. Experimental Psychology: Human Perception and Performance, 5, 315–323.

Blake, R., 1989. A neural theory of binocular rivalry. Psychological Review, 96, 145-167.

Blake, R., 2001. A primer on binocular rivalry, including current controversies. Brain and mind, 2(1), 5-38.

Blake, R. and Logothetis, N. K., 2002. Visual competition. Nature Reviews Neuroscience, 3, 12-21.

Bolanowski, S.J., and Doty, R.W., 1987. Perceptual “blankout” of monocular homogeneous fields (Ganzfelder) is prevented with binocular viewing. Vision research, 27(6), 967-982.

Bonneh, Y.S., Cooperman, A., and Sagi, D., 2001. Motion-induced blindness in normal observers. Nature, 411(6839), 798-801.

Brascamp, J.W., Klink, P.C., and Levelt, W.J.M., 2015. The ‘laws’ of binocular rivalry: 50 years of Levelt’s propositions. Vision Research, 109, 20-37.

Brascamp, J., Blake, R., and Knapen, T., 2015. Negligible fronto-parietal BOLD activity accompanying unreportable switches in bistable perception. Nature neuroscience, 18, 1672-1678.

Breese, B.B., 1909. Binocular rivalry. Psychological Review, 16(6), 410.

Brown, R.J. and Norcia, A.M., 1997. A method for investigating binocular rivalry in real-time with the steady-state VEP. Vision research, 37(17), 2401-2408.

Cao, Y., Sarria, I., Fehlhaber, K.E., Kamasawa, N., Orlandi, C., James, K.N., Hazen, J.L., Gardner, M.R., Farzan, M., and Lee, A., 2015. Mechanism for selective synaptic wiring of rod photoreceptors into the retinal circuitry and its role in vision. Neuron, 87(6), 1248-1260.

Carlson, T.A., and He, S., 2004. Competing global representations fail to initiate binocular rivalry. Neuron, 43(6), 907-914.

Cerrolaza, J.J., Villanueva, A., and Cabeza, R., 2012. Study of polynomial mapping functions in video-oculography eye trackers. ACM Transactions on Computer-Human Interaction, 19(2), 10.

Cong, F., Lin, Q.H., Kuang, L.D., Gong, X.F., Astikainen, P., and Ristaniemi, T., 2015. Tensor decomposition of EEG signals: A brief review. Journal of neuroscience methods, 248, 59-69.

Davson, H., Ed., 1962. The eye. IAcademic Press, Oxford.

Davson, H., 1972. Dynamic aspects of cerebrospinal fluid. Developmental Medicine & Child Neurology, 14(27), 1-16.

Dawson, S., 1917. The experimental study of binocular color mixture, British Journal of Psychology, 8, 510-551.

de Weert, C.M.M. and Levelt, W.J.M., 1976. Comparison of normal dichoptic coloer mixing. Vision Research, 16. 59-70.

de Weert, C.M.M., and Wade, N.J., 1988. Compound binocular rivalry. Vision research, 28(9), 1031-1040.

Delorme, A., and Makeig, S., 2004. EEGLAB: an open source toolbox for analysis of single-trial EEG dynamics including independent component analysis. Journal of neuroscience methods, 134(1), 9-21.

Diza-Caneja, E., 1928. Sobre la binocularidad en aparatos monoobjetivos. Archivos de Oftalmologia Hispano-Americanos, 28(334), 599-600.

Doolan, P.D., Alpen, E.L., and Theil, G.B., 1962. A clinical appraisal of the plasma concentration and endogenous clearance of creatinine. The American Journal of Medicine, 32(1), 65-79.

Dowling, J.E., and Boycott, B.B., 1966. Organization of the primate retina: electron microscopy. Proceedings of the Royal Society of London B: Biological Sciences, 166(1002), 80-111.

Emery, S.E., Daffner, S.D., France, J.C., Ellison, M., Grose, B.W., Hobbs, G.R. and Clovis, N.B., 2015. Effect of Head Position on Intraocular Pressure During Lumbar Spine Fusion. J Bone Joint Surg Am, 97(22), 1817-1823.

Fuensanta, A.V.D., and Doble, N., Eds., 2012. The Human Eye and Adaptive Optics. INTECH Open Access Publisher.

Gray, H., Ed., 1918. Anatomy of the human body. Lea & Febiger.

Grimsley, G., 1943. A study of individual differences in binocular color fusion. Journal of Experimental Psychology, 32(1), 82.

Gunter, R., 1951. The absolute threshold for vision in the cat. The Journal of physiology, 114(1-2), 8-15.

Haldat, C., 1806. Experiences sur la double vision, Journal de Physique, 63, 387–401.

Haldenwang, P., Labrosse, G., and Abboudi, S., 1984. Chebyshev 3-D spectral and 2-D pseudospectral solvers for the Helmholtz equation, Journal of Computational Physics, 55(1), 115-128.

Hardy, J., Delehunt, P., Okajima, K., Werner, J.S., 2005. Senescence of chromatic contrast sensitivity 1. Threshold measurements. J. Opt. Soc. Am. A., 22, 49-59.

Haynes, J.D., and Rees, G., 2006. Decoding mental states from brain activity in humans. Nature Reviews Neuroscience, 7(7), 523-534.

Helmholtz, H., 1866. Handbuch der physiologischen Optik,Voss Press.

Hering, H., 1864. Vom binocularen Tiefsehen, In Beitrdge zur Physiologic V, Engelmann. Leipzig, 5, 287-358.

Hering, E., 1878. Zur lehre vom lichtsinne, K. Akademie der Wissenschaften Press, 68.

Hohwy, J., Roepstorff, A., and Friston, K., 2008. Predictive coding explains binocular rivalry: an epistemological review. Cognition, 108(3), 687-701.

Hollins, M., 1980. The effect of contrast on the completeness of binocular rivalry suppression. Perception & psychophysics, 27(6), 550-556.

Hollins, M., and Hudnell, K., 1980. Adaptation of the binocular rivalry mechanism. Investigative Ophthalmology & Visual Science, 19(9), 1117-1120.

Hopfinger, J.B., Buonocore, M.H., and Mangun, G.R., 2000. The neural mechanisms of top-down attentional control. Nature neuroscience, 3(3), 284-291.

Hovis, J.K., 1989. Review of dichoptic color mixing. Optometry and Vision Science, 66, 181-190.

Howard, I.P. and Rogers, B.J. (Eds), 1995. Binocular Vision and Steropsis. Oxford university press.

Howard, I.P., 2002. Seeing in depth(I Porteous). Chap. 7.

Hu, L., Zhang, Z.G., Mouraux, A., and Iannetti, G.D., 2015. Multiple linear regression to estimate time-frequency electrophysiological responses in single trials. NeuroImage, 111, 442-453.

Huynh-Thu, Q., Callet, P.L., and Barkowsky, M., 2010. Video quality assessment: from 2D to 3D- challenges and future trends, Proc. IEEE International Conf. Image Processing, 4025-4028.

Ikeda M. and Sagawa K.,1979. Binocular color fusion limit. J. Opt .Soc. Am., 69, 316-321.

Ikeda M. and Nakashima Y., 1980. Wavelength difference limit for binocular color fusion. Vision Research, 20, 693-697.

Ikeda M., Kusumi A., Obama T and Shinoda H., 2003. Color Appearance of Color Charts Observed with a Cataract Experiencing Goggle. J. Color Sci. Assoc. Jpn., 27(2), 113-124.

Jamison, K.W., Roy, A.V., He. S., Engel, S.A., and He, B., 2015. SSVEP signatures of binocular rivalry during simultaneous EEG and fMRI. Journal of neuroscience methods, 243, 53-62.

Johannsen, D.E., 1930. A quantitative study of binocular color vision, J. Gen. Psychol, 4, 282-308.

Johnston, J.A., Kawamura, M., Kirken, R.A., Chen, Y.Q., Blake, T.B., Shibuya, K., Ortaldo, J., Mcvicar, D.W., O'Shea, J.J., 1994. Phosphorylation and activation of the Jak-3 Janus kinase in response to interleukin-2, Nature, 370, 151-153.

Jacobson, M., 1993. Foundations of neuroscience (2nd ed.). Springer.

Jung, Y.J., Sohn, H., Lee, S.I., Ro, Y.M., and Park, H.W., Quantitative measurement of binocular color fusion limit for non-spectral colors. Optics Express, 19(8), 7325-7338.

Judd, D.B., and Wyszecki, G., 1975. Color in Business, Science and Industry. Wiley Series in Pure and Applied Optics (3rd ed.). New York: Wiley-Interscience.

Kaplan, I.T., and Metlay, W., 1964. Light intensity and binocular rivalry. Journal of Experimental Psychology, 67(1), 22.

Knoblauch, K., Saunders, F., Kusuda, M., Hynes, R., Podgor, M., Higgins, K.E., and Monasterio, F.M., 1987. Aged and illuminance effect in the Farnsworth-Munsell 100 hue test. Appl. Opt., 26, 1441-1448.

Kolb, H., Ed., 1995. Webvision: Simple anatomy of the retina. The Organization of the Retina and Visual System

Lambooij, M., Ijsselsteijn, W., Fortuin, M., and Heynderickx, I., 2009. Visual discomfort and visual fatigue of stereoscopic displays: a review. J. Imaging Sci. Technol., 53(3), 1-14.

Law, P.C.F., Paton, B.K., Riddiford, J.A., Gurvich, C.T., Ngo, T.T., and Miller, S.M., 2015. No Relationship Between Binocular Rivalry Rate and Eye-Movement Profiles in Healthy Individuals: A Bayes Factor Analysis. Perception, 44(6), 643-661.

Lehky, S.R., 1988. An astable multivibrator model of binocular rivalry. Perception, 17(2), 215-228.

Lehky, S.R., and Sejnowski, T.J., 1988. Network model of shape-from-shading: neural function arises from both receptive and projective fields. Nature, 333(6172), 452-454.

Leopold, D.A., Logothetis, N.K., et al., 1996. Activity changes in early visual cortex reflect monkeys' percepts during binocular rivalry. Nature, 379(6565), 549-553.

Leopold, D.A., and Logothetis, N.K., 1999. Multistable phenomena: changing views in perception. Trends in cognitive sciences, 3(7), 254-264.

Ling, S., and Blake, R., 2009. Suppression during binocular rivalry broadens orientation tuning. Psychol. Sci., 20(11), 1348-1355.

Logothetis, N.K., and Schall, J.D., 1989. Neuronal correlates of subjective visual perception. Science, 245(4919), 761-763.

Logothetis, N.K., Leopold, D.A., and Sheinberg, D.L., 1996. What is rivalling during binocular rivalry? Nature, 380, 621-624.

Logothetis, N.K., 1998. Single units and conscious vision. Philosophical Transactions of the Royal Society B: Biological Sciences, 353(1377), 1801-1818.

Lumer, E.D., Friston, K.J. and Rees, G., 1998. Neural correlates of perceptual rivalry in the human brain. Science, 280(5371), 1930-1934.

Makeig, S. Jung. T.P., Bell. A.J., Ghahremani, D., and Sejnowski, T.J., 1997. Blind separation of auditory event-related brain responses into independent components. Proceedings of the National Academy of Science, 94(20), 10979-10984.

Makous, W., and Sanders, R.K., 1978. Suppression interactions between fused patterns, Visual psychophysics and physiology, Academic Press, New York.

Markand, O.N.,1990. Alpha rhythms. Journal of Clinical Neurophysiology, 7(2), 163-190.

Meenes, M., 1930. A phenomenological description of retinal rivalry. The American Journal of Psychology, 260-269.

Mitchell, J.F., Stoner, G.R., and Reynolds, J.H., 2004. Object-based attention determines dominance in binocular rivalry. Nature, 429(6990), 410-413.

Monty, R.A., and Senders, J.W., 1976. Eye movements and psychological processes, DTIC document, Tec. Rep.

Morgan, K.N., and Tromborg, C.T., 2007. Sources of stress in captivity. Applied Animal Behaviour Science, 102(3), 262-302.

Nguyen, V.A., Freeman, A.W., and Alais, D., 2003. Increasing depth of binocular rivalry suppression along two visual pathways. Vision research, 43(19), 2003-2008.

Norcia, A.M., Appelbaum, L.G., Ales, J.M., Cottereau, B.R., and Rossion, B., 2015. The steady-state visual evoked potential in vision research: A review. Journal of Vision, 15(6), 4.

O'Shea, R.P., and Blake, R., 1986. Dichoptic temporal frequency differences do not lead to binocular rivalry. Perception & psychophysics, 39(1), 59-63.

Pickford, R.W., 1947. Binocular color combinations, Nature, Lond 159, 268-269.

Pokorny, J., Smith, V.C. and Lutze, M., 1987. Aging of the human lens. Appl. Opt., 26, 1437-1440.

Polyak, S.L., 1941. The retina. Univ. Chicago Press.

Qin, D.M., Takamatsu, Nakashima, Y., and Qin, X.,2006. Change of wavelength difference limit for binocular color fusion with wavelength and brightness of stimuli. J. Light Vis. Env., 30(1), 43–45.

Qin, X., Nakashima, Y., Takamatsu, M, Qin, D.M., Sassa K. and Katoh Z., 2005. Analysis of Wavelength Difference Limit for Binocular Color Fusion. The 5th Lux Pacifica, 225-228.

Qin, X., Nakashima, Y., Takamatsu, M., and KIDOH, Y., 2007. Research of Binocular Color Fusion Limit on Peripheral Visual Field. J. Light & Vis. Env., 31, 155-156

Qin, X., Nakashima, Y. and Takamatsu, M., 2009. Effects of Luminance and Size of Stimuli upon Binocular Color Fusion Limit. Opt. Rev., 16(3), 404-408.

Qin, X., Jiang, S., Takamatsu, M., and Nakashima, Y., 2009. Research of Binocular Color Fusion Limit on Peripheral Visual Field. J.Light & Vis.Env., 33, 156-160.

Rivers, T.J., Sirota, M.G., Guttentag, A.I., Ogorodnikov, D.A., Shah, N.A., and Beloozerova, I.N., 2014. Gaze shifts and fixations dominate gaze behavior of walking cats. Neuroscience, 275, 477-499.

Robinsion, M.H., 1968. The defensive behavior of the stick insect oncotophasma martini (Griffini). Proc. of the Royal Entomological Society of London, A, General Entomology, 43, 183-187.

Rodriguez-Fortuno, F.J., Marino, G., Ginzburg, P., O'Connor, D., Martinez, A., Wurtz, G.A., and Zayats, A.V., 2013. Near-field interference for the unidirectional excitation of electromagnetic guided modes. Science, 340(6130), 328-330.

Roeber, U., 2012. Neural processing of orientation differences between the eyes' images. Journal of vision, 12(13), 20.

Romany, F.M., 2012. Using genetic algorithm for identification of diabetic retinal exudates in digital color images. Journal of Intelligent Learning Systems and Applications, 4(3), 188-198.

Sagawa, K., 1981. Minimum light intensity required for color rivalry. Vision Research, 21(10), 1467-1474.

Said, C.P., and Heeger, D.J., 2013. A model of binocular rivalry and cross-orientation suppression. PLoS Comput. Biol., 9(3), e1002991.

Sandberg, K., Bahrami, B., Kanai, R., Barnes, G.R., Overgaard, M., and Rees, G., 2013. Early visual responses predict conscious face perception within and between subjects during binocular rivalry. Journal of cognitive neuroscience, 25(6), 969-985.

Sereno, M.I., Dale, A.M., Reppas, J.B., Kwong, K.K., Belliveau, J.W., Brady, T.J., Rosen, B.R., and Tootell, R.B., 1995. Borders of multiple visual areas in humans revealed by functional magnetic resonance imaging. Science, 268(5212), 889-893.

Shigeru, C., 1996. 3D consortium safety guidelines for popularization of human-friendly 3D. Tech. Rep. 3D Consortium, Japan.

Siegel, M., Buschman, T.J., and Miller, E.K., 2015. Cortical information flow during flexible sensorimotor decisions. Science, 348(6241), 1352-1355.

Slagter, H.A., Prinssen, S., Reteig, L.C., and Mazaheri, A., 2016. Facilitation and inhibition in attention: Functional dissociation of pre-stimulus alpha activity, P1, and N1 components. NeuroImage, 125, 25-35.

Smelser, G.K., Ed., 1961. The structure of the eye. Academic Press, New York.

Soon, C.S., Brass, M., Heinza, H.J., and Haynes, J.D., 2008. Unconscious determinants of free decisions in the human brain. Nature neuroscience, 11(5), 543-545.

Sun, P., Chubb, C., and Sperling, G., 2015. Two mechanisms that determine the Barber-Pole Illusion. Vision research, 111, 43-54.

Suzuki, T.A., Qing, Y., Sakuragawa, S., Tamura, H., and Okajima, K., 2006. Age-related changes of reaction time and p300 for low-contrast color stimuli: effects of yellowing of the aging human lens. J. Physiol. Anthropol., 25(2), 179-187.

Tang, T., Chen, L.Y., Liu, Z., Liu, C., and Zhou, Y., 2012. Low-level processing deficits underlying poor contrast sensitivity for moving plaids in anisometropic amblyopia. Visual neuroscience, 29(6), 315-323.

Thomas, F.H., Dimmich, F.L. and Luria, S.M. , 1961. A study of binocular color mixture. Vision Research., 1, 108-120.

Tong, F., Meng, M., and Blake, R., 2006. Neural bases of binocular rivalry. Trends in cognitive sciences, 10(11), 502-511.

Tononi, G. and Edelman, G.M., 1998. Consciousness and complexity. Science, 282(5395), 1846-1851.

Tononi, G., Edelman, G.M., and Sporns, O., 1998. Complexity and coherency: integrating information in the brain. Trends in cognitive sciences, 2(12), 474-484.

Tononi, G., Srinivasan, R., Russell, D.P., and Edelman, G.M., 1998. Investigating neural correlates of conscious perception by frequency-tagged neuromagnetic responses. Proceedings of the National Academy of Sciences, 95(6), 3198-3203.

Trapp, S., and Bar, M., 2015. Prediction, context, and competition in visual recognition. Annals of the New York Academy of Sciences, 1339(1), 190-198.

Ujike, H. et al., 2005. ISO international workshop agreement-IWA3 image safety-reducing the incidence of undesirable biomedical effects caused by visual image sequence. IWA 3:2005(E), ISO copyright office, case postale 56, CH-1211 Geneva 20.

Ungerleider, S.K., and Leslie, G., 2000. Mechanisms of visual attention in the human cortex. Annual review of neuroscience, 23(1), 315-341.

van de Grind, W.A., Koenderink, J.J., and Van Doorn, A.J., 1986. The distribution of human motion detector properties in the monocular visual field. Vision Research, 26(5), 797-810.

van de Grind, W.A., 2002. Physical, neural, and mental timing. Consciousness and cognition, 11(2), 241-264.

van den Berg, T.J.T.P. and Tan, K.E.W.P., 1994. Light transmittance of the human cornea from 320 to 700 nm for different ages. Vision Res., 34, 1453-1456.

Voytek, B., Kayse, A.S., Badre, D., Fegen, D., Chang, E.F., Crone, N.E., Parvizi, J., Knight, R.T., and D'Esposito, M., 2015. Oscillatory dynamics coordinating human frontal networks in support of goal maintenance. Nature Neuroscience, 18, 1318-1324.

Walls, G.L., 1942. The vertebrate eye and its adaptive radiation. Cranbrook Institute of Science.

Wandell, B.A., Ed., 1995. Visual perception. Stanford University.

Weale, R.A., 1988. Age and transmittance of the human crystalline lens. J. Physiol., 395, 577-587.

Werner, J.S., and Steele, V.G., 1988. Sensitivity of human foveal color mechanisms throughout the life span. J. Opt. Soc. Am. A., 12, 2122-2130.

Werner, J.S., Peterzell, D.H., and Scheetz, A.J., 1990. Light, vision, and aging. Optom. Vis. Sci., 67, 214-229.

Werner, J.S., and Schefrin, B.E., 1993. Loci of achromatic points throughout the life span. J. Opt. Soc. Am. A., 10, 1509-1516.

Werner, J.S., 1996. Visual problems of the retina during aging: compensation mechanisms and color constancy across the life span. Prog. Retin Eye Res., 15, 621-645.

Wheatstone, C., 1938. Some remarkable phenomena of binocular vision. Philosophical Transactions of the Royal Society. 128, 371-394.

Wright, W.D. and Pitt, F.H.G., 1934. Hue discrimination in normal color-vision. Proc.Phys.Soc. 46, 459-473.

Wu, C.W., Gu, H., Zou, Q., Lu, H., Stein, E., and Yang, Y., 2012. TE-dependent spatial and spectral specificity of functional connectivity. Neuroimage, 59(4), 3075-3084.

Xu, J., Pokorny, J., and Smith, V.C., 1997. Optical density of the human lens. J. Opt. Soc. Am. A., 14, 953-960.

Young, T., 1802. The bakerian lecture: on the theory of light and colors, Philosophical Transactions of the Royal Society of London, 92, 12-48.

Zhang, L. and Tam, W. J., 2005. Stereoscopic image generation based on depth images for 3D TV. IEEE Transactions on Broadcasting, 51(2), 191-199.

Papers and Conferences List

Original Papers list

1. Shi Wang, Mamoru Takamatsu, "Analysis of the Difference between the Normal Vision and the Experiencing Cataract Vision on Binocular Color Fusion Limit," Int. Journal of Engineering Research an Applications, Vol. 5, Issue. 10, pp. 45-49, 2015

2. Shi Wang, Mamoru Takamatsu, "Empirical and EEG Evidences on the Fusion Limit of Binocular Vision in Cataract Experiencing Vision," International Journal of Applied Science and Technology, Vol. 5, No. 5, pp. 19-24, 2015

International Conferences list

1. Shi Wang, Chen, J., Ma, Y.C., Nakashima, Y., and Takamatsu, M., "Basic study on the limits of binocular colour fusion in retinal fovea", 5th CJK Lighting Conference, Tokyo, 2012.

2. Lin Ma, Nakashima, Y., Takamatsu, M., Shi Wang, and Sawa, K., Color temperature illumination of history buildings, 4th CJK Lighting Conference, Dalian, 2011.

3. Jia Chen, Lin Ma, Shi Wang, Nakashima, Y., and Takamatsu, M., "Evaluation of landscape lighting for urban nightscape in a snowy region", 5th CJK Lighting Conference, Tokyo, 2012.

4. Jia Chen, Shi Wang, Nakashima, Y., Takamatsu, M., and Fujita, H., "Binocular colour fusion limits in retinal fovea for three-dimensional display" IADIS International Conference Interfaces and Human Computer Interaction, Prague, 2013.

Domestic Conferences list (in japan)

1. 王　石，藤田 博樹，高松 衛，中嶋 芳雄:“高齢者における「色」の両眼融合限界に関する基礎的研究”平成２３年度電気関係学会北陸支部連合大会，福井(2011 年 9 月)．

2. 王 石，藤田 博樹，高松 衛，中嶋 芳雄:“「色の両眼融合限界」に関する研究”平成２３年度人間工学会東海支部連合大会, 三重(2011 年 10 日).

3. 王 石，马 云超，藤田 博樹，高松 衛，中嶋 芳雄“「色」の両眼融合限界の定量化に関する研究–高齢者における–”平成２４年度電気関係学会北陸支部連合大会, 富山(2012 年 9 月)．

4. 王 石，马 云超，藤田 博樹，高松 衛，中嶋 芳雄:“高齢者における色の両眼融合限界の定量化”日本照明学会第 45 回全国大会, 山口(2012 年 9 月)．

5. 王 石，马 云超，藤田 博樹，高松 衛，中嶋 芳雄:“「色」の両眼融合限界に関する研究–若年者と高齢者の差における–”日本人間工学会第 54 回全国大会, 千葉(2013 年 6 月)．

6. 王 石，马 云超，高松 衛，中嶋 芳雄:“周辺視における「色」の両眼融合限界に関する研究”平成２５年度電気関係学会北陸支部連合大会, 石川(2013 年 9 月)．

7. 王 石，华 斌，藤田 博樹，高松 衛，中嶋 芳雄:“色差と両眼融合限界点の推移に関する研究” 平成２６年度電気関係学会北陸支部連合大会, 富山(2014 年 9 月)．